Dear Dr. Yool,

We sincerely thank you and the two reviewers for the valuable comments, which have helped us improve the manuscript. We have considered carefully the comments and revised the manuscript accordingly. Please see below for detailed point-by-point replies (*in italics*) to the comments (in plain text). We hope that our revisions will be satisfactory to you and the reviewers.

Best regards,
Bingzhang Chen
S. Lan Smith

****

Reviewer 1

The lognormal distribution is a fundamental assumption in the authors' model. In their revised manuscript, they concede that it is also an unusual one. It is perfectly fine to say that the lognormal can be fit well to empirical data (e.g. Quintana et al. 2008, though another citation or two here would be nice) and has been used in other continuous size models and therefore is used here. However, the mathematical arguments used for why the lognormal was used instead of the power law are uncompelling and/or incorrect.

The authors say that the power-law distribution does not have an upper or lower limit on size, whereas the lognormal does; this is wrong. Power laws are supported (i.e. have non-zero probability density) on the range [x_min, infinity), whereas lognormals are supported on the range [0, infinity), so these distributions are not different in this regard. In fact, it is much more common to specify an upper cutoff on power laws via an exponential truncation than it is for a lognormal. It is quite easy to calculate the mean and variance of a power law, so these are bad examples of mathematical manipulations for which the power law is hard. The power law also has zero probability of negative size; actually if x_min for the power law can be set to the size of the smallest phytoplankton in the system (e.g. Pro), which means that the power law has a zero probability for a cell smaller than x_min, while the lognormal always has a nonzero probability for arbitrarily small phytoplankton. The skewness of the log-size distribution discussed by the authors is further evidence for the power law potentially giving better results than the lognormal.

It's fine to justify the lognormal by citing that it can be fit to data well and has been used in continuous size models, but the other arguments for its use should be reconsidered, and the authors should be clear that their model hinges upon this unusual, even if justifable, assumption. I recommend the authors read the paper "Power laws, Pareto distributions, and Zipf's law" by M. E. J. Newman, which gives a clear description of many of the relevant mathematical properties of power laws.

All other changes I found satisfactory!

[Response]
First of all, we sincerely thank the reviewer for suggesting the paper of Newman (2005), which is extremely inspiring. Also thanks for suggesting the truncated power-law distribution, which could be a potential alternative to the lognormal distribution. We have looked into the literature and found that the controversy concerning the power law versus lognormal distribution has long existed in many fields of science.

We apologize that in the previous revised text, due to lack of statistics knowledge, we wrote incorrectly that the power-law distribution is unrealistic in representing phytoplankton at the size limits. We were also incorrect in stating that its mathematical manipulation is difficult. Now we have thoroughly revised Sect. 4.2.1. For the sake of space, we will not copy the whole text here, but just summarize the main points of Sect. 4.2.1:

1) *The power law is indeed more often used to fit phytoplankton size data.*

2) *We need to impose an upper cutoff for power law to calculate mean and variance of phytoplankton size.*
3) *It is difficult to tell which distribution is better for fitting empirical data. The two distributions are intrinsically connected.*
4) *Neither of them can deal with the problem of multimodal distributions, which may be solved by having multiple functional groups, assuming a particular distribution for each group.*

****

Reviewer 2

I have read with interest the revised version of the manuscript by Bingzhang Chen and S. Lan Smith as well as their answers to the editor and the three referees' comments. The manuscript has been substantially improved. Indeed, the authors have extensively reworked some parts of the study which adds a significant value to the manuscript in terms of both methodological implications of their work and scientific outcome. In particular, new simulations have been conducted with a modified version of the model equations, including e.g. a second zooplankton variable corresponding to the mesozooplankton with grazing preferences scaled with prey size.

As suggested, and importantly, the method that has been conducted in this study, namely using the observations at two distinct stations to set up a single set of parameters values that can later be used as an initial estimate for new simulations (e.g. 3D simulations), has been clarified in the new version of the manuscript. Moreover, some efforts have also been made to validate the model and the previously obtained unique set of parameters using an independent station (ALOHA) with only limited success in reproducing the observed biogeochemical features in this region (understimation of Chl, NPP and PON). Some suggestions have been proposed to improve the optimization of the parameters for 3D

GCM's simulations (Transport Matrix Technique).

The results section 3.4 has also been further developed with a detailed description of the relative weight of the different factors and their relationship in driving the simulated size variance (i.e diversity) and its variability over time at the two stations. Finally, the discussion section (4.1) has been deeply improved and better structured which contributes to a better connection between this work and more general concepts with regards to ecological mechanisms explaining plankton diversity (exclusive competition, evolutionary processes (trait diffusion) and physical transport, see section 4.1.1).

Overall, convincing and detailed arguments have been given by the authors on every points requested by the referees. Therefore, I recommend this revised manuscript for publication in GMD. Hereafter, I give a few remaining minor suggestions to improve the clarity of the manuscript.

[Response] Thank you very much for the encouragement!

P4 L.13-19 : 'The trait variance, treated as a tracer in the model, serves as a measure of trait diversity; although it cannot be simply equated to species richness, it can be converted to other diversity metrics such as the continuous entropy (Quintana et al., 2008). The diversity of functional traits is arguably a better diversity index than species richness relating to ecosystem functioning (Loreau et al., 2001).

Thus, the continuous trait-based model has the advantage that the factors controlling diversity can be directly quantified …'

Due to the inclusion of new sentences, text organization results in poor transitioning. I would suggest restructuring as follows:

'The trait variance, treated as a tracer in the model, serves as a measure of trait diversity. Thus, the continuous trait-based model has the advantage that the factors controlling diversity can be directly quantified … . Although the size variance cannot be simply equated to species richness, it can be converted to other diversity metrics such as the continuous entropy (Quintana et al., 2008). Moreover, the diversity of functional traits is arguably a better diversity index than species richness relating to ecosystem functioning

(Loreau et al., 2001).’

[Response] The suggested revisions are very nice. We have completely followed the suggestions.

P.5 L26-P.6 L4: Section 2: This added overview paragraph at the beginning of the model description section is very useful. However, the use of the term ‘CITRATE 1.0’ (P.4, L.26) is sometimes confusing as the reader might not know whether the authors are talking about the name of the model (which should be the correct use for CITRATE 1.0) or the method conducted in this study. Moreover, it would also be useful to mention here that the method that has been used aims at calibrating the model parameters to be applied for different oceanic regions. I would suggest something like:
The aim of the present study is to design and implement a continuous trait-based model (CITRATE 1.0) at two representative stations in the North Pacific. The overall goal of this model is not only to simulate the phytoplankton size diversity but also to faithfully reproduce the seasonal and vertical dynamics of other important quantities such as nutrients Chl a, and productivity in for later investigations of the roles of phytoplankton diversity in biogeochemical cycles in different oceanic regions (using 3D regional/global simulations). Therefore, the two contrasted stations were used to provide a single set of parameters values by fitting the model results to observations before the obtained model was validated in another independent station (ALOHA). Hence, CITRATE 1.0 consists of the following key features:

[Response] Thanks for the suggested revisions, which are really helpful. We have completely followed the suggestions.

P. 21 L. 6-10: For consistency reasons, this part on the comparison of estimated growth rate with literature values should be moved P. 20 L. 21 together with the paragraph on the test of sensitivity of the growth rate.

[Response] We are sorry that we might have caused confusion between

“u”and “μ”. This part is actually on the sensitivity analysis of the trait diffusion coefficient “u”, not on comparing simulated phytoplankton growth rates (μ) with those reported in the literature. To make it clearer, we have corrected the sentence to: “The optimized trait diffusion coefficient (u) was much higher than in Acevedo-Trejos et al. (2016).”

CITRATE 1.0: Phytoplankton continuous trait-distribution model with one-dimensional physical transport applied to the North Pacific

Bingzhang Chen, S. Lan Smith

Research Center for Global Change Research, JAMSTEC (Japan Agency for Marine-Earth Science and Technology), 3173-25 Showa-machi, Kanazawa-ku, Yokohama 236-0001, Japan

Correspondence to: Bingzhang Chen (bzchen@jamstec.go.jp)

删除的内容: 1.1

删除的内容: 0

删除的内容: west

删除的内容: bingzhang.chen@gmail.com

Abstract. Diversity plays critical roles in ecosystem functioning, but it remains challenging to model phytoplankton diversity in order to better understand those roles and reproduce consistently observed diversity patterns in the ocean. In contrast to the typical approach of resolving distinct species or functional groups, we present a ContInuous TRAiT-basEd phytoplankton model (CITRATE) that focuses on macroscopic system properties such as total biomass, mean trait values, and trait variance. This phytoplankton component is embedded within a Nitrogen-Phytoplankton-Zooplankton-Detritus-Iron model that itself is coupled with a simplified one-dimensional ocean model. Size is used as the master trait for phytoplankton. CITRATE also incorporates "trait diffusion" for sustaining diversity, as well as simple representations of physiological acclimation, i.e. flexible chlorophyll-to-carbon and nitrogen-to-carbon ratios. We have implemented CITRATE at two contrasting stations in the North Pacific where several years of observational data are available. The model is driven by physical forcing including vertical eddy diffusivity imported from three-dimensional general ocean circulation models (GCMs). One common set of model parameters for the two stations is optimized using the Delayed Rejection Adaptive Metropolis-Hasting Monte Carlo (DRAM) algorithm. The model faithfully reproduces most of the observed patterns and gives robust predictions on phytoplankton mean size and size diversity. CITRATE is suitable for applications in GCMs and constitutes a prototype upon which more sophisticated continuous trait-based models can be developed.

删除的内容: remains unclear how best

删除的内容: is still

带格式的: 字体:非 粗体

删除的内容: ed

删除的内容: 1.0

删除的内容: west

删除的内容: i

删除的内容: physics

删除的内容: wa

删除的内容: d

删除的内容: observational

删除的内容: a

删除的内容: With proper physical forcing,

删除的内容: 1.0

删除的内容: can be applied to any oceanic station where either nitrogen or iron limits phytoplankton growtha starting step

删除的内容: and applications within GCMs

删除的内容: and couple

删除的内容: d within general ocean circulation models

1 Introduction

Phytoplankton are a polyphyletic group of oxygenic organisms that account for nearly half of the global primary production (Fields et al., 1998) and also play indispensable roles in other biogeochemical cycles in the Earth system (Falkowski, 2012). They have astonishingly high diversity, with several thousand species already documented and many remaining to be explored (Sournia et al., 1991; Moon-van der Staay et al., 2001). Their equivalent spherical diameter (ESD) can range from less than one micron for cyanobacteria such as *Prochlorococcus* (Chisolmn et al., 1988) to more than 1 mm for some giant diatoms (Villareal, 1993). Furthermore, physiology differs substantially even within the same genera or species and the role of intraspecific variability in population dynamics and biogeochemical cycles remains to be investigated (Strzepek and Harrison, 2004; Johnson et al., 2006; Palenik et al., 2006; Kooistra et al., 2008; Biller et al., 2015). The roles of phytoplankton diversity in marine ecosystem functioning have not been understood as thoroughly as those of plant diversity in terrestrial ecosystems (Tilman et al., 1997, 2014).

Although various ocean models have been developed by accounting for different functional groups or categories of phytoplankton (e.g., Le Quéré et al., 2005; Hashioka et al., 2013), the finite number of such distinct types included limits their ability to resolve the vast diversity of trait values. Some pioneering studies have considered greater numbers of species, each of which is defined by particular set of multivariate trait axes that constitute a hyper-volume niche space (Follows et al., 2007; Barton et al., 2010; Follows and Dutkiewicz, 2011; Matsuda et al., 2016). (It is worth noting that these diversity models usually focus on “functional traits” which are the key to linking phytoplankton diversity, environmental conditions, and ecosystem functioning. Important phytoplankton traits include maximal growth rate, the light absorption and nutrient uptake affinities, optimal growth temperature, and edibility (i.e., susceptibility to grazing), etc (Litchman et al., 2007; Litchman and Klausmeier, 2008; Edwards et al., 2011, 2012, 2015; Merico et al., 2009; Barton et al., 2010, Thomas et al., 2012; Chen, 2015)). The total species pool in these modelling studies should ideally cover the entire multi-dimensional trait space constrained by trade-offs (Barton et al., 2010; Smith et al., 2011), although

删除的内容: Both species identity (functional traits) and diversity play critical roles in ecosystem functioning (Tilman et al., 1997, 2014).

删除的内容: sizes

删除的内容: the

删除的内容:

删除的内容: various

删除的内容: such as cyanobacteria, diatoms, diazotrophs, etc.

删除的内容: has a

删除的内容: F

删除的内容: of all possible species

删除的内容: trait

删除的内容: which is however

computational limits make this impossible in practice. As a compromise, only a limited set of trait combinations is sampled from the entire trait space. Although this approach has effectively generated large-scale patterns of plankton diversity, it generally underestimates local diversity, for two reasons: 1) lack of appropriate mechanisms for sustaining diversity (but *see* Vallina et al., (2014)), and 2) insufficient trait resolution, so that fitness differences between species are too large to allow coexistence (i.e. insufficient equalizing effect; *see* Chesson, 2000). In any case, a substantial proportion of the idealized species so modelled cannot survive under realistic oceanic conditions, and therefore the models do not capture the functions associated with many species.

Continuous trait-based models have been developed to address the above questions (Wirtz and Eckhardt, 1996; Norberg et al., 2001; Bruggeman, 2009; Merico et al., 2009, 2014; Terseleer et al., 2014; Acevedo-Trejos et al., 2015, 2016; Smith et al., 2016). Instead of modeling the dynamics of individual species, continuous trait-based models or so-called "adaptive dynamics" models focus on macroscopic or aggregate properties of a community such as total biomass, average trait, and trait variance by assuming that phytoplankton traits follow some distribution (usually Gaussian) (Smith et al., 2011). These models do not have the problem of inadequate trait resolution, because they have infinitesimally fine trait resolution. The trait variance, treated as a tracer in the model, serves as a measure of trait diversity. Thus, the continuous trait-based model has the advantage that the factors controlling diversity can be directly quantified and better understood because the sources (e.g. speciation or immigration) and sinks (e.g. resource competition) for diversity are specified explicitly. Although the size variance cannot be simply equated to species richness, it can be converted to other diversity metrics such as the continuous entropy (Quintana et al., 2008). Moreover, the diversity of functional traits is arguably a better diversity index than species richness relating to ecosystem functioning (Loreau et al., 2001). In addition, these models are computationally much more efficient than classic discrete species approaches. For example, assuming two independent traits for the phytoplankton community, a continuous trait-based model only requires 1 (biomass) + 2 x 2 (trait mean and variance) = 5 tracers for the phytoplankton community, while a discrete species-based model requires 2 x 10 = 20 tracers if assuming ten discrete values in each trait dimension, which still provides only coarse trait resolution. Furthermore, this difference increases linearly with trait dimension.

删除的内容: practically impossible in practice due to

删除的内容: at

删除的内容: such models

带格式的: 字体:斜体

删除的内容: of the trait space

带格式的: 字体:斜体

删除的内容: ;

删除的内容: ,

删除的内容: a

删除的内容: it

删除的内容: but

删除的内容: may

删除的内容: like

删除的内容: Shannon-Wiener index

删除的内容: T

删除的内容: Thus, the continuous trait-based model has the advantage that the factors controlling diversity can be directly quantified and better understood because the sources (e.g. speciation or immigration) and sinks (e.g. resource competition) for diversity can beare specified explicitly given.

删除的内容: species-based models

删除的内容: exponentially

Relatively few continuous trait-based models have been coupled with physics transport and calibrated against oceanic observations. Here we describe a new one-dimensional model, **CITRATE 1.0**, built upon the classic nitrogen-phytoplankton-zooplankton-detritus (NPZD) model with a phytoplankton community represented using a continuous distribution of size, taken as a master trait (Fig. 1). In this way, not only total phytoplankton biomass, but also phytoplankton mean size and size variance are explicitly modeled. The distributions of other important functional traits are implicitly modeled via well-established scaling power laws. Although this approach might overlook some other important traits that are not related to size and thereby underestimate trait diversity to some extent, it serves as a starting point for later development of more comprehensive diversity models that can include more traits or be integrated with the discrete functional group approach. For the model to be implemented in the subarctic North Pacific, a well-known high nitrate low chlorophyll (HNLC) region, **CITRATE** also incorporates an iron limitation module. We optimized the model parameters against the extensive observational data at two contrasting stations (K2: 160 ºE, 47 ºN; S1: 145 ºE, 30ºN) in the North Pacific (Fig. 2a). The station K2 is located within the western subarctic North Pacific gyre and is characterized by low temperature, high nitrate, and high carbon export (Matsumoto et al., 2014; Wakita et al., 2016). Iron limitation on phytoplankton growth has been suggested at this station (Fujiki et al., 2014). The station S1 is located within the western subtropical North Pacific and is characterized by high sea surface temperature, low levels of nitrate and carbon export efficiency (Matsumoto et al., 2016; Sasai et al., 2016; Wakita et al., 2016). To independently validate the model, we also use the optimized model parameters from stations K2 and S1 to run the model for station ALOHA (158 ºW, 22.75 ºN) and compare the model outputs with the extensive observational data collected there.

删除的内容: validated

删除的内容: **1.0**

删除的内容: **1.1**

删除的内容: While we admit that

删除的内容: at

删除的内容: the

In the following sections, we first describe the details of the model structure and the parameter optimization subroutine. Then we show the results of parameter optimization and modeled patterns of nutrients, phytoplankton biomass, mean size and size diversity. We also discuss the merits and limitations of the model and of the continuous trait-distribution approach. **CITRATE** is intended as a prototype for later incorporation into three-dimensional (3D) general ocean circulation models (GCMs) and for further development of more comprehensive trait-based models.

删除的内容: 1.0

删除的内容: to be

删除的内容: starting model

2 Model description

The aim of the present study is to design and implement a continuous trait-based model (**CITRATE** 1.0) at two representative stations in the North Pacific. The overall goal of this model is not only to simulate the phytoplankton size diversity but also to faithfully reproduce the seasonal and vertical dynamics of other important quantities such as nutrients, Chl *a*, and productivity for later investigations of the roles of phytoplankton diversity in biogeochemical cycles in different oceanic regions (using 3D regional/global simulations). Therefore, these two contrasting stations were used to provide a single set of parameters values by fitting the model to observations before the obtained model was validated against data from another independent station (ALOHA). Hence, **CITRATE** 1.0 consists of the following key features:

1) It models the mean and variance of a continuous phytoplankton size (i.e. log cell volume (μm^3)) distribution and incorporates "trait-diffusion" to sustain size diversity (Merico et al., 2014).
2) It contains an iron cycle in addition to the nitrogen cycle because in the subarctic and equatorial Pacific iron instead of nitrogen should be the main limiting nutrient for phytoplankton growth (Behrenfeld et al., 2006; Fujiki et al., 2014).
3) The phytoplankton cells have variable chlorophyll-to-carbon (θ) and nitrogen-to-carbon (Q_N) ratios that respond to light and nutrient conditions in a realistic fashion.
4) A single set of model parameters are optimized against field observational data at two time-series stations in the Northwest Pacific.

2.1 Description of the ecosystem model

CITRATE 1.0 contains 9 tracers in total: dissolved inorganic nitrogen (DIN, abbreviated as ***N*** in all the equations; unit: μmol N L^{-1}), phytoplankton biomass (***P***; μmol N L^{-1}), microzooplankton biomass (***MIC***; μmol N L^{-1}), mesozooplankton biomass (***MES***; μmol N L^{-1}), detritus in terms of nitrogen (***D***; μmol N L^{-1}) and iron (***D$_{Fe}$***; nmol Fe L^{-1}), dissolved iron (***fer***; nmol Fe L^{-1}), the products of

删除的内容: overall…aim of CITRATE 1.01.11.0 …

删除的内容: the…“adaptive dynamics”…ontinuous trait-base …

带格式的: 字体:非 粗体

带格式的: 字体:粗体

删除的内容: for modeling phytoplankton size diversity under realistic environmental conditions at the two representative stations in the North Pacific. …heAnd…our …

带格式的: 字体:斜体

删除的内容: ed

删除的内容: results

带格式的: 正文

删除的内容: in

带格式的: 字体:粗体

删除的内容: ,

删除的内容: is not only to model phytoplankton size structure, but also to faithfully simulate the seasonal and vertical dynamics of other important quantities such as nutrients, Chl *a*, and productivity for later investigations of the roles of phytoplankton diversity in biogeochemical cycles. The constructed model structure and optimized model parameters are to be used for later application of the “adaptive dynamics” approach in three-dimensional ocean general circulation models (GCMs). Hence, **CITRATE 1.01.11.0** consists of the following key features:

带格式的: 字体:斜体

带格式的 …

带格式的: 列出段落, 已编号 + 级别: 1 + 编号样式: 1, 2, 3, … + 起始于: 1 + 对齐方式: 左 + 对齐位置: 0 cm +

带格式的: 字体:粗体, 英语(美国)

删除的内容: For simplicity, we assume that phytoplankton size is the master trait that determines all physiological functions (Litchman et al., 2007; Finkel et al., 2010; Edwards et al., 2011, 2012, 2015). In addition to phytoplankton total biomass (***P***), we also include phytoplankton mean log size (

带格式的: 左对齐

删除的内容: , ln μm^3) and log size variance (***v***, (ln μm^3)^2) as independent tracers in the model. We use the product of

…

删除的内容: slightly improved the model fitting. Because in certain parts of the North Pacific iron instead of nitrogen is the main limiting nutrient for phytoplankton growth (Fujiki et al., 2014), we also include dissolved iron (***fer***) as another independent tracer. Hence the model includes 7 tracers in total (Fig. 1).

删除的内容: **General d…escription of the 1D** …

带格式的: 字体:粗体

带格式的: 缩进: 首行缩进: 2.13 字符

删除的内容: **1.0**

删除的内容: **1.1**

带格式的 …

$P\bar{l}$ and $P(v+\bar{l}^2)$ where $\bar{l}$ (ln μm^3) is the phytoplankton mean log cell volume and v ((ln μm^3)^2) is the log volume variance (Fig. 1).

We assume that phytoplankton size is the master trait that determines all physiological functions (Litchman et al., 2007; Finkel et al., 2010; Edwards et al., 2011, 2012, 2015; Marañón, 2015). We also assume that phytoplankton size follows a lognormal distribution, which is supported by some observational data (Finkel, 2007; Quintana et al., 2008, 2016). Since $\bar{l}$ and v are not real standing stocks that can be directly transported in hydrodynamic models but are emergent properties of phytoplankton size structure, we follow Bruggeman (2009) to use the raw moments of biomass probability (i.e. $P\bar{l}$ and $P(v+\bar{l}^2)$ for mean and variance) as independent tracers involved in transport. All the assumptions made here will be discussed later in **Sect.** 4.

Below we will describe the equations for each tracer. For simplicity, phytoplankton cells are assumed not to excrete inorganic nitrogen or to have any natural mortality to be converted into detritus. Phytoplankton are eaten by both micro- and mesozooplankton:

$$\frac{dP}{dt} = P\mu_{com} \text{-} e^{\frac{E_Z}{k}\left(\frac{1}{T_0}-\frac{1}{T}\right)}\left[MIC g_{max,1}\frac{{P_{T,1}}^2}{{P_{T,1}}^2+K_{P,1}^2} + MES g_{max,2}\frac{(P_{T,2}+MIC)P}{(P_{T,2}+MIC)^2+K_{P,2}^2}\right] + \frac{d}{dz}\left(K_v\frac{dP}{dz}\right) \qquad (1)$$

where μ_{com} is the phytoplankton specific growth rate (d^{-1}) of the whole community (i.e. integrated over the whole size spectra). The equation of μ_{com}, along with those of $\bar{l}$ and v, will be described later in Sect. 2.2. E_z is the activation energy (in electron volts [eV], 1 eV = 96.49 kJ mol^{-1}) for heterotrophic processes. $g_{max,i}$ (i = 1 for microzooplankton and 2 for mesozooplankton) is zooplankton maximal grazing rate (d^{-1}). $K_{P,i}$ is the grazing half-saturation constant of zooplankton. Here we have assumed that zooplankton grazing follows a Holling Type III functional response. $P_{T,i}$ is total palatable prey concentration for zooplankton (μmol N L^{-1}), the details of which will be given later in Sect. 2.3. If

带格式的： 字体：非 粗体

删除的内容: size (i.e.

删除的内容:)

删除的内容: ((ln μm^3)^2)

带格式的： 字体：粗体，英语(英国)

删除的内容: For simplicity, w

删除的内容: the

删除的内容: In addition to phytoplankton total biomass (***P***), we also include phytoplankton mean log size (

删除的内容: , ln μm^3) and log size variance (***v***, (ln μm^3)^2) as independent tracers in the model.

删除的内容: W

删除的内容:

删除的内容: the product of

删除的内容: and

删除的内容: , respectively,

删除的内容: for

删除的内容: the

删除的内容: of mean and variance

删除的内容: diffusion

删除的内容: .

删除的内容: Note that we prefer

删除的内容: over

删除的内容: because we found that the use of

删除的内容: slightly improved the model fitting.

删除的内容: Because in certain parts of the North Pacific iron instead of nitrogen is the main limiting nutrient for phytoplankton growth (Fujiki et al., 2014), we also include dissolved iron (***fer***) as another independent tracer. Hence the model includes 7 tracers in total (Fig. 1).

删除的内容: The 1D model focuses on the upper 1500 meters of the ocean. The vertical grid, a total of 30 layers, follows a stretched vertical coordinate with increasing resolution towards the sea surface (surface stretching parameter = 2.0), similar to that used in the Regional Ocean Modelling System (ROMS) (Shchepetkin and McWilliams, 2005). For computational efficiency, the 1D model contains only biological tracers. The physics variables are imported as external data (*see* Sect. 2.3 for details).

带格式的： 正文，右对齐，缩进：首行缩进： 0 字符，行距：

删除的内容:

带格式的： 字体：粗体

带格式的： 字体：非 粗体

带格式的： 上标

带格式的： 字体：非 粗体

带格式的： 字体：斜体

带格式的： 字体：斜体，下标

zooplankton grazing has no size selectivity on phytoplankton, then $P_T = P$. We assume that microzooplankton preferably feed on small phytoplankton while mesozooplankton prefer large phytoplankton (Table 1). Mesozooplankton also feed on microzooplankton. More descriptions of zooplankton size-dependent grazing will be given later. z is the depth of the model grid (m). K_v is the vertical eddy diffusivity (m^2 s^{-1}).

The total amount of food ingested by zooplankton is divided among three fates: zooplankton net growth, excretion into the inorganic nitrogen pool, and defecation of unassimilated food into the detritus pool (Buitenhuis et al., 2010). Mesozooplankton mortality is set to be proportional to the squares of its biomass and is also converted into detritus pool. As such, the dynamics of micro- and mesozooplankton follow:

$$\frac{dMIC}{dt} = e^{\frac{E_Z}{k}\left(\frac{1}{T_0}-\frac{1}{T}\right)}\left(MICg_{max,1}\frac{P_{T,1}{}^2}{P_{T,1}{}^2+K_{P,1}^2}NGE_1\text{-}MESg_{max,2}\frac{(P_{T,2}+MIC)MIC}{(P_{T,2}+MIC)^2+K_{P,2}^2}\right)+\frac{d}{dz}\left(K_v\frac{dMIC}{dz}\right) \qquad (2a)$$

$$\frac{dMES}{dt} = e^{\frac{E_Z}{k}\left(\frac{1}{T_0}-\frac{1}{T}\right)}\left(MESg_{max,2}\frac{(P_{T,2}+MIC)^2}{(P_{T,2}+MIC)^2+K_{P,2}^2}NGE_2\text{-}m_zMES^2\right)+\frac{d}{dz}\left(K_v\frac{dMES}{dz}\right) \qquad (2b)$$

where NGE_i is the net growth efficiency of zooplankton. m_z is the mesozooplankton mortality coefficient (d^{-1} (μmol N L^{-1})$^{-1}$).

Detritus is converted to DIN at a rate (R_{dn}, d^{-1}) that has the same temperature sensitivity with zooplankton grazing. Detritus is also assumed to have a constant sinking rate (W_d, d^{-1}).

$$\frac{dD}{dt} = e^{\frac{E_Z}{k}\left(\frac{1}{T_0}-\frac{1}{T}\right)}\Big(MICg_{max,1}\frac{P_{T,1}{}^2}{P_{T,1}{}^2+K_{P,1}^2}unass_1+MESg_{max,2}\frac{(P_{T,2}+MIC)^2}{(P_{T,2}+MIC)^2+K_{P,2}^2}unass_2+$$
$$m_zMES^2\text{-}R_{dn}D\Big)\text{-}W_d\frac{dD}{dz}+\frac{d}{dz}\left(K_v\frac{dD}{dz}\right) \qquad (3)$$

where $unass_i$ represents the fraction of unassimilated food by zooplankton.

带格式的: 字体:斜体

带格式的: 字体:粗体, 英语(美国)

删除的内容: phytoplankton

带格式的: 缩进: 首行缩进: 0 字符

带格式的: 缩进: 首行缩进: 0 字符

带格式的: 下标

带格式的: 上标

带格式的: 上标

带格式的: 字体:粗体, 英语(美国)

带格式的: 上标

带格式的: 缩进: 首行缩进: 0 字符

带格式的: 字体:斜体

带格式的: 字体:斜体, 下标

DIN is taken up by phytoplankton and is replenished by zooplankton excretion, detritus regeneration and diffusion from the depth:

$$\frac{dN}{dt} = -P\mu_{com} + e^{\frac{E_Z}{k}\left(\frac{1}{T_0}-\frac{1}{T}\right)}\left(MICg_{max,1}\frac{{P_{T,1}}^2}{{P_{T,1}}^2 + K_{P,1}^2}(1 - NGE_1\text{-}unass_1)\right.$$

$$\left.+MESg_{max,2}\frac{\left(P_{T,2}+MIC\right)^2}{\left(P_{T,2}+MIC\right)^2+K_{P,2}^2}(1 - NGE_2\text{-}unass_2) + DR_{dn}\right) + \frac{d}{dz}\left(K_v\frac{dN}{dz}\right) \qquad (4)$$

The sources and sinks of *fer* largely follow DIN with an additional source (atmospheric deposition; Fe$_{depo}$) and sink (scavenging; *fer*$_{scav}$) (Aumont et al., 2003; Buitenhuis et al., 2010; Nikelsen et al., 2015):

$$\frac{dfer}{dt} = \begin{bmatrix} -P\mu_{com} + e^{\frac{E_Z}{k}\left(\frac{1}{T_0}-\frac{1}{T}\right)}\left(MICg_{max,1}\dfrac{{P_{T,1}}^2}{{P_{T,1}}^2 + K_{P,1}^2}(1 - NGE_1\text{-}unass_1)\right. \\ \left.+MESg_{max,2}\dfrac{\left(P_{T,2}+MIC\right)^2}{\left(P_{T,2}+MIC\right)^2+K_{P,2}^2}(1 - NGE_2\text{-}unass_2) + DR_{dn}\right) \end{bmatrix} R_{fer_N}$$

$$+Fe_{depo}\text{-}fer_{scav} + \frac{d}{dz}\left(K_v\frac{dfer}{dz}\right) \qquad (5a)$$

To translate between nitrogen and iron in phytoplankton and zooplankton, a constant *fer*:*N* ratio (R_{fer_N}) of 0.0265 is assumed. The data of monthly atmospheric deposition of total soluble iron are extracted from the Scenario III in Luo et al. (2008). Following Nikelsen et al. (2015), iron scavenging rate (*fer*$_{scav}$) is composed of both linear scavenging rate (k_{scm}) and particle absorption rate (k_{sc}):

$$fer_{scav} = \left(k_{scm} + k_{sc}De^{\frac{E_Z}{k}\left(\frac{1}{T_0}-\frac{1}{T}\right)}\right)Fe_{prime} \qquad (5b)$$

in which Fe_{prime} is the concentration of free iron:

$$Fe_{prime} = \frac{\left(-A+\sqrt{4ferk_{eq}+A^2}\right)}{2k_{eq}} \qquad (5c)$$

$$A = 1 + \left(l_{fe}\text{-}fer\right)k_{eq} \qquad (5d)$$

where k_{eq} is the equilibrium constant between free iron and ligands and is assumed to depend only on temperature:

带格式的: 字体:Times New Roman, 非 斜体

带格式的: 居中

带格式的: 字体:斜体

带格式的: 字体:斜体, 下标

带格式的: 字体:非 粗体

带格式的: 字体:斜体

带格式的: 字体:斜体, 下标

带格式的: 字体:(默认) Times New Roman, 非 斜体

带格式的: 缩进: 首行缩进: 0 字符

带格式的: 缩进: 首行缩进: 0 字符

$$k_{eq} = 10^{\left(17.27-\frac{1565.7}{T}\right)} \qquad (5e)$$

Note that *T* is in absolute temperature (K). l_{fe} is the total iron ligand concentration that is assumed constant (0.6 nM).

The equation for $\boldsymbol{D_{Fe}}$ is:

$$\frac{dD_{Fe}}{dt} = e^{\frac{E_Z}{k}\left(\frac{1}{T_0}-\frac{1}{T}\right)}\left(MICg_{max,1}\frac{{P_{T,1}}^2}{{P_{T,1}}^2+K_{P,1}^2}unass_1 + MESg_{max,2}\frac{\left(P_{T,2}+MIC\right)^2}{\left(P_{T,2}+MIC\right)^2+K_{P,2}^2}unass_2 + m_zMES^2 - R_{dn}D\right)R_{fe_N} - W_d\frac{dD_{Fe}}{dz} + fer_{scav} + \frac{d}{dz}\left(K_v\frac{dD_{Fe}}{dz}\right) \qquad (6)$$

2.2 Continuous trait-based phytoplankton model

Following the moment closure techniques in Merico et al. (2009) and the introduction of "trait diffusion" (Merico et al., 2014), the equations for μ_{com}, *l*, and *v* can be written as:

$$\mu_{com} \approx \left(\mu(l) + \frac{v}{2}\left(\frac{d^2\mu(l)}{dl^2} + u\frac{d^4\mu(l)}{dl^4}\right) - 3u\frac{d^3\mu(l)}{dl^3}\right)\Bigg|_{l=\bar{l}} \qquad (7a)$$

$$\frac{d\bar{l}}{dt} \approx \left[v\left(\frac{d\mu(l)}{dl} - \sum_{i=1}^{2}\frac{dg_i(l)}{dl} + u\frac{d^3\mu(l)}{dl^3}\right) - 3u\frac{d\mu(l)}{dl}\right]\Bigg|_{l=\bar{l}} \qquad (7b)$$

$$\frac{dv}{dt} \approx \left\{v\left[v\left(\frac{d^2\mu(l)}{dl^2} - \sum_{i=1}^{2}\frac{d^2g_i(l)}{dl^2} + u\frac{d^4\mu(l)}{dl^4}\right) - 5u\frac{d^2\mu(l)}{dl^2}\right] + 2u\mu(l)\right\}\Bigg|_{l=\bar{l}} \qquad (7c)$$

where $\mu(\boldsymbol{l})$ is the phytoplankton growth rate (d^{-1}) at mean size $\boldsymbol{l}$, *u* is the trait diffusion parameter, which describes the probability of the parental size *l*(*i*) changing to adjacent size values *l*(*i*–1) or *l*(*i*+1) in offspring cells (Merico et al., 2014). Eqs. (7a-c) are approximations because the higher-order moments such as the skewness and kurtosis have been ignored and a Gaussian distribution needs to be assumed for $\boldsymbol{l}$. $\frac{dg_i(l)}{dl}$ and $\frac{d^2g_i(l)}{dl^2}$ are the first and second derivatives of zooplankton clearance rate (d^{-1}) against phytoplankton size and will be described in detail in Sect. 2.3.

The equations of $P\bar{l}$ and $P(v+\bar{l}^2)$ follow:

带格式的: 字体:粗体，斜体

带格式的: 字体:粗体，斜体，下标

带格式的: 字体:非 粗体

带格式的: 正文，右对齐，缩进：首行缩进： 0 字符，行距：单线

删除的内容: ,

删除的内容:) and log size variance (*v*) wereare set to be 1. Initial dissolved iron concentration wais set to the vertical profile of iron in January from a 3D global biogeochemical model output (Aumont et al., 2003). The time step of the model wasis 30 minutes. All the fixed model parameters are shown in Table 1 and the model parameters that are optimized to match observational data are shown in Tal

带格式的: 字体:粗体，斜体

带格式的: 字体:粗体

删除的内容: 1

带格式的: 两端对齐，缩进：首行缩进： 2.13 字符

删除的内容: ,

删除的内容: differential

带格式的: 字体:斜体，下标

删除的内容: *P*

删除的内容: ,

删除的内容: (1a)

删除的内容:

删除的内容: 1

删除的内容: b

删除的内容:

删除的内容: 1c

删除的内容: ,

带格式的: 字体:斜体

带格式的: 字体:斜体

带格式的: 字体:非 斜体

删除的内容: , K_v is the vertical eddy diffusivity ($m^2\ s^{-1}$)

删除的内容: 1

带格式的: 上标

带格式的: 缩进：首行缩进： 2.36 字符

删除的内容: differential

$$\frac{d(P\bar{l})}{dt} = P\frac{d\bar{l}}{dt} + \bar{l}\frac{dP}{dt} + \frac{d}{dz}\left(K_v\frac{d(P\bar{l})}{dz}\right) \qquad (7d)$$

$$\frac{d(P(v+\bar{l}^2))}{dt} = P\left(\frac{dv}{dt} + 2\bar{l}\frac{d\bar{l}}{dt}\right) + (v+\bar{l}^2)\frac{dP}{dt} + \frac{d}{dz}\left(K_v\frac{d(P(v+\bar{l}^2))}{dz}\right) \qquad (7e)$$

Following previous studies (Flynn, 2003; Geider et al., 1997; Follows et al., 2007; Chen and Laws, 2017), phytoplankton growth rate (μ) depends on temperature (T, K), light (I, W m^{-2}), DIN and ***fer***:

$$\mu = \mu_m \min\left(\frac{N}{N+K_N}, \frac{fer}{fer+K_{fer}}\right)\left(1 - e^{-\frac{\alpha_C I}{\mu'_{0,m} e^{\frac{Ep}{k}\left(\frac{1}{T_0}-\frac{1}{T}\right)}}}\right) \qquad (8)$$

in which μ_m is a function of T:

$$\mu_m = \mu'_m e^{\frac{Ep}{k}\left(\frac{1}{T_0}-\frac{1}{T}\right)} \qquad (9)$$

The trait parameters μ'_m, K_N, K_{fer}, and α_c are all dependent on cell size ***l***:

$$\mu'_m = \mu'_{0,m} e^{\alpha_\mu l + \beta_\mu l^2} \qquad (10a)$$

$$K_N = K_{0,N} e^{\alpha_K l} \qquad (10b)$$

$$K_{fer} = K_{0,fer} e^{\alpha_{fer} l} \qquad (10c)$$

$$\alpha_c = \alpha_{0,c} e^{\alpha_I l} \qquad (10d)$$

删除的内容:

删除的内容: 1

删除的内容:

删除的内容: 1

删除的内容: P

带格式的: 字体:斜体

删除的内容: dissolved inorganic nitrogen (N, μmol L^{-1})

删除的内容: ***iron concentrations (fer, nmol L^{-1})***

带格式的: 字体:粗体，斜体

带格式的: 英语(美国)

删除的内容:

删除的内容: 2

删除的内容: 3

删除的内容: μ'_m

带格式的: 英语(美国)

带格式的: 字体:粗体，斜体

删除的内容: 4

删除的内容: 4

删除的内容: 4

删除的内容: 4

Eq. (10a) follows that maximal phytoplankton growth rate is a unimodal function of phytoplankton size (Chen et al., 2010, 2011; Marañón et al., 2013). It is worth noting that the light term of phytoplankton growth (the right side of Eq. 8) is usually modelled as $\mathbf{1\text{-}e^{-\frac{\alpha_c I}{\mu_m}}}$ (Flynn, 2003), in which both α_c and μ_m are dependent on size. We use α_I to represent the net effect of size on $\frac{\alpha_c}{\mu_m}$ for mathematical convenience, which leads to Eq. 8.

Following Flynn (2003), we have derived equations to directly calculate phytoplankton chlorophyll-to-carbon (θ, g Chl (mol C)$^{-1}$) and nitrogen-to-carbon (Q_N, mol N (mol C)$^{-1}$) ratios from ambient light and nutrient levels:

$$\theta = \theta_{min} + \frac{\mu}{I\alpha_C}(\theta_{max}\text{-}\theta_{min}) \tag{11a}$$

$$Q_N = \frac{Q_{min}}{1-\left(1-\frac{Q_{min}}{Q_{max}}\right)\frac{N}{N+K_N}} \tag{11b}$$

where θ_{min} and θ_{max} are minimal and maximal Chl:C ratios, respectively. Q_{min} and Q_{max} are minimal and maximal N:C ratios, respectively. The total Chl *a* concentrations (*Chl*, μg L^{-1}) and net primary production (*NPP*, μgC L^{-1} d^{-1}) integrated over the whole size spectra can be calculated as:

$$Chl = P\left(\frac{\theta}{Q_N} + \frac{v}{2}\frac{d^2\left(\frac{\theta}{Q_N}\right)}{dl^2}\right)\Bigg|_{l=\bar{l}} \tag{11c}$$

$$NPP = P\left(\frac{\mu}{Q_N} + \frac{v}{2}\frac{d^2\left(\frac{\mu}{Q_N}\right)}{dl^2}\right)\Bigg|_{l=\bar{l}} \tag{11d}$$

To calculate the fractions of Chl within a size range (i.e. <1 μm, 1–3 μm, 3–10 μm and > 10 μm), we had to discretize the size spectra into 60 even size classes between $\bar{l}\text{-}6\sqrt{v}$ and $\bar{l} + 6\sqrt{v}$ and calculated the μ, α_c, K_N, Q_N, θ, and eventually Chl of each size class following Eq. (11a-c). This is

删除的内容: 5
带格式的: 英语(美国)
带格式的: 字体:非 粗体
带格式的: 字体:非 粗体, 斜体
带格式的: 字体:非 粗体, 斜体, 下标
删除的内容: light-dependent growth
带格式的: 英语(美国)
删除的内容: are also able
删除的内容:
删除的内容: estimate
带格式的: 英语(美国)
带格式的: 英语(美国), 上标
带格式的: 英语(美国)
删除的内容: directly
删除的内容: 5
带格式的: 英语(英国)
删除的内容: 5
删除的内容: 5
删除的内容: 5
带格式的: 字体:斜体
带格式的: 字体:斜体
带格式的: 字体:斜体
带格式的: 字体:斜体
带格式的: 字体:斜体
带格式的: 字体:斜体
带格式的: 字体:斜体, 下标
带格式的: 字体:斜体
带格式的: 字体:斜体, 下标
带格式的: 字体:斜体
带格式的: 字体:斜体, 下标
带格式的: 字体:斜体

because the distributions of Chl do not follow the lognormal distribution of cell volume and an analytic solution is not yet available for calculating only a fraction of Chl. Fortunately, this approach only adds a minor computational cost because we only need to calculate the size-fractionated Chl once per day when saving model outputs.

2.3 Zooplankton size-dependent grazing

Following Smith et al. (2016), the ingestion rate of zooplankton on size class l can be formulated as:

$$G(l) = g_{max} Z \frac{\rho(l)P(l)}{P_T+\varepsilon} \frac{(P_T+\varepsilon)^2}{(P_T+\varepsilon)^2+K_P^2} = g_{max} Z \rho(l) P(l) \frac{P_T+\varepsilon}{(P_T+\varepsilon)^2+K_P^2} \quad (12a)$$

where $G(l)$ is the zooplankton ingestion rate (μmol N L^{-1} d^{-1}) on the size class l. $\rho(l)$ is the relative grazing preference on size class l. Z is the biomass of either micro- or mesozooplankton. ε is the food other than phytoplankton (ε = 0 for microzooplankton and MIC for mesozooplankton). P_T (total palatable phytoplankton food) is formulated as:

$$P_T = \int_{-\infty}^{\infty} \rho(l) P(l) dl \quad (12b)$$

with $P(l)$ is the phytoplankton concentration at size l:

删除的内容: data
带格式的: 英语(美国)
删除的内容: Light levels (I_z) at depth z were calculated base
删除的内容: (12)
带格式的: 英语(美国)
删除的内容: **2.2 General description of the 1D model (nut**
删除的内容: (6)
删除的内容: (7a)
删除的内容: (7b)
删除的内容: (7c)
删除的内容: (7d)
删除的内容: (8a)
删除的内容:
删除的内容:
删除的内容:) and log size variance (v) are set to be 1. Initial
带格式的: 正文
带格式的: 字体:粗体, 斜体
带格式的: 正文, 右对齐
删除的内容: 3
带格式的: 正文
带格式的: 字体:斜体
带格式的: 字体:斜体
带格式的: 字体:斜体
带格式的: 上标
带格式的: 上标
带格式的: 字体:粗体, 斜体
带格式的: 字体:斜体
带格式的: 字体:斜体
带格式的: 字体:斜体
带格式的: 英语(美国)
带格式的: 字体:斜体
带格式的: 英语(美国)
带格式的: 字体:非 斜体, 英语(美国)
带格式的: 字体:斜体
带格式的: 字体:斜体, 英语(美国)
带格式的: 字体:斜体, 英语(美国), 下标
带格式的: 英语(美国)
带格式的: 正文, 右对齐
删除的内容: 3
带格式的: 正文
带格式的: 字体:斜体
带格式的: 字体:斜体
带格式的: 字体:粗体, 斜体

$$P(l) = \frac{P}{\sqrt{2\pi v}} e^{-\frac{1}{2}\frac{(l-\bar{l})^2}{v}} \qquad (12c)$$

Zooplankton clearance rate (g, d^{-1}) on size class l can be formulated as:

$$g(l) = g_{max} Z \frac{P_T+\varepsilon}{(P_T+\varepsilon)^2+K_P^2} \rho(l) \qquad (12d)$$

For mathematic convenience, we parameterize $\rho(l) = e^{bl+c}$, where b and c are constants. P_T can be approximated as:

$$P_T \approx P\rho(l)\left(1+\frac{v}{2}b^2\right)$$

And:

$$\frac{dP_T}{dl} = bP_T$$

$$\frac{d^2P_T}{dl^2} = b^2P_T$$

Thus, the first derivative of $g(l)$ can then be derived as:

$$\frac{dg(l)}{dl} = bg(l)\left\{\frac{[K_P^2-(P_T+\varepsilon)^2]P_T}{[(P_T+\varepsilon)^2+K_P^2](P_T+\varepsilon)}+1\right\} \qquad (12e)$$

And:

$$\frac{d^2g(l)}{dl^2} = bg(l)\left\{\left\{\frac{[K_P^2-(P_T+\varepsilon)^2]P_T}{[(P_T+\varepsilon)^2+K_P^2](P_T+\varepsilon)}+1\right\}^2 + bP_T\left\{-\frac{4K_P^2P_T}{[(P_T+\varepsilon)^2+K_P^2]^2}+\frac{[K_P^2-(P_T+\varepsilon)^2]}{[(P_T+\varepsilon)^2+K_P^2]}\frac{\varepsilon}{(P_T+\varepsilon)^2}\right\}\right\} \qquad (12f)$$

Note that we do not optimize the parameters of b and c because the zooplankton data are insufficient to constrain the parameters (Table 1, 2).

2.4 One-dimensional (1D) model

The 1D model focuses on the upper 150 meters of the ocean. The vertical grid, a total of 30 layers, follows a stretched vertical coordinate with increasing resolution towards the sea surface (surface stretching parameter = 2.0), similar to that used in the Regional Ocean Modelling System (ROMS) (Shchepetkin and McWilliams, 2005). For computational efficiency, instead of explicitly solving the

删除的内容: 3
带格式的: 正文，右对齐
带格式的: 字体:斜体
带格式的: 上标
带格式的: 字体:斜体
带格式的: 正文
删除的内容: 3
带格式的: 正文，右对齐
带格式的: 正文
带格式的: 英语(美国)
带格式的: 正文，居中
带格式的: 正文
带格式的: 正文，居中
带格式的: 正文
删除的内容: T
带格式的: 字体:斜体
带格式的: 字体:斜体
带格式的: 正文，右对齐
删除的内容: 3
带格式的: 字体:粗体
带格式的: 正文
带格式的: 正文，右对齐
删除的内容: 3
带格式的: 正文
带格式的: 字体:斜体
带格式的: 英语(美国)
带格式的: 英语(美国)
删除的内容: **External physics data for o**
带格式的: 缩进：首行缩进： 0 字符

complete moment, temperature, and salinity equations, we imported the physics variables that are directly relevant to the ecological processes from external data products.

Four types of external physics forcing data were imported into the 1D model: vertical eddy diffusivity (K_v), surface photosynthetic available radiation (PAR_0), atmospheric dust deposition, and vertical temperature profiles. Vertical advection of water was neglected, which had been shown relatively unimportant (Fernández-Castro et al., 2016). The most important physics forcing data, K_v, determined the upward nutrient flux to the upper euphotic zone and were imported from the output of a three dimensional (3D) eddy-permitting model targeted for North Pacific (Hashioka et al., 2009). This 3D model was able to faithfully simulate the Kuroshio Current and the spatial distributions of the Chl *a* fields. The extracted vertical profiles of K_v were also consistent with the *in situ* estimated mixed layer depths (MLD) at the three stations (Fig. 2). PAR_0 were imported from SeaWIFS satellite monthly climatology products. Seasonal temperature vertical profiles were imported from WOA2013 monthly climatology.

带格式的: 正文, 缩进: 首行缩进: 2.36 字符, 行距: 单线

Light levels (I_z) at depth z were calculated based on PAR_0 and Chl *a* concentrations following the Beer-Lambert law:

$$I_z = PAR_0 e^{-z\left(K_w + K_{chl}\int_z^0 Chl(x)dx\right)} \tag{13}$$

in which K_w and K_{chl} are the attenuation coefficients for seawater and Chl *a*, respectively. To realistically estimate the average light field that a phytoplankton cell should experience in a mixing water column (Franks, 2015), the ambient light level for phytoplankton within the surface mixed layer is calculated as the average light throughout the surface mixed layer, which is defined as the deepest depth with $K_v > 10^{-3}$ m^2 s^{-1}. This calculation is based on eq. (1) in Franks (2015), which gives that the average time for a phytoplankton cell to move 100 m (an approximate estimate of MLD) at the local diffusivity of 10^{-3} m^2 s^{-1} is roughly half a day. However, to compare with *in situ NPP* estimates that were calculated from incubation bottles without continuous mixing, phytoplankton μ, θ, and Q_N are recalculated from I_z based on the Beer-Lambert law (Eq. 13).

带格式的: 正文, 缩进: 首行缩进: 0 字符, 行距: 单线

带格式的: 英语(美国)

The initial condition of inorganic nitrogen was set to the vertical profile of nitrate in January of the World Ocean Atlas (WOA) 2013 monthly climatology. Initial phytoplankton, microzooplankton, and detritus biomass were all set to 0.1 μmol N L^{-1} in each grid. Mesozooplankton biomass was initialized as 0.05 μmol N L^{-1}. Initial D_{Fe} concentrations were set as detritus times R_{fer_N}. Initial phytoplankton mean log size ($\bar{l}$) and log size variance (v) were set as –2.2 log μm^3 and 0.09 (log μm^3)^2, respectively. Initial dissolved iron concentration was set to the vertical profile of iron in January from a 3D global biogeochemical model output (Aumont et al., 2003). The time step of the model was 5 minutes. All the fixed model parameters are shown in Table 1 and the model parameters that are optimized to match observational data are shown in Table 2.

We employed a Dirichlet boundary condition at the bottom for DIN and ***fer*** with the values predefined by the WOA2013 climatology and the model output from Aumont et al. (2003), respectively. For other tracers, we assumed no diffusive flux at the bottom. Detritus was allowed to sink out of the system with the loss of nitrogen and iron replenished by diffusion.

2.5 Delayed Rejection Adaptive Metropolis-Hasting Monte Carlo (DRAM) algorithm

The Metropolis-Hasting Monte Carlo (MHMC) algorithm aims to find the posterior distribution (including mean and covariance matrix) of the parameter vectors, given the data provided. The key here is to develop an appropriate proposal covariance matrix (P_{cvm}), which determines the magnitude and direction of the proposed perturbations to the parameter values, as the algorithm explores the parameter space. At each iteration of the algorithm, the newly proposed parameter set is either accepted or rejected based on the model-data mismatch, as explained below. In the classical random walk MHMC algorithm, the P_{cvm} must be specified by the user to achieve sufficient acceptance rates for the proposed parameters, which typically requires a great deal of effort and many trials.

The adaptive MHMC (Haario et al., 2001), uses the already accepted parameters to approximate P_{cvm}, which is periodically updated as more simulations are conducted. Specifically, the P_{cvm} is tuned based on the covariance matrix (C_{vm}) of the already accepted parameter sets after a fixed number of iterations following Gelman et al. (2014) (i.e. $P_{cvm} = C_{vm} \bullet 2.4^2/d$, where d is the length of the target

带格式的: 字体:斜体

带格式的: 字体:斜体, 下标

删除的内容: to be

带格式的: 字体:斜体

带格式的: 上标

带格式的: 上标

删除的内容: 1

删除的内容: 30

带格式的: 缩进: 首行缩进: 2.36 字符

删除的内容: Four types of external physics forcing data were imported into the 1D model: vertical eddy diffusivity (K_v), surface photosynthetic available radiation (PAR_0), atmospheric dust deposition, and vertical temperature profiles. Vertical advection of water was neglected, which had been shown relatively unimportant (Fernández-Castro et al., 2016). The most important physics forcing data, K_v, determined the upward nutrient flux to the upper euphotic zone and were imported from the output of a three dimensional (3D) eddy-permitting model targeted for North Pacific (Hashioka et al., 2009). This 3D model was able to faithfully simulate the Kuroshio Current and the spatial distributions of the Chl *a* fields. The extracted vertical profiles of K_v were also consistent with the *in situ* estimated mixed layer depths (MLD) at the threewo stations (Fig. 2). Practically, any reasonable outputs of seasonal K_v profiles can be used. PAR_0 were imported from SeaWIFS satellite monthly climatology products. Seasonal temperature vertical profiles were imported from WOA2013 monthly climatology.

删除的内容: 4

删除的内容: with reasonable search efforts

删除的内容: is used to generate a new set of parameters based on current position of the parameters.

删除的内容: should

删除的内容: msut

删除的内容: designed

删除的内容: which

删除的内容: and this

删除的内容: however is not

删除的内容:

删除的内容: always an easy task and may

删除的内容: need

删除的内容: substantial

删除的内容: s for

带格式的: 缩进: 首行缩进: 2.36 字符

删除的内容: , developed by

删除的内容: (

删除的内容: t

删除的内容: s

parameter vector). Thus, the algorithm alters the magnitude and direction of proposed 'jumps' in order to efficiently explore the parameter space.

With the delayed rejection MCMC (Mira, 2001), when a newly proposed set of parameters is rejected, P_{cvm} is temporarily downscaled (to 1% of the original P_{cvm} in our case) and a second set of parameters is proposed based on the rejected parameters and the downscaled P_{cvm}. This approach is particularly efficient because low acceptance rates typically result when the P_{cvm} is too large (the parameter jumps are too wide) to find the target distribution of the parameters. Temporarily reducing P_{cvm} can substantially increase the acceptance rate. By using multiple stages of P_{cvm}, the algorithm can also effectively deal with the problem of non-Gaussian posteriors, which can reduce the efficiency of the adaptive MHMC (Haario et al., 2006).

The DRAM algorithm, built upon the classic Metropolis-Hasting Monte Carlo (MHMC) algorithm, incorporates the merits of both adaptive and delayed-rejection MHMC algorithm to increase the acceptance rate and thus more efficiently find the target distribution of parameter values (Haario et al., 2006; Laine, 2008). It has been shown to better explore the parameter space compared to other algorithms such as the families of Simulated Annealing, possibly because of its two-stage proposal covariance matrices (Villagran et al., 2008). Compared with the widely used ensemble Kalman filter, DRAM is more suitable for the nonlinear response typically of ecosystems (Annan and Hargreaves, 2007).

Here we briefly outline the DRAM algorithm. For further details and proofs see Haario et al. (2006) and Laine (2008).

1) Initialize the parameter values and P_{cvm}, assuming no correlation among parameters, and a standard deviation equaling to one sixth the difference between the maximal and minimal value for each parameter, respectively (Table 1).
2) Run the model with the current parameter values (θ_{curr}) and calculate the likelihood (L). Note that all the parameter values must be within the boundaries shown in Table 2.
3) Propose a new set of parameters (θ_{pro}) based on θ_{curr} and P_{cvm}, rerun the model, and obtain a new likelihood (L_l).

删除的内容: Based on this
删除的内容: directed by P_{cvm}
删除的内容: more
删除的内容: usually the main cause for the
删除的内容: of the newly proposed parameters is that the
删除的内容: i.e.,
删除的内容: By t
删除的内容: ,
删除的内容: the acceptance rate
删除的内容: be
删除的内容: d
删除的内容: lead to the low
删除的内容: DRAM
删除的内容: than some
删除的内容: possibly due to the use of
删除的内容: perhaps more
带格式的: 缩进: 首行缩进: 1.77 字符
删除的内容: workflow of the
删除的内容: The
删除的内容: have been given in
带格式的: 列出段落, 缩进: 左: 0 cm, 悬挂缩进: 4.26 字符, 已编号 + 级别: 1 + 编号样式: 1, 2, 3, … + 起始于: 1 + 对齐方式: 左 + 对齐位置: 0.75 cm + 缩进位置: 1.98 cm
删除的内容: . The initial P_{cvm} is constructed to have
删除的内容: and parameter
删除的内容: a
删除的内容: ing
删除的内容: of
删除的内容: s
删除的内容:
删除的内容: based on
带格式的: 字体:斜体
带格式的: 字体:斜体, 下标
带格式的: 字体:斜体
带格式的: 字体:(中文) Times New Roman, 英语(美国)
带格式的: 下标
带格式的: 字体:(中文) Times New Roman, 英语(美国)

4) If the ratio of L_1/L is larger than a random number between 0 and 1, then accept θ_{pro} ($\theta_{curr} = \theta_{pro}$) and return to step 2).

5) Otherwise, propose a second set of parameters (θ_{pro2}) based on θ_{pro} and P_{cvm2} (= $0.01P_{cvm}$), rerun the model, and obtain the second likelihood (L_2).

6) If the ratio of $\frac{L_2}{L}\frac{q_1(\theta_{pro2},\theta_{pro1})q_2(\theta_{pro2},\theta_{pro1},\theta_{curr})}{q_1(\theta_{curr},\theta_{pro1})q_2(\theta_{curr},\theta_{pro1},\theta_{pro2})}\frac{1-min\left(1,\frac{L_1}{L_2}\right)}{1-min\left(1,\frac{L_1}{L}\right)}$ is larger than a random number between 0 and 1, then accept θ_{pro2} ($\theta_{curr} = \theta_{pro2}$) and return to step 2). Otherwise retain the current position, θ_{curr}. Here $q_1(y,x)$ is the probability of proposing y given x and $q_2(z,y,x)$ is the probability of proposing z given x and y.

7) After a certain interval, update P_{cvm} based on C_{vm} calculated from the accepted θ.

To increase the computational efficiency and avoid being trapped in local minima due to insufficient chain length, we modified the DRAM algorithm for parallel computing (Calderhead, 2014). That is, we initialize θ and P_{cvm} simultaneously for n processes. Each process runs the above procedure from 1) to 7) except that at 7) all accepted θ are consolidated to update the global estimate of P_{cvm}, which is then distributed to all sub-processes to propose new θ.

Preliminary model runs suggested that from the third year, the model reached a quasi-steady state, exhibiting regular seasonal cycles under the climatological forcing (Fig. 3). As such, we ran the model for four years and the output of the final year was used for validation against observational data. The model outputs were linearly interpolated to the observational depths and time. To allow fair comparisons among different data types and downplay the effects of extreme values, both the model outputs and observational data were transformed to their 1/4 power and normalized between 0 and 1 to achieve a quasi-normal distribution before calculating sum of squared errors ($SSqE$):

$$SSqE_{k,i} = \sum_{j=1}^{n_{k,i}}\left(\frac{m_{k,i,j}^{0.25}-o_{k,i,min}^{0.25}}{o_{k,i,max}^{0.25}-o_{k,i,min}^{0.25}}-\frac{o_{k,i,j}^{0.25}-o_{k,i,min}^{0.25}}{o_{k,i,max}^{0.25}-o_{k,i,min}^{0.25}}\right)^2 \quad (14a)$$

where $SSqE_{k,i}$ is the sum of squared errors of data type i at station k. $n_{k,i}$ is the number of observations for data type i at station k. $o_{k,i,j}$ is the observed jth value for data type i at station k. $o_{k,i,min}$ and $o_{k,i,max}$ are minimal and maximal observed values for data type i at station k, respectively (Note that for all size-fractions of Chl a, we intentionally set $o_{k,i,min} = 0$ and $o_{k,i,max} = 1$ to minimize the effects of the large

带格式的: 字体:斜体

删除的内容: go

带格式的: 字体:非 斜体

带格式的: 字体:(中文) Times New Roman, 英语(美国)

删除的内容: go to

带格式的: 字体:斜体

带格式的: 下标

带格式的: 字体:斜体

带格式的: 字体:斜体

带格式的: 字体:斜体

带格式的: 字体:斜体

带格式的: 字体:斜体

带格式的: 字体:斜体

带格式的: 列出段落, 缩进: 左: 0 cm, 悬挂缩进: 4.26 字符, 已编号 + 级别: 1 + 编号样式: 1, 2, 3, … + 起始于: 1 + 对齐方式: 左 + 对齐位置: 0.75 cm + 缩进位置: 1.98 cm

删除的内容: of

带格式的: 英语(美国)

带格式的: 英语(美国)

带格式的: 缩进: 首行缩进: 1.77 字符

删除的内容: um

删除的内容: due to

删除的内容: because of

带格式的: 英语(美国)

删除的内容: from

带格式的: 字体:斜体

带格式的: 英语(美国)

删除的内容: at sub-processes

删除的内容: transfered

删除的内容: transferred

带格式的: 英语(美国)

删除的内容: to the main process

带格式的: 英语(美国)

带格式的: 英语(美国)

删除的内容: The adaptive component uses information from previous model runs to approximate the distribution of parameter values as a multivariate Gaussian, which it periodically updates as more simulations are conducted. Based on this, the algorithm alters the magnitude and direction of proposed ‘jumps’ in parameter space (i.e., the proposal covariance matrix (P_{cvm})) in order to more efficiently explore the parameter space. Specifically, the P_{cvm} is tuned based on the covariance matrix (C_{vm}) of the already accepted parameter sets after a fixed number of iterations following Ge … ...

删除的内容: both model

删除的内容: 0

measurement variability). $m_{k,i,j}$ is the value linearly interpolated from model outputs to the same depth and date of $o_{k,i,j}$.

Following Laine (2008), the likelihood function was calculated as the product of the exponential of the sum of squared errors, scaled by a measure of the model-data error for each data type, respectively:

$$L=\prod_{k=1}^{2}\left[\prod_{i=1}^{9}(2\pi)^{-\frac{n_{k,i}}{2}}\sigma_{k,i}^{-n_{k,i}}e^{-\frac{SSqE_{k,i}}{2\sigma_{k,i}^{2}}}\right] \quad (14b)$$

in which $\sigma_{k,i}$ is the standard deviation of the Gaussian errors of data type i at station k.

Following Laine (2008), we applied Gibbs sampling, which estimates the distribution of each $\sigma_{k,}$ so as to match the ensemble distribution of model output to that of the data. This entails assuming that the prior of $1/\sigma_{k,i}$ follows a gamma distribution, with the prior mean as S_0^2 and prior accuracy as n_0. At each step the value of $1/\sigma_{k,i}$ was sampled from a conditional gamma distribution $\Gamma\left(\frac{n_0+n_{k,i}}{2},\frac{n_0S_0^2+SSqE_{k,i}}{2}\right)$. The model parameters were assumed to follow multivariate normal distributions. The likelihood function contributed by the priors of the parameters was:

$$L_{pri}=(2\pi)^{-\frac{n_p}{2}}\left(\prod_{i=1}^{n_p}\eta_i^{-1}\right)e^{-\sum_{i=1}^{n_p}\left(\frac{\theta_i-\gamma_i}{\eta_i}\right)^2} \quad (14c)$$

in which n_p is the number of parameters to be estimated, γ_i and η_i are the prior estimates of the i^{th} parameter and its standard deviation, respectively (Table 2). Values of η_i were calculated as one-sixth of the difference between the preset maximal and minimal parameter boundaries. θ_i is the current parameter value. The MCMC chain was run for an ensemble of 10000 simulations with five processes running in parallel (i.e. a total of 50000 parameter sets were obtained). Although the model contains more than 20 parameters, we only selected 9 parameters for optimization, to minimize the possibility of parameter unidentifiability and avoid optimising highly correlated parameters such as g_{max} and K_p simultaneously (Table 2).

2.6 Observational data

For stations K2 and S1, the observations including MLD and nine types of data (DIN, CHL, NPP, PON, Fer, and four size fractions of CHL) were obtained from the K2S1 project (https://ebcrpa.jamstec.go.jp/k2s1/en/index.html; Honda, 2016; Table 3). The observations spanned

删除的内容: for the nineeight types of observational data (total dissolved inorganic nitrogen (TINDIN), total Chl *a* concentration, *NPP*, particulate organic nitrogen (PON), dissolved inorganic iron (*fer*), and the fractions of four size-fractionated (> 10 µm, 3–10 µm, 1–3 µm, <1 µm) Chl *a*; Table 3) at two stations

删除的内容: is

带格式的: 字体:斜体

删除的内容: 1

带格式的: 英语(美国)

删除的内容: y

删除的内容: t

删除的内容: a

删除的内容: e

带格式的: 英语(美国)

带格式的: 英语(美国)

删除的内容: i

删除的内容: are

删除的内容: i

删除的内容: 2

带格式的: 英语(美国)

带格式的: 英语(美国)

带格式的: 英语(美国)

带格式的: 英语(美国)

删除的内容: (e.g.

带格式的: 字体:斜体

带格式的: 字体:斜体, 下标

带格式的: 字体:斜体

带格式的: 字体:斜体, 下标

删除的内容:)

删除的内容: The data used are described below.

带格式的: 英语(美国)

删除的内容: 5

删除的内容: T

删除的内容: nal data

删除的内容: eight

删除的内容: f

删除的内容: used in DRAM

删除的内容: (*see* Sect. 2.4)

from 2010 to 2013 at seasonal sampling frequencies. Part of the data have been published in Wakita et al. (2016), Fujiki et al. (2016), Matsumoto et al. (2016), and Sasai et al. (2016). DIN was calculated as the sum of nitrate, nitrite, and ammonia, which were measured with a continuous flow analyzer (QuAAtro 2-HR system, BL-Tech). CHL was measured using the nonacidification method following Welschmeyer (1994). NPP was measured with the technique of $NaH^{13}CO_3$ uptake (Matsumoto et al., 2016). PON was measured by an elemental analyser (Wakita et al., 2016). Size fractions of CHL were measured by filtering seawater sequentially through 10 µm, 3 µm, 1 µm polycarbonate membrane filters and finally a GF/F glass-fibre filter. The filters were soaked in N,N-dimethylformamide (DMF) and chlorophyll concentrations retained on the filters were measured with the same protocol as total CHL (Fujiki et al., 2016).

For station ALOHA, the data were downloaded from http://hahana.soest.hawaii.edu/hot/. All the data were pooled together to generate a quasi-climatological seasonal pattern and inter-annual variations were treated as random noise. To improve data coverage, we also included the nitrate data of World Ocean Atlas (WOA) 2013 for observed DIN. Due to the lack of *in situ* observational data, the data of *fer* were obtained from a global biogeochemistry model (Aumont et al., 2003). To calculate MLD from depth profiles of temperature and salinity, MLD was defined as the first depth that the seawater density exceeds surface density by 0.125 kg m^{-3} (Shigemitsu et al., 2012).

3 Results

3.1 External physics forcing

The validity of external physics forcing data, particularly vertical mixing that determines upward nutrient diffusive supply to the surface mixed layer, is essential for correct results and parameter optimization with the ecosystem model. Here we show in Fig. 2 a representative year of seasonal variations of K_v, temperature, surface PAR, and atmospheric iron deposition. Vigorous winter mixing precedes summer water column stratification at K2 and S1, while the seasonal variations of mixing are less pronounced at ALOHA. At all three stations, the model estimates of mixed layer depths are consistent with those measured from *in situ* temperature and salinity profiles (Fig. 2b,f,j). Water temperatures and surface PAR values at the subarctic station K2 are significantly lower than at the

带格式的: 上标

带格式的: 下标

删除的内容: Part of the data have been published in Wakita et al. (2016), Fujiki et al. (2016), Matsumoto et al. (2016), and Sasai et al. (2016).

删除的内容: TIN

带格式的: 字体:斜体

删除的内容: calculated

删除的内容: dust

删除的内容: d

删除的内容: both

删除的内容: stations

删除的内容: ,

删除的内容: with

删除的内容: were

subtropical stations S1 and ALOHA. The station K2 is also characterized by a pronounced spring peak of atmospheric dust deposition.

3.2 Parameter optimization and sensitivity analysis

For all the five parallel sub-processes, the log-likelihood continued to increase with the number of model runs and reached a plateau after 1000 iterations (Fig. 4). For most (but not all) types of data, model–data mismatches (*SSqE*) consistently decreased. Comparing the two stations, the model fits to the Chl, and NPP were better at station K2 than S1. The model fits to the size fractions of 1 ~ 3 μm were better at S1 than K2.

Most values of the optimized parameters fell into reasonable ranges (Table 2; Fig. 5). For example, the estimated $K_{0,N}$ is close to the value (0.2 μM) given in Ward et al. (2012). For some of the parameters such as W_d and μ, the final optimized value differed substantially from initial estimates, an expected outcome of the algorithm striving to match with the nine different types of observations at both stations with contrasting environments. Below we show some preliminary results of sensitivity analysis particularly on those differing with *a prior* estimates (Table 4).

The mean $\mu'_{0,m}$ estimated from laboratory phytoplankton data is around 0.4 d^{-1}, half of the optimized value (Chen and Laws, 2017). Reducing $\mu'_{0,m}$ to 0.4 d^{-1} mainly generated worse fits to the size fractions of <1 μm fractions of CHL at both stations. This is because the lower phytoplankton growth led to higher nutrient concentrations and lower estimates of <1 μm fractions.

The estimate of W_d of 20 m d^{-1} is a relatively high sinking speed. Reducing W_d to 10 m d^{-1} only led to slightly worse fits to DIN data at station S1 (but better fits to DIN at K2) and overall did not deteriorate the results substantially.

The estimate of m_z (0.2 (μM N)$^{-1}$ d^{-1}) is also at the high end of those used in the literature. We found that the model results were quite sensitive to the value of the closure term m_z. Reducing m_z to 0.1 (μM N)$^{-1}$ d^{-1} led to higher mesoplankton biomass and generated much worse fits particularly for DIN at K2.

We also tested whether we could assume that the light component of phytoplankton growth is size independent (i.e. $\alpha_I = 0$). The results suggested that with $\alpha_I = 0$, the model predicted much worse fits to

删除的内容: Compared to station S1, t
删除的内容: wa
删除的内容: **O**
删除的内容: **efficiency**
删除的内容: **optimized parameter distributions**
删除的内容: As expected
删除的内容: 2
删除的内容: Except that the *SSqE* of NPP and the largest size fraction (> 10 μm) increased with time at S1
删除的内容: all the other
删除的内容: TIN,
删除的内容: and large size fractions (> 3 μm) of Chl
删除的内容: small
删除的内容: (
删除的内容: <
删除的内容:)
带格式的: 字体:斜体
带格式的: 字体:斜体, 下标
带格式的: 字体:斜体, 下标
带格式的: 字体:斜体
删除的内容: some
带格式的: 字体:斜体
带格式的: 字体:斜体, 下标
带格式的: 字体:斜体
删除的内容: such as $K_{0,N}$, W_d, $\alpha_{0,C}$, and $K_{0,fer}$
删除的内容: eight
带格式的: 字体:斜体
带格式的: 上标
带格式的: 字体:斜体
带格式的: 上标

带格式的: 字体:斜体
带格式的: 字体:斜体, 下标
带格式的: 字体:斜体
带格式的: 字体:小四
带格式的: 字体:小四
带格式的: 字体:小四
带格式的: 字体:小四, 非 粗体
带格式的: 字体:小四
带格式的: 字体:小四
带格式的: 字体:小四

the data. An optimized value of –0.26 for α_l is also consistent with the size scaling relationship of light dependent growth in Finkel (2001) and Edwards et al. (2015), suggesting that light limitation could drive phytoplankton being small.

The optimized trait diffusion coefficient (u) was much higher than in Acevedo-Trejos et al. (2016). Reducing μ to 0.05 led to worse fits to the size-fractionated chlorophyll since lower size variance failed to capture the observed size scatter. It also relates to the limitation of the model that has to assume a lognormal distribution of size (*see* Sect. 4.2.1). However, an abnormally high μ could drive the model to unstable conditions in which the size variance kept increasing.

3.3 Comparison between best model outputs and observation

The best model outputs in terms of the highest likelihood could capture most of the observational patterns quantitatively (Figs. 6–9). At both stations, the model could reproduce the vertical increasing trend of DIN with depth and the higher surface concentrations of DIN during winter than summer and autumn. It is noteworthy that the model could also successfully reproduce the relatively abundant summer DIN concentrations at surface at station K2 due to the incorporation of iron and light limitation. The vertical and seasonal patterns of Chl *a* and NPP could also be well reproduced at station K2. The only problem is that, at station S1, the high NPP at surface could not be well reproduced (Fig. 7).

Validation against observed phytoplankton size data is critical for testing **CITRATE** 1.0 in which phytoplankton size structure is the core component. The model could reproduce most patterns of the proportions of size-fractionated CHL at both stations (Figs. 8, 9). For example, the model correctly reproduced the relative dominance of picophytoplankton (<3 μm) at both stations, although nitrate concentration was high at station K2. The seasonal and vertical fractions of 3–10 μm were generally well simulated at both stations, except for an artificial surface peak at K2. The model could also simulate the relative larger sizes at K2 than at S1.

We also note some deficiencies of the model. At both stations, the fractions of > 10 μm Chl were close to zero at both stations in the model, in contrast to the substantial fractions of > 10 μm during summer at K2 and in the winter at S1. The model also tended to overestimate the 1–3 μm fractions at both stations and underestimate the <1 μm fractions occasionally. All these problems relate to the assumption of a fixed trait distribution as discussed later.

删除的内容: toward
带格式的: 字体:(中文) ＭＳ 明朝
删除的内容: Note that t
删除的内容: value
带格式的: 字体:斜体
删除的内容: , which might be a necessary condition to match with the observed distributions of
删除的内容: We also note that
删除的内容: increasing *u* beyond some threshold (e.g. 0.2)
带格式的: 字体:斜体
带格式的: 字体:斜体
删除的内容: .
删除的内容: TIN
删除的内容: TIN
删除的内容: TIN
删除的内容: A
删除的内容: depth of the nutricline seems to be underestimated
删除的内容: , mostly related to the shallow mixed layer depth from spring to summer (Fig. 2b).
删除的内容: .
带格式的: 字体:斜体
删除的内容: Although with some deviations, t
删除的内容: show
删除的内容: dominance of
删除的内容: and smaller sizes
删除的内容: At station S1, the model also reproduced the relatively invariant proportions of size-fractionated Chl with depth during stratified seasons. This is not expected because of a steep vertical gradient of TIN around 100 m, which was expected to enhance the growth of large phytoplankton. The relative constancy of phytoplankton size structure with depth suggests that large phytoplankton are more susceptible to light limitation as previously suggested (Finkel, 2001; Edwards et al., 2015).
删除的内容: ,
带格式的: 字体:斜体
删除的内容: including the overestimation of
删除的内容: 3~
删除的内容: 10
带格式的: 字体:斜体
删除的内容: K2
带格式的: 字体:斜体
删除的内容: The model also tended to underestimate >10 μm fractions at station S1.

3.4 Modelled seasonal patterns of nutrients, phytoplankton biomass, mean size, and size diversity

At both stations, DIN concentrations were higher during winter in the surface mixed layer due to more vigorous mixing (Figs. 10, 11). Significant drawdown of DIN occurred in surface water following water column stratification which occurred earlier in S1 than K2. At station K2, after an increase during June and July due to the peak of atmospheric deposition, dissolved iron concentration also decreased in the fall due to phytoplankton uptake. By contrast, surface iron concentrations accumulated from late summer to fall due to nitrogen limitation at station S1.

In accordance with the DIN patterns, higher concentrations of Chl *a* were found during winter at station S1, which resulted from both increased phytoplankton biomass and chlorophyll-to-carbon ratios (Fig. 11). Starting from spring to fall, subsurface maximal layers of Chl *a* formed and progressively deepened with time. By contrast, at station K2, Chl *a* concentrations peaked in summer and subsurface chlorophyll maximum layers were not evident (Fig. 10), suggesting light limitation played a stronger role in limiting phytoplankton growth at K2 than S1.

At both stations, in spite of the nutrient increases in winter, phytoplankton mean size peaked in spring or summer. This is mostly attributed by the light limitation on large cells, which can be reflected by the negative value of α_I (Table 2) . At both stations, the main periods of size increases were in spring when light level increased and there were still nutrients left from winter mixing. The increases in light were contributed by both increases in surface PAR and shallower mixing. Nutrient (dissolved iron in the case of K2) depletion together with light decreases led to negative values of $\frac{d\mu(l)}{dl}$ since late spring or summer at both stations, resulting in subsequent decreases in mean size. In general, the modelled mean sizes were significantly larger at station K2 than S1, mainly due to less severe nutrient limitation.

The modelled patterns of size variances (i.e. size diversity) are the focus of **CITRATE**. Within the surface mixed layer, modelled phytoplankton size diversity showed an opposite pattern with mean size, with the peaks in fall at S1 and in winter at K2 (Fig. 10,11). At first glance, we also seemed to find a negative correlation between the growth rate μ_{com} and size diversity at both stations (Fig. 12a). When growth rates were high, size variances were low, and vice versa. The paired scatterplots between μ_{com}

删除的内容: TIN

删除的内容: TIN

删除的内容: s

删除的内容: the patterns of

删除的内容: mirrored those of TIN

删除的内容: , suggesting

删除的内容: that the spring peak of dust deposition was counteracted by stimulated phytoplankton growth

删除的内容: TIN

删除的内容: s

删除的内容: from spring to

删除的内容: early

删除的内容: even during the summer

删除的内容: around

删除的内容:

删除的内容: because wintertime conditions, with high nutrient concentrations, favour large sizes, and phytoplankton mean size continues to increase, i.e.

删除的内容: values are usually positive throughout the winter, until spring

删除的内容: Thus, the spring peak of mean size results from winter mixing that favours large size. This scenario is similar to the spring bloom cycles described by Behrenfeld (2010) that spring bloom is also a result of winter mixing that favours phytoplankton growth

删除的内容: .

... ...

删除的内容: the

带格式的: 字体:粗体

删除的内容: **1.0**

带格式的: 字体:非 粗体

删除的内容: M

删除的内容: variances

删除的内容: largely followed the patterns of nutrients

删除的内容: Similar to mean size, size variance also increased from fall when mixing started to intensify. However, size variance decreased with nutrient depletion appreciably faster than mean size because the rate of change of size variance is a function of the square of size variance, while the rate of change of mean size is only a function of size variance (Eq. 1). This led to a temporal decoupling of mean size and size diversity. We also observed a temporal decoupling of μ and size variance.

删除的内容: T

带格式的: 下标

and size variances in surface waters suggested that these two quantities were not linearly correlated, particularly at S1. Instead, their relationships depended on the timing of the season. At station S1, during the transition from the end of winter to early spring, phytoplankton cells experience a rapid increase in growth rate without much change in size diversity. During the rest of spring, phytoplankton growth rate decreased from the maximum to nearly the minimum; while size diversity first underwent a phase of moderate decrease and then recovered. From the beginning of summer to mid-fall, there were no big changes in growth rate, but size diversity increased dramatically. From mid-fall to the beginning of the winter, phytoplankton growth rate increased, but size diversity decreased to winter values. At station K2, the variability of size diversity was smaller, with high growth rates and low size diversity in summer and the opposite patterns in winter.

We decomposed the different factors in affecting the dynamics of size diversity in surface waters at both stations (Eq. 7c,e; Fig. 12b,c). Three points need to be mentioned. First, the calculated net combined effects, including the second derivatives of growth and grazing ($\frac{d^2\mu(l)}{dl^2}$ and $\frac{d^2g(l)}{dl^2}$), trait diffusion ($\frac{d^4\mu(l)}{dl^4}$ and *μ*(*l*)), and vertical mixing (i.e. diffusion), were consistent with the net changes of size variances (some minor differences were because we saved the above quantities at daily interval which could not account for the changes within one day), validating our computation. Second, the contributions from the second derivatives of growth and trait diffusion (dominated by 2*μμ*(*l*) with the contributions from $\frac{d^4\mu(l)}{dl^4}$ being minor; Eq. 7c) were the two largest terms, which usually offset against each other. It is the margin of these two terms plus vertical mixing that drove the changes of size variance. The values of $\frac{d^2\mu(l)}{dl^2}$ were always negative in all times at both stations, suggesting that without "trait diffusion", size variance would decrease toward zero (Eq. 7c). This highlights the importance of trait diffusion (which can be interpreted as genetic mutation or transgenerational phenotypic plasticity) to sustain diversity. The values of $\frac{d^2\mu(l)}{dl^2}$ were more negative when growth rates were higher. For example, in early April of S1, the decrease of size variance was induced by a more negative $\frac{d^2\mu(l)}{dl^2}$ (*see*

删除的内容: peaked during spring and summer at S1 and K2, respectively, due to the improved light condition and high temperature. In other words, although spring or summer blooms can be characterized by high biomass, growth rate, and large size, the size diversity could be higher during winter.

带格式的: 缩进: 首行缩进: 1.18 字符

带格式的: 字体:斜体

带格式的: 字体:斜体

带格式的: 字体:斜体

删除的内容: ,

删除的内容: a surrogate for the intensity of competition,

删除的内容: indicative of the effect of resource competition that reduces diversity

删除的内容: T

带格式的: 字体:非 粗体

删除的内容: and it is the margin of these two terms that (partially) drove the changes of size variance

删除的内容: less negative in nutrient-replete wintertime and deep waters, suggesting that enhanced nutrient supply relieved the nutrient competition among phytoplankton species, providing a window for large species to thrive, and thus increasing diversity

带格式的: 字体:斜体

also Fig. 11h). Similar situations also occurred at the end of December. Third, water column mixing also played a significant role in affecting size diversity, which was the main factor leading to the peak of size diversity in fall in surface waters at S1. The effect of mixing became important because at this time, a subsurface maximum of phytoplankton biomass still existed below the surface mixed layer. With the deepening of surface mixed layer, substantial biomass of phytoplankton was entrained into surface waters and these phytoplankton communities had different trait properties with surface ones, thereby enhancing diversity (*see* Sect. 4.1.1 for discussion).

The model also generated reasonable patterns of Chl:C and N:C ratios, which were largely determined by light and nutrient concentrations (Fig. 10i,j; Fig. 11i,j). Both Chl:C and N:C ratios were high in winter when nutrient concentrations were high and light levels were low due to strong mixing. And both ratios were low in surface stratified waters where nutrient supply from below became diminished due to strong stratification and also light levels became strong due to both increased surface PAR and shallow mixing layers.

3.5 Validations of the model at station ALOHA

We used the optimal parameter sets obtained at stations S1 and K2 to run the model at station ALOHA. As there were no data of size-fractionated Chl at ALOHA, we only compared the model outputs of DIN, CHL, NPP, and PON with the observational data. While the modelled profiles of DIN matched well with the observed data, the model underestimated CHL, NPP, and PON, although the qualitative patterns could be reproduced (Fig. 13).

4 Discussion

4.1 Model merits

4.1.1 Understanding ecological mechanisms

Besides the improved computational efficiency (Acevedo-Trejos et al., 2016), the most important advantage of the continuous trait-based ‘adaptive dynamics’ approach is expressed well in the following quote from Bak (1996): “If, following traditional scientific methods, we concentrate on an accurate description of the details, we lose perspective.” (p. 10) and “It is a futile endeavour to try to explain most natural phenomena in detail by starting from particle physics and following the trajectories of all

删除的内容: . The absolute magnitude of

带格式的: 字体:斜体

删除的内容: were less negative and trait diffusion estimates were also relatively high, phytoplankton size diversity kept increasing. With stratifying water column starting from spring, the values of

删除的内容: positively correlated to μ, indicating that higher growth rates induced greater resource competition. This agrees well with the “dynamic equilibrium theory” proposed by Huston (

删除的内容: became more negative and trait diffusion became critically important for sustaining diversity in the system by counteracting the effect of competitive exclusion in nutrient depleted waters.

带格式的: 英语(美国)

删除的内容:

带格式的: 字体:非 粗体

带格式的: 缩进: 首行缩进: 1.18 字符

带格式的: 字体:非 粗体

带格式的: 缩进: 首行缩进: 0 字符

删除的内容: **Facilitating u**

删除的内容: **on**

删除的内容: T

删除的内容: or the

删除的内容:

删除的内容: can be quoted

删除的内容: also

particles." (p. 5). This modelling approach has the potential to make it much easier to understand the mechanisms regulating phytoplankton diversity, because the functional trait diversity itself (quantified by the trait variance) is a tracer in the model, and the sources and sinks of diversity are given explicitly (Eq. 7). In particular, the second derivative of the growth rate, $\frac{d^2\mu(l)}{dl^2}$, evaluated at the mean size, is a proxy for the intensity of resource competition. The more concave is the curve of $\mu(l)$, the more intense is the competition, i.e., the fitness of suboptimal species decreases more steeply with distance from the optimal size. In models resolving a number of discrete species, the typical index for the intensity of resource competition under steady-state is R*, the lowest nutrient concentration allowing positive net growth (Tilman, 1982; Litchman et al., 2007; Barton et al., 2010). Under non-equilibrium conditions, it is the maximal growth rate instead of R* that determines the outcome of competition (Hutson, 1979; Barton et al., 2010). In any case, it is the realised growth rate that determines the outcome of competition. Compared to R*, the second derivative $\frac{d^2\mu(l)}{dl^2}$ has two advantages as a proxy for quantifying the intensity of competition: 1) it applies under both equilibrium and non-equilibrium conditions and 2) it circumvents the problem of tracking many species. Using this approach, it is straightforward to test some ecological theories such as Huston's "general hypothesis of species diversity" (Huston, 1979). For example, the absolute magnitude of $\frac{d^2\mu(l)}{dl^2}$ correlates positively with μ (Fig. 13), indicating that resource competition is more intense when growth rates are high. This is a mathematical manifestation of the verbal argument of the "dynamic equilibrium theory" proposed in Huston (1979), who emphasized that in natural environments where equilibrium is rarely achieved fast-growing species tend to outcompete slow-growing species (*see* also Barton et al., 2010), and hence growth rates play a greater role in determining diversity than R* values.

Similarly, Eq. 7b specifies concisely the factors affecting mean phytoplankton size. In fact, Eqs. 7a-c can be understood as derived from a Taylor expansion representing an infinite number of discrete trait classes (Merico et al. 2009). Hence, even if a discrete version of a diversity model is used, it may

删除的内容: We believe that t…is merit …

删除的内容: overweighs other technical advantages such a… …

删除的内容: can…greatly facilitate…ake it much easier to …

删除的内容: computational efficiency (Acevedo-Trejos et al., 2016)

删除的内容: in terms of

删除的内容: equations themselves (Eq. 1) have already provided the genuine insights for…and the mechanisms regulating …

删除的内容: for…f diversity have been already…re explicitl …

删除的内容: For example

$d^2\mu(l)$ …

带格式的 …

删除的内容: since …he fitness of suboptimal species drops …

删除的内容:)

删除的内容: typical NPZD-type

删除的内容: Thus, we propose that…ompared to R*, the sec …

删除的内容: the trajectories of

删除的内容: a…any number of …pecies the competition is n …

删除的内容: 'adaptive dynamics', it is easier to ability to easily quantify competition intensity (and other ecological quantities), which makes…his approach, it is straightforwardeasier …

删除的内容: y

删除的内容: T

域代码已更改

删除的内容: positively …orrelates positively withd to…μ (F …

删除的内容: agrees well with

删除的内容: proposed by Huston (1979).

删除的内容: .

删除的内容: the …rowth rates play a greater role instead of …

删除的内容: do steady state competitive abilities as typically quantified by

删除的内容: and fast-growing species tend to outcompete slow-growing species (*see* also Barton et al., 2010)

带格式的: 字体:斜体

删除的内容: (Tilman, 1982????; Litchman et al., 2007)

删除的内容: When

删除的内容: This is because when environmental conditions favour highfast growth rates, it takes less time for the dominant species to predominate, thusand reducing diversitydiversity decreases. The positive correlation between the absolute value of … QUOTE and μ is a mathematical manifestation of the verbal

argument in Huston (1979). …

删除的内容: also gives…pecifies the sources and sinks of m …

be also helpful to calculate the terms in Eqs. 7a-c in order to understand the factors affecting species diversity, biomass, and productivity.

The set of Eqs. 7 also provides an excellent platform to investigate the underlying mechanisms for the relationship between biodiversity and ecosystem functioning (productivity, in this case), which have been extensively studied (Loreau et al., 2001; Tilman et al., 2014). While the negative relationship between productivity (μ_{com}) and diversity suggests that enhanced productivity can induce greater competition and reduce diversity (Huston, 1979), diversity can also be affected by other factors besides competition.

The incorporation of trait diffusion originally developed for continuous trait-based models (Merico et al., 2014) provides a means of representing mutation and other processes that sustain diversity, thus linking ecological and evolutionary processes (Rosenzweig, 1995). This allows control of the level of diversity in simulation experiments such as those conducted herein to investigate diversity-productivity relationships. The increasing effect of trait diffusion with growth rate is consistent with the Metabolic Theory of Ecology, in that metabolic rates, which are closely coupled with growth rates and generation time, are expected to correlate with mutation rates. Therefore, growth rates are expected to affect speciation and potentially contribute to the latitudinal diversity gradient (Rohde, 1992; Allen et al., 2006; Dowle et al., 2013). Our results have shown that trait diffusion can be the largest term counter-balancing competitive exclusion (Fig. 13). Without considering this mechanism, diversity could be underestimated in productive waters due to strong competition.

The approach of transporting trait moments across spatial grids, originally developed by Bruggeman (2009), also allows water mixing to affect diversity patterns. Although this approach is not perfect (*see* Sect. 4.2.2 and Fig. 14), it does allow that the mixing of two communities with different mean traits can generate trait variance greater than the weighed mean variance of the two original communities. The larger difference of the mean traits, the greater the increase in trait variance upon mixing. Consider the case of mixing two communities with biomass P_1 and P_2, mean size l_1 and l_2, size variance v_1 and v_2. The biomass and mean size of mixed community are $P_1 + P_2$ and $\frac{P_1 l_1 + P_2 l_2}{P_1 + P_2}$, respectively. After some algebraic manipulation, we can derive the size variance (v') after mixing:

删除的内容: In typical NPZD-type models in which phytoplankton species compete for the same set of nutrients but do not directly confront each other, the parameters representing the direct interactions among species (such as in the Lotka–Volterra equations) are usually not available. Thus, in traditional approaches that model the trajectories of a number of species, the competition is not easily quantifiable and therefore is rarely quantified. The ability to easily quantify competition intensity makes it easy to test ecological theories such as Huston's "general hypothesis of species diversity" (Huston, 1979).

删除的内容: 1

删除的内容: correlation

带格式的 ... ...

删除的内容: certainly

删除的内容: One insight from the results of the temporal decoupling of growth rate and size diversity on the seasonal scale is that productivity and diversity are not necessarily correlated because the productivity can strongly depend on *current* environmental condition, while diversity emerges over time, depending on standing stocks, which themselves are contingent upon *historical* events.

删除的内容: also …rovides a mechanism similar to speciatio ... ...

删除的内容: evolutionary theory…he Metabolic Theory of E ... ...

删除的内容: and…affect speciation and ... ...

删除的内容: This could also contribute to the latitudinal diversity gradient sincebecause in warm, tropical regions (ectothermic) organisms tend to growth fast (i.e. short generation time) due to high temperature and therefore have high mutation and speciation rates (Rohde, 1992; Allen et al., 2006; Dowle et al., 2013).

删除的内容: This

带格式的: 字体:斜体

删除的内容: a population with the …rait variance at ... ...

带格式的 ... ...

$$v' = \frac{P_1(l_1^2+v_1)+P_2(l_2^2+v_2)}{P_1+P_2} - \left(\frac{P_1 l_1+P_2 l_2}{P_1+P_2}\right)^2 = \frac{P_1 P_2 (l_1 - l_2)^2}{(P_1+P_2)^2} + \frac{P_1 v_1+P_2 v_2}{P_1+P_2} \qquad (15)$$

Thus, it is clear from Eq. (15) that the difference between *v'* and biomass weighed mean variance $\frac{P_1 v_1+P_2 v_2}{P_1+P_2}$ depends on the difference of mean traits. Hence, mixing can enhance diversity to the extent that the traits of the original communities differ. Barton et al. (2010) have shown that the "hotspots" of high phytoplankton diversity are usually located along areas where mixing is strong enough to allow coexistence of multiple populations with different traits. Our simulations are consistent with that view and show that vertical mixing can significantly enhance diversity, particularly during ocean mixed layer entrainment.

4.1.2 Flexible stoichiometry

We also consider realistic phytoplankton physiology and optimized model parameters guided by real data. For example, our model has incorporated some features of phytoplankton plasticity (acclimation) such as variable Chl:C ratio and N:C ratios. Although, for the sake of simplicity, these variable ratios do not directly influence phytoplankton specific growth rate as in Geider et al. (1997), they are able to reproduce the high Chl:C ratios in the DCM layer, thus providing a more realistic mechanism for the formation of the DCM layer than with models that assume fixed ratios (Fennel and Boss, 2003). Similarly, the variable N:C ratio also allows phytoplankton cells to achieve higher carbon-based NPP in surface waters compared to models with fixed N:C ratios (Christian, 2005). Although cellular chlorophyll and nitrogen quota are not calculated as independent tracers, model comparisons suggest that more complex models do not always yield better fits to the data (Flynn, 2003).

4.1.3 Realistic mechanisms for controlling phytoplankton size structure

In CITRATE 1.0 we have provided both bottom-up and top-down mechanisms to affect the size structure of phytoplankton. First, we employ an observation-based unimodal relationship between maximal growth rate and size to give the nanophytoplankton the advantage under nutrient-replete conditions (Chen and Liu, 2010, 2011; Marañón et al., 2013), thus allowing a trade-off between nutrient affinity and maximal growth rate within the pico- and nano-size range. Thus, bottom-up factors alone are sufficient to reproduce the observed decrease in the fraction of small phytoplankton with nutrient

带格式的: 右对齐，允许文字在单词中间换行

带格式的: 字体:斜体

删除的内容: the extent that

删除的内容: relates

删除的内容: how

删除的内容: in

删除的内容: were

删除的内容: were

删除的内容: wa

批注 [SS1]: Should this be 'communities'?

删除的内容: is

删除的内容: specifically

删除的内容: in

删除的内容: fall inin the surface waters at S1

带格式的: 字体:粗体

带格式的: 缩进：首行缩进： 0 字符

带格式的: 字体:粗体

删除的内容: By solving these theoretical differential equations under quasi-realistic ocean conditions, we can evaluate the relative roles of each mechanism that structures the community properties mentioned above.

删除的内容: Although any model is necessarily an abstraction of the real world, to avoid being too far away from reality, w

删除的内容: ed

删除的内容: acclimatory

删除的内容: the

删除的内容: with

删除的内容: than the

带格式的: 字体:粗体

带格式的: 缩进：首行缩进： 0 字符

删除的内容: W

删除的内容: in **CITRATE 1.01.11.0**

带格式的: 字体:粗体

删除的内容: Instead

删除的内容: large

删除的内容:

删除的内容: the

删除的内容: should be

删除的内容: abl

删除的内容: e

删除的内容: pattern that the

删除的内容: decreases

enrichment (Marañón et al., 2012). We also impose a size-dependent feeding preference of zooplankton based on the general understanding that smaller microzooplankton tend to prefer smaller phytoplankton, whereas larger mesozooplankton tend to prefer larger phytoplankton (Frost, 1972; Hansen and Hansen, 1994; Liu et al., 2005; Ward et al., 2012). These top-down factors have additional effects on phytoplankton size structure. Our assumption about the preference of microzooplankton on small phytoplankton is similar to Terseleer et al., (2014) and Acevedo-Trejos et al., (2015), who assumed a combination of decreasing maximal phytoplankton growth rate with increasing size and a grazing preference for small phytoplankton in order to offset the growth advantage of small phytoplankton in eutrophic waters. In our case, small phytoplankton lose the advantage in eutrophic waters, where larger phytoplankton grow faster because of the imposed unimodal relationship between maximal growth rate and size. Meanwhile, in eutrophic waters, mesozooplankton dominate and preferentially feed on larger phytoplankton to balance the growth advantages of larger cells.

Interestingly, counter to our intuition, field incubation experiments have often found that microzooplankton feed on diatoms faster than on picophytoplankton, and that diatoms grow faster than picophytoplankton even in oligotrophic waters (Latasa et al., 1997; Zhou et al., 2015). These results raise a paradoxical question: "How can diatoms grow so fast with negligible nutrients in oligotrophic waters, but without accumulating high biomass?". Whether this is because of experimental bias is an open question. The feeding preference of mesozooplankton on large prey seems less disputable (Frost, 1972; Liu et al., 2005), but *see* Terseleer et al. (2014) for an assumption of decreasing feeding preference of copepods on large diatoms. This implies strong top-down control of large phytoplankton in eutrophic waters where mesozooplankton dominate, limiting the biomass of large phytoplankton. However, this implication is at odds with the common observation that large phytoplankton dominate total biomass in eutrophic waters (Marañón et al., 2012). Future refinements might include a unimodal feeding preference, similar to the grazing kernel proposed earlier (Hansen and Hansen, 1994; Poulin and Franks, 2010). In any case, for model calibration and validation, more and better data are much needed concerning the size-scaling of both phytoplankton traits and zooplankton grazing preference.

4.2 Model limitations

删除的内容: Compared to previous continuous trait-based models (Terseleer et al., 2014; Acevedo-Trejos et al., 2015, 2016), **CITRATE** 1.0…e also does not…impose a size-dependent fe

删除的内容: the …maller microzooplankton tend to

删除的内容:

删除的内容: of…bout the preference of microzooplankton o

删除的内容: oligotrophic

删除的内容: the growth superiority of …mall phytoplankton

删除的内容: oligotrophic…utrophic waters, where larger

删除的内容: disappears due to the

删除的内容: so that the grazing preference of microzooplankton on small phytoplankton is necessarily weaker

删除的内容: .…Meanwhile, in eutrophic waters, mesozoopla

删除的内容: opposite…ounter to our intuition, field incubati

删除的内容: fast-growing

删除的内容: also …row faster than picophytoplankton even

带格式的: 字体:斜体

删除的内容: ,…(2014) for an assumption of decreasing feedi

带格式的: 字体:非 粗体

删除的内容: rther

删除的内容: Another feeling from such modeling exercise is that

删除的内容: addition…ny case, for model calibration and

删除的内容: Instead, we employ an observation-based unimodal relationship between maximal growth rate and size to give the large phytoplankton the advantage under nutrient-replete conditions (Chen and Liu, 2010, 2011; Marañón et al., 2013), thus allowing a tradeoff between nutrient affinity and maximal growth rate. One reason is that, in the open ocean, such size-dependent feeding preference is either very weak or does not have a robust pattern for the dominant grazers, microzooplankton (Hansen and Hansen, 1994; Chen et al., 2009, 2010). While previous studies usually assume that the specific clearance rates of zooplankton on phytoplankton decrease with increasing phytoplankton size, which is usually based on the copepod data, field dilution experiments often suggest that the grazing rates of microzooplankton are higher on fast-growing diatoms (Latasa et al., 1997; Zhou et al., 2015). Because our model incorporates a generic zooplankton compartment, which should have an adaptive feeding behaviour on phytoplankton (Behrenfeld and Boss, 2014), we feel that it is justifiable not to apply any size-related feeding preference in **CITRATE** 1.0. Thus, phytoplankton mean size and size diversity are controlled only by bottom-up factors, although zooplankton grazing plays an indirect role in affecting nutrient regeneration and phytoplankton mortality. Whether or not size-dependent zooplankton grazing plays an important role in determining patterns of phytoplankton mean size and size diversity (Terseleer et al., 2014) deserves to be further investigated in future work

带格式的: 英语(美国)

带格式的: 缩进: 首行缩进: 0 字符

4.2.1 Assumption of trait distribution

To facilitate calculation of trait moments, a certain distribution has to be assumed for the trait (Merico et al., 2009, 2014). The lognormal distribution can be fitted well to empirical data (Quintana et al., 2008, 2016), and because of its mathematical convenience, it has been widely used in continuous size distribution models (Terseleer et al., 2014; Acevedo-Trejos et al., 2015, 2016; Smith et al., 2016). For these reasons we have assumed a lognormal distribution in the present study.

However, other probability distributions can also describe phytoplankton size. In the literature, phytoplankton abundance (*N*, cells L^{-1}) within the size interval from *V* to *V* + d*V* is more often modelled as a power-law function of cell volume *V* (unit: μm^3; Gin et al., 1999; Cavender-Bares et al., 2001; Cermeño et al., 2006):

$$N(V) = N_0 V^{\alpha} \qquad (16a)$$

where N_0 represents the abundance of phytoplankton having cell volume 1 μm^3, and α is the exponent of the power law. Because models typically represent phytoplankton biomass, instead of abundance, we can convert the abundance to biomass (*B*, μm^3 L^{-1}):

$$B(V) = N(V)V = N_0 V^{\alpha+1} \qquad (16b)$$

Although the power law of Eq. (16b) may seem to be a suitable alternative distribution for continuous size-based models, empirical data suggest that α tends to vary between –0.7 and –1 (Cermeño et al., 2006), which means that the exponent (α + 1) of the power law relating *B* and *V* should be between 0 and 0.3. In this case both the mean and variance of the power law distribution as shown in Eq. (16b) are infinite (Newman, 2005). This problem can be solved by adding an upper cutoff via an exponential truncation (Clauset et al., 2009):

$$B(V) = N_0 V^{\alpha+1} e^{-\lambda V} \qquad (16c)$$

where λ is a positive constant.

Whether the power law or the lognormal distribution fits better to empirical data has been widely debated in the literature, and many results show that both can fit the data equally well (Allen et al., 2001; Mitzenmacher, 2004; Clauset et al., 2009). This is not surprising given that the two distributions are intrinsically connected (Mitzenmacher, 2004; Newman, 2005). We suspect that the power law with an

删除的内容: ;

删除的内容: . And also b…cause of its mathematical

删除的内容: lognormal is not the only…ther probability

删除的内容: I… the literature, phytoplankton abundance (*an*

带格式的: 缩进: 首行缩进: 1.77 字符

带格式的

删除的内容: usually…ore often modelled as a power-law fur

带格式的

带格式的: 右对齐, 允许文字在单词中间换行

带格式的: 左对齐

带格式的

删除的内容: with…aving the …ell volume of … μm^3.

带格式的: 字体:斜体

删除的内容: the common unit of …odels typically represent

带格式的: 字体:斜体

带格式的

带格式的: 英语(美国)

删除的内容: .

带格式的: 缩进: 首行缩进: 1.18 字符

删除的内容: While…lthough the power law of Eq. (16b) ma

删除的内容: The slope of log abundance versus log size (e.g

带格式的: 字体:斜体

删除的内容: be

带格式的: 英语(美国)

删除的内容: , suggesting

删除的内容: with the consequence tha…hich means thatt

带格式的: 英语(美国)

删除的内容: slope

删除的内容: between

删除的内容: *log biomass*

删除的内容: versus log size

带格式的: 字体:斜体

带格式的: 字体:斜体

删除的内容: This causes the problem that

批注 [SS2]: Is this term simply added to the eq. above? If s

带格式的

删除的内容: *B*(*V*)= *N*⍰0⍰ *V*⍰*α*+1⍰ *e*⍰-*γV*⍰*B*(*V*)= *N*⍰0⍰

带格式的: 左对齐

带格式的

删除的内容: In the literature, there have been lots of debates

带格式的: 左对齐, 缩进: 首行缩进: 1.18 字符

删除的内容: since

upper cutoff may be able to capture better the right skewness of phytoplankton size distributions, as is common in oligotrophic waters where large diatoms coexist with the dominant cyanobacteria such as *Prochlorococcus* (Campbell et al., 1994; Liu et al., 1997; Villareal et al., 1999). It remains to be investigated whether changing the distribution to the truncated power law can help solve the problem of underestimating the fraction of > 10 μm size in the current study.

Neither the lognormal nor the power law with an upper cutoff can capture multimodal size distributions, as exemplified in fig. 1b of Marañón (2015) and reported by other studies (Banas, 2011; Bonachela et al., 2016; Coutinho et al., 2016). This is an inevitable consequence of aggregating the description of the entire community into only the three descriptors (i.e. total biomass, mean and variance), which reduces the degrees of freedom, thus sacrificing detailed accuracy for generality and perspective.

One remedy for this problem might be to assign more functional groups in phytoplankton and assume a probability distribution for each group, respectively (Terseleer et al., 2014). Having a number of functional groups also circumvents the problem of size-independent functional differences among phytoplankton, such as the different maximal growth rates of diatoms and dinoflagellates despite their similar sizes (Chen and Laws, 2017). We expect that in the near future such a combination of continuous trait distributions and functional groups will likely provide more realistic representations of marine phytoplankton diversity.

4.2.2 Transport of moments

Another potential problem is the transport of trait moments in ocean circulation models. Unlike nutrients or plankton biomass, trait moments are not real "concentrations" that can be directly involved in advection and diffusion. In general two Gaussian curves differing in area (i.e., total biomass), mean, and variance do not sum to a perfect Gaussian curve (Fig. 14a). Bruggeman (2009) has derived that, if following the assumption of normal distribution of traits, the raw moments of the biomass distribution can behave as normal tracers in GCMs. We have shown a few examples of mixing of communities of different biomass, mean size, and size variance in Fig. 14. These examples demonstrate that when the mean sizes and size variances differ greatly and biomasses are similar, the mixed

删除的内容: might…ay be able to capture better cope with …

删除的内容: unicellular…cyanobacteria such as *Prochloroc*

删除的内容: deal with the problem of

带格式的: 缩进：首行缩进： 1.18 字符

删除的内容: However, aside from fact that the power-law distribution is unrealistic in predicting phytoplankton biomass at the size limits (there must be upper and lower limits of size at which phytoplankton biomass becomes close to zero, which cannot be predicted bywhich the power-law cannot reproduce), the power-law distribution is much more inconvenient in terms of for mathematical manipulations (e.g. calculating mean and variance) thancompared to the normal distribution. TheA lognormal distribution is usually appropriatea much better alternative for phytoplankton size in terms of mathematic properties (e.g., zero probability of negative size) and can be fit well to empirical data (Finkel, 2007Quintana et al., 2008). Therefore, it is not surprising that the lognormal distribution has been widely used in continuous size models; (Terseleer et al., 2014; Acevedo-Trejos et al., 2015, 2016; Smith et al., 2016).

带格式的: 英语(美国)

删除的内容: lognormal

删除的内容: ces…of …aximal growth rates between …f diat

删除的内容: The immediate summation of…n general two G

删除的内容: certainly

删除的内容: usually …ot sum to … another

删除的内容: 2…). However, if we consider that during one s

删除的内容: A schematic diagram is shown in

删除的内容: al…raw moments

删除的内容: Fig. 12b shows an to represent one example of such approximationa water mass mixed with a small fraction of an adjacent water mass, which seems to work well to the first order, which seems to work well to the first order. Therefore, the robustness of such approximation depends on the difference of phytoplankton biomass in the present grid and that transported from adjacent grids into the present grid. Since within the mixed layer, the three quantities (*P*,

带格式的

域代码已更改

删除的内容: From t…hese examples, we could sense…demo community may deviate from the assumed normal distribution, making this a poor approximation. For now, we assume that across adjacent grids, phytoplankton communities should in most cases be similar enough for this approximation to work reasonably well.

4.2.3 Lack of multiple traits

As a first step, we incorporated only size as the master trait that affects all physiological functions of phytoplankton. In reality, many phytoplankton functional traits, such as optimal temperature, diazotrophy, and mixotrophy, are independent of size. For example, the optimal growth temperature of phytoplankton is closely related to environmental temperature, but only weakly relates to size (Thomas et al., 2012; Chen, 2015). The optimal growth temperature and irradiances are certainly function traits that deserve to be incorporated into trait-based models (Follows et al., 2007; Norberg, 2004; Edwards et al., 2015) and are expected to strongly affect phytoplankton functional diversity at large scales.

4.2.4 Difficulty in modelling surface peaks of NPP at oligotrophic stations

The near-surface peak of NPP at the oligotrophic stations S1 and ALOHA during summer is not expected if we assume that the source of nutrients comes from below the euphotic zone. Even if variable N:C ratios are used in the model to allow more carbon to be fixed given the same amount of nitrogen near surface waters, surface NPP is still likely to be underestimated even with the presence of N_2 fixation because of phosphorus limitation (Christian, 2005). It is possible that other mechanisms such as vertical migration of phytoplankton need to be taken into account (Villareal et al., 1999; Chavez et al., 2012). Therefore, this problem is not only restricted to **CITRATE** 1.0.

4.2.5 Optimized parameters for 3D GCM

One purpose of optimizing a common parameter set for two stations with contrasting environmental conditions is to use this parameter set for 3D GCMs. This is based on the expectation that, such a parameter set that can work for the two stations should work for other locations as well. However, our validation exercise at station ALOHA reveals that the parameter set optimized for stations K2 and S1 only succeeds in matching the DIN data well, but underestimates CHL, NPP and PON at station ALOHA. This suggests that we might be overlooking some unique but important processes at ALOHA. Alternatively, it is also possible that the uneven sampling at K2 and S1 might bias the parameter optimisation to some extent. Similar difficulties in parameter optimisation have been shown previously

删除的内容: s

删除的内容: and hence the approximation cannot work very well

删除的内容:

删除的内容: can

删除的内容: es

删除的内容: properties

删除的内容: , and

带格式的: 字体:非 粗体

删除的内容:

删除的内容:) should be similar due to strong mixing, the approximation is not a big concern. The problem mainly lies at the bottom of the mixed layer where there is a sharp gradient of phytoplankton properties particularly biomass (Fig. 12c). We can roughly estimate that, based on the eddy diffusivity (~2 x 10^5 m^2 s^{-1}), grid distance (20 m), and the phytoplankton biomass differenc ... ...

带格式的: 字体:非 粗体

带格式的: 字体:斜体

带格式的: 上标

带格式的: 字体:粗体, 斜体

带格式的: 字体:非 粗体

带格式的: 字体:粗体, 斜体

带格式的: 字体:斜体

带格式的: 字体:粗体, 斜体

删除的内容: should work wellbe reliable in most cases

删除的内容: and may potentially be a concern only under th ... ...

带格式的: 字体:非 粗体

带格式的: 上标

带格式的: 上标

带格式的: 上标

删除的内容: N_2 fixatio

删除的内容: n

删除的内容: identity and

删除的内容: **S1**

删除的内容: 1.0

删除的内容: 1.1

删除的内容: **Deficiency of the external physics driver**

带格式的: 缩进: 首行缩进: 1.77 字符

删除的内容: finding

删除的内容: optimized to

删除的内容: with t

删除的内容: since this

删除的内容: , it

删除的内容: stations

删除的内容: disappointingly

(Ward et al., 2010). For optimising parameters for 3D GCMs, a better approach might be to use the "Transport Matrix" technique that has been successfully implemented for some biogeochemistry models (Khatiwala, 2007; Kriest et al., 2017). Nonetheless, our optimized parameters can provide a useful initial estimate for modelling other stations and for use in 3D GCMs.

4.3 Future directions

Considering the above limitations, one future direction is to increase the number of traits in the model to generate more realistic phytoplankton diversity patterns, which requires both an "envelope" function relating the maximal growth rate with the optimal trait value and a relationship between growth rate and trait value for each species (Norberg, 2004). Another refinement as noted above is to model a continuous trait distribution for each functional group, respectively, thus combining the continuous trait-distribution and functional group approaches to better capture deviations of overall trait distributions from normality and to better represent key ecosystem functions.

It is relatively easy to couple the one-dimensional **CITRATE** model with 3D global or regional ocean models in order to model the large-scale patterns of phytoplankton size and size diversity. Furthermore, it should be possible in the near future to optimize parameters for such a 3D model using the "transport matrix" technique. In particular, by including both trait diffusion and competitive exclusion it may be possible to begin to untangle the relative roles of ecological versus evolutionary processes in shaping global phytoplankton diversity patterns.

5. Conclusions

- We present a 1D model with continuous size distribution for phytoplankton (**CITRATE**). The dynamics of phytoplankton mean size and size variance are directly linked to environmental factors and moments of the size distribution (Eq. 7), facilitating understanding of the underlying mechanisms controlling phytoplankton size and diversity. **CITRATE** 1.0 also incorporates "trait diffusion" as an eco-evolutionary process to sustain phytoplankton diversity.
- We optimized the parameters of **CITRATE** using the DRAM algorithm, which revealed that the model can faithfully reproduce observed seasonal patterns of inorganic nitrogen, Chl *a*, and

带格式的: 字体:非 粗体, (中文) 中文(中国), (其他) 英语(美国)

删除的内容: We note that various aspects of the external environmental drivers such as vertical mixing coefficients (K_v) and iron deposition rates may still have some deficiencies that can bias model results and parameter optimization. For example, it is puzzling that although the MLDs derived from K_v seemed consistent with *in situ* temperature and salinity profiles (Fig. 2b), they were usually shallower than the observed nutricline from spring to fall at station S1. It is also possible that this problem arose because certain aspects of phytoplankton biology such as the varying adaptive response to light (Moore et al., 1998) were not included in the model. For example, we expect that including another functional group adapted to low light environments would deepen the nutricline.

删除的内容: each functional group with

删除的内容: -based model

删除的内容: mixing

删除的内容: discrete trait

删除的内容: trait distributions that

删除的内容: e

删除的内容: .

删除的内容: ,

删除的内容: thus providing a means

删除的内容:

删除的内容: and later optimising

删除的内容: the

删除的内容: with

删除的内容: in

删除的内容: (

删除的内容: 1

删除的内容: 1.0

删除的内容: 1.1

phytoplankton size structure at two contrasting time-series stations. The model structure and associated parameters obtained herein can be useful for 3D regional and global ocean modelling.

- The limitations of **CITRATE** include its assumption of a lognormal distribution for phytoplankton size as the sole master trait, which to some extent limits the precision with which it can reproduce large size classes of phytoplankton. These limitations and others may be overcome in future studies by building on **CITRATE** 1.0 to construct more elaborate continuous trait-distribution models capable of reproducing more realistic patterns of phytoplankton diversity.

6. Code and data availability

The code and data of **CITRATE** 1.0 are freely available at: https://github.com/BingzhangChen/citrate under the MIT license.

6.1 General instruction

Tutorial: The code for CITRATE 1.0 (DOI: 10.5281/zenodo.1034805) is written in Fortran90 with the Intel Fortran compiler used. We have tested the codes on macOS Sierra 10.12.5 (i386 processor) and also a GNU/Linux cluster with x86-64 architechture. The user is supposed to be familiar with the Fortran language and has some basic knowledge of BASH. Some post-processing scripts are also written in the free software R (version 3.3.2). Before compiling the codes and running the model, the user needs to install the mpi (e.g. openmpi) library for parallel computation. Below we give some instructions and explanations of the codes and how to run the model.

1) Go to the directory you want to run the model (we assume that the root directory is under home directory: ~/).

2) To download the codes, type: "git clone https://github.com/BingzhangChen/citrate.git".

3) Type: "cd DRAM/NPZDcont/BOTH_TD" to go to the working directory.

4) Type: "vi run" to change the setting for model run:

Test = 0 means a fast run, usually for a formal model run for a large number of iterations. Test = 1 means running a model for debugging, which is much slower than the fast run. The user can also modify the compiler flags depending on the purpose in the script. The user needs to specify the directory where the library of mpifort exists.

删除的内容: .
删除的内容: models
删除的内容: shortcomings
带格式的: 制表符:不在 10.04 字符
删除的内容: .
删除的内容: continuous trait-based models can be built
删除的内容: 1.0
删除的内容: 1.1
删除的内容: e
删除的内容: , for example by accounting for multi-dimensional trait distributions
删除的内容: 1.1
删除的内容: 0
删除的内容: NPZDFeCONT
删除的内容: 1
删除的内容: 0
删除的内容: 999151
删除的内容: 895996
删除的内容: 1. How to run the model: .
删除的内容: confirm

5) Type "./run", the model will compile and an executable (CITRATE) will be generated.

6) Type "vi Model.nml", which contains two namelists. The namelist &Model contains the options for station names, the type of ecological model, the type of nutrient uptake function (1 only for CITRATE), and the type for grazing function (four different grazing functions including the three Holling type functions and the Ivlev function). The station name determines the right physics files to be read and the filenames for model output. For now we only allow three possible stations: S1, K2, and HOT. Other station names will generate an error. If the user wants to add more station names, the subroutine Setup_OBSdata within MOD_1D.f90 is the place to be modified. A number of ecological models besides **CITRATE** have been developed. It is beyond the scope of the present study to describe all of them in detail. Just note that the model lists are in the fortran file bio_MOD.f90 and some other details are in choose_model.f90 and MOD_1D.f90.

The namelist &MCMCrun contains the options for defining the total length of the MCMC chain which is at least 2, the number of the ensemble runs, the number of days for each model run, whether the model should start from previous runs (Readfile = 1) or start a new run (Readfile = 0), and the number of runs in the historical files (enssig and enspar).

7) After defining all the model settings, type “mpirun –np 5 citrate” and then the model will run with 5 parallel processes and some outputs will be shown on the screen. Type “mpirun –np 5 citrate > out” to make the model outputs stored in the “out” file. For each model run, the model saves the current parameters into the “enspar” file and the current values of σ and $SSqE$ into the ‘enssig’ file. In this way, even if the model crashes, the user can pick up the current parameter position and updated parameter covariance matrix. The model also generates the files of best parameters, best σ and $SSqE$ files, best model output files that correspond to observational data, and model output files at daily resolution at each grid after an ensemble run.

For each station, four different physics forcing data including vertical profiles of eddy diffusive coefficients and temperatures, surface PAR and atmospheric dust deposition. We already provided the relevant data for stations S1 and K2. The temporal resolution is one day for the vertical eddy diffusivity and one month for three other types of data.

6.2 Code structure

带格式的：字体：粗体

删除的内容：./

删除的内容：./

带格式的：字体：斜体

带格式的：字体：斜体

删除的内容：*s*

带格式的：字体：斜体

带格式的：字体：斜体

带格式的：缩进：首行缩进： 2.36 字符

删除的内容：The code for **CITRATE** 1.0 is written in Fortran90 with the Intel Fortran compiler used. The running environment is Linux or Unix. The user is supposed to be familiar with the Fortran language.

带格式的：英语(美国)

带格式的：英语(美国)

All the source files including the makefile are stored in the *src* folder. Here we briefly describe the functions of the most important source files:

- Main.f90: The main program for DRAM that calls each subroutine in serial.

- MOD_1D.f90: The major module that sets up and runs the 1D model. The module also generates model output that matches with the observational data.

- Interface_MOD.f90: the module that initializes the absolute and normalized parameter vectors, the covariance matrix of the parameters, the prior parameter values, and the upper and lower parameter boundaries.

- SUB_MOD.f90: the module that calculates sum of squared errors (SSqE) between model outputs and observational data. This module also contains the I/O subroutines that save the parameters, σ, and SSqE for each iteration. It also contains the major subroutine MCMC_adapt that determines whether to accept new parameters, updates covariance matrix, proposes new parameter vectors and calls the subroutine that runs the 1D model with the newly proposed parameters.

- choose_model.f90: the subroutine that defines the number and indices of tracers and the model outputs that need to be written into the output file.

- NPZD_cont.f90: the major biological subroutine for the CITRATE model.

- bio_MOD.f90: the module that declares most of the model names, indices for model input and output variables and parameters.

带格式的： 英语(美国)

带格式的： 两端对齐，行距： 1.5 倍行距

删除的内容： .

Table 1. Fixed parameters of the **CITRATE** 1.0 model.

Symbol	Description	Value	Unit
K_w	Light attenuation coefficient of seawater	0.04^a	m^{-1}
K_{chl}	Light attenuation coefficient of chlorophyll	0.025^a	(mg Chl *a* $m^{-2})^{-1}$
E_p	Activation energy of phytoplankton rates	0.41^b	eV
E_z	Activation energy of heterotrophic rates	0.65^b	eV
θ_{min}	Minimal chlorophyll-to-carbon ratio	0.02^c	gChl $molC^{-1}$
θ_{max}	Maximal chlorophyll-to-carbon ratio	0.47	gChl $molC^{-1}$
$unass_1$	Fraction of unassimilated food by microzooplankton	0.24^d	dimensionless
$unass_2$	Fraction of unassimilated food by mesozooplankton	0.31^e	dimensionless
NGE	Net growth efficiency of zooplankton	0.3^d	dimensionless
R_{dn}	Conversion rate of detritus to inorganic nitrogen	0.1	d^{-1}
l_{fe}	Total iron ligand concentration	0.6^f	nM
K_{scm}	Minimal iron scavenging rate	$5 \times 10^{-3\ f}$	d^{-1}
K_{sc}	Particle dependent scavenging rate	0.03^f	$(\mu M\ N)^{-1}\ d^{-1}$
R_{Fe_N}	Plankton iron-to-nitrogen ratio	0.0265	nM:μM
α_μ	First-order size scaling component for μ_m	0.2^b	$(\ln \mu m^3)^{-1}$
β_μ	Second-order size scaling component for μ_m	-0.01^b	$(\ln \mu m^3)^{-2}$
α_K	Size scaling exponent for K_N	0.27^g	$(\ln \mu m^3)^{-1}$
α_{fer}	Size scaling exponent for K_{fer}	0.27^g	$(\ln \mu m^3)^{-1}$
Q_{0N}	Phytoplankton minimal N:C ratio	0.06	mol N: mol C
$g_{max,1}$	Maximal microzooplankton specific ingestion rate for phytoplankton of 1.24 μm (1 μm^3) at 15 ºC	1.35^h	d^{-1}
$g_{max,2}$	Maximal mesozooplankton specific ingestion rate for phytoplankton of 10 μm at 15 ºC	0.53^h	d^{-1}
$K_{p,2}$	Grazing half-saturation constant of mesozooplankton	0.5^h	μM N
b_1	Size-dependent feeding selectivity of microzooplankton	-0.05	$(\ln \mu m^3)^{-1}$
b_2	Size-dependent feeding selectivity of mesozooplankton	0.02	$(\ln \mu m^3)^{-1}$

[a]Fennel et al., (2006); [b]Chen and Laws, (2017); [c]Flynn, (2003); [d]Buitenhuis et al., (2010); [e]Buitenhuis et al. (2006); [f]Nickelsen et al., (2015); [g]Ward et al., (2012); [h]Chai et al., (2002).

删除的内容: including units and values

删除的内容: 1.0

删除的内容: 1.1

带格式的: 行距: 1.5 倍行距

删除的内容: 5

删除的内容: 5

删除的内容: *Unass*

删除的内容: K_p ... ...

删除的内容:

删除的内容: ^{d}

删除的内容: 3

删除的内容: ^{5}

删除的内容: ^{d}

删除的内容: ^{d}

带格式的: 上标

带格式的: 行距: 1.5 倍行距

带格式的: 上标

带格式的: 上标

Table 2. Parameters optimized by the DRAM algorithm. The values inside the parentheses of the initial values indicate the “hard” boundaries for the parameters. The numbers inside the parentheses of the optimized values indicate the standard deviation after the first 10000 iterations have been removed.

Symbol	Description	Initial	Optimized	Unit
W_d	Sinking rate of detritus	4 (1, 20)	19.6 (1.0)	m d^{-1}
K_p	Grazing half-saturation constant of microzooplankton	0.5 (0.05, 2)	0.28 (0.01)	μM N
m_z	Coefficient of mortality rate of mesozooplankton	0.1 (0.05, 0.2)	0.20 (0.002)	$(\mu M\ N)^{-1}\ d^{-1}$
$\alpha_{0,c}$	Initial slope of photosynthesis versus light at 1 μm^3	0.055[a] (0.01, 0.1)	0.05 (0.004)	$(W\ m^{-2})^{-1}\ d^{-1}$
α_I	Size scaling exponent for α_c	-0.1 (–0.3, 0.1)	-0.26 (0.01)	$(\ln \mu m^3)^{-1}$
$K_{0,N}$	Growth half-saturation constant for nitrogen for a phytoplankton cell of 1 μm^3	0.2[b] (0.05, 0.5)	0.29 (0.03)	μM N
$\mu'_{0,m}$	Phytoplankton maximal growth rate at 1 μm^3 at 15 ºC	1.2[c] (0.3, 2.7)	0.85 (0.05)	d^{-1}
$K_{0,fer}$	Growth half-saturation constant for iron of phytoplankton with 1 μm^3	0.08[d] (0.02, 0.2)	0.17 (0.02)	nM Fe
u	Trait diffusion parameter	0.08[e] (0, 0.1)	0.1 (0.0008)	$d^{-1}\ (\ln \mu m^3)^{-2}$

[a]Fennel et al., (2006); [b]Ward et al., (2012); [c]Flynn et al., (2016); [d]Gregg et al., (2003); [e]Merico et al., (2014)

删除的内容: “burn-in” period…(…02…00 iterations)…have

删除的内容: 1…(0.0…, 21

删除的内容: 3.3…(1.00.3

删除的内容: Q_{0N}

删除的内容: 3

删除的内容: 094…(0.00202

删除的内容: [b]

删除的内容: 19…(0.00413

删除的内容: 0.08…(–0.3, 0.12

删除的内容: 0.097…(0.01017

删除的内容: dimensionless

删除的内容: 5…(0.0501… 0.53

删除的内容: 0.89…(0.031

删除的内容: α_K

删除的内容: [d]…(0.3, 2.73

删除的内容: 1.34…(0.0518

删除的内容: α_μ

删除的内容: [f]…(0.024

删除的内容: 058…(0.00…1

删除的内容: α_{fer}

删除的内容: [g]…(0.01… 0.12

删除的内容: 092…(0.00…0816

删除的内容: dimensionless

删除的内容: *dustso*

带格式的: 字体:小五, 西班牙语

删除的内容: Marañón et al., (2013); [b]…ennel et al., (2006);

带格式的: 西班牙语

Table 3. Observational data at stations S1 and K2. N: number of observations. Min and Max are minimal and maximal values used in data normalization (*see* Sect. 2.4 for details). DIN: dissolved inorganic nitrogen (μmol L^{-1}). Chl *a*: total chlorophyll a concentration (μg L^{-1}). NPP: net primary production measured by ^{13}C uptake (μgC L^{-1} d^{-1}). PON: particulate organic nitrogen (μmol L^{-1}). Fer: dissolved iron concentration (nmol L^{-1}). SF Chl: percentages of four size fractionated Chl *a*. Note that the data of Fer were from model outputs of Aumont et al., (2003) instead of real observations.

删除的内容: TIN

	K2			S1		
Type	N	Min	Max	N	Min	Max
DIN	974	4.1	45.7	902	0	11.2
Chl *a*	470	0	3.4	426	0	1.0
NPP	112	0.1	37.1	128	0.1	34.9
PON	29	0.1	2.2	32	0.1	1.0
Fer	168	0.02	1.12	168	0.02	0.95
SF Chl	143 x 4	0	1.0	166 x 4	0	1.0

删除的内容: TIN

Table 4. Sum of squared errors between model outputs and observational data for sensitive analysis. The standard run used the optimized parameter values in Table 2. In other runs, only the value of the parameter shown was changed while others were kept constant.

	Stn	DIN	CHL	NPP	PON	%3–10 µm	%1–3 µm	%<1 µm
Standard	K2	21.5	8.1	3.0	0.92	3.6	7.3	13.3
	S1	11.2	16.5	6.7	1.5	4.9	4.0	4.1
$\mu'_{0,m} = 0.4$	K2	19.7	11.6	5.4	0.86	6.7	7.1	23.4
	S1	13.2	12.8	6.6	1.3	4.4	4.3	16.3
$W_d = 10$	K2	15.3	8.1	3.0	1.1	3.6	7.3	13.4
	S1	17.8	12.7	4.6	1.0	2.9	4.6	6.6
$\alpha_I = 0$	K2	167.3	35.8	11.8	2.0	10.4	8.6	36.4
	S1	13.0	16.1	6.1	1.8	22.0	5.4	56.4
$m_z = 0.1$	K2	523.8	17.6	8.0	1.9	12.9	6.5	11.3
	S1	11.5	17.7	7.4	1.6	9.1	2.9	3.0
$\mu = 0.05$	K2	22.2	8.3	3.2	0.94	4.7	8.5	15.4
	S1	11.1	16.9	6.8	1.6	11.0	4.2	4.0

带格式的: 字体:非 粗体
带格式的: 行距: 双线
带格式的: 字体:非 粗体
带格式的: 字体:五号
带格式的: 空格 段前: 0 磅
带格式表格
带格式的: 字体:五号
带格式的: 空格 段前: 0 磅
带格式的: 字体:五号
带格式的: 空格 段前: 0 磅
带格式的: 左对齐, 空格 段前: 0 磅
带格式的: 字体:五号
带格式的: 空格 段前: 0 磅
带格式的: 字体:五号
带格式的: 空格 段前: 0 磅
带格式的: 字体:五号
带格式的: 空格 段前: 0 磅
带格式的: 字体:五号
带格式的: 空格 段前: 0 磅
带格式的: 字体:五号
带格式的: 空格 段前: 0 磅
带格式的: 字体:五号
带格式的: 空格 段前: 0 磅
带格式的: 字体:五号
带格式的: 空格 段前: 0 磅
带格式的: 字体:五号
带格式的: 空格 段前: 0 磅
带格式的: 字体:五号
带格式的: 空格 段前: 6 磅
带格式的: 字体:五号, (中文) 日语, (其他) 英语(美国)
带格式的: 字体:五号
带格式的: 字体:五号
带格式的: 空格 段前: 6 磅
删除的内容: .

Author contribution

B. Chen and S. L. Smith conceived and designed the study. S. L. Smith wrote the initial code of Adaptive Metrapolis-Hasting Monte Carlo algorithm. B. Chen acquired and organized the observational data, did subsequent coding, and wrote the first draft of the manuscript. Both authors contributed to later revision of the manuscript.

删除的内容: MCMC

Competing interests

The authors declare that they have no conflict of interest.

Acknowledgments

删除的内容: .

We sincerely thank S. Vallina, E. Acevedo-Trejos, and C. Carcia-Comas for useful discussions. The comments from the editor and three anonymous reviewers have substantially improved an earlier draft of the manuscript. This study would not be possible without the cruise data shared by the K2S1 project personnel, particularly M. C. Honda, T. Fujiki, and K. Matsumoto. We also sincerely thank T. Hashioka for sharing the data of vertical eddy diffusivity. This study is supported by CREST (Grant Number JPMJCR12A3; P.I. SLS) funded by the Japan Science and Technology (JST) Agency and a Grants-in-Aid for Scientific Research (KAKENHI) (Grant Number JP16K21701; P.I. BC) funded by Japan Society for the Promotion of Science (JSPS).

删除的内容: We sincerely thank

删除的内容: , for sharing the cruise data

References

Acevedo-Trejos, E., Brandt, G., Bruggeman, J. and Merico, A., Mechanisms shaping size structure and functional diversity of phytoplankton communities in the ocean, Sci. Rep., 5, 8918, doi: 10.1038/srep08918, 2015.

Acevedo-Trejos, E., Brandt, G., Smith, S. L. and Merico, A., PhytoSFDM version 1.0. 0: Phytoplankton Size and Functional Diversity Model, Geosci. Model Dev., 9, 4071–4085, doi: 10.5194/gmd-9-4071-2016, 2016.

Allen, A. P., Li, B. L. and Charnov, E. L.: Population fluctuations, power laws and mixtures of lognormal distributions, Ecol. Let., 4, 1–3, 2001.

Allen, A.P., Gillooly, J.F., Savage, V.M. and Brown, J.H.: Kinetic effects of temperature on rates of genetic divergence and speciation. Proc. Nat. Acad. Sci., 103, 9130-9135, 2006.

Annan, J. D., and Hargreaves, J. C.: Efficient estimation and ensemble generation in climate modelling. Phil. Trans. R. Soc. A, 365, 2077–2088, 2007.

Aumont, O., Maier-Reimer, E., Blain, S., and Monfray, P.: An ecosystem model of the global ocean including Fe, Si, P colimitations. Global Biogeochem. Cycles, 17, 1060, doi:10.1029/2001GB001745, 2003.

Bak, P.: How nature works: the science of self-organized criticality, New York: Copurnicus, 1996.

Banas, N. S: Adding complex trophic interactions to a size-spectral plankton model: Emergent diversity patterns and limits on predictability, Ecol. Mod., 222, 2663–2675, 2011.

Behrenfeld, M. J.: Abandoning Sverdrup's critical depth hypothesis on phytoplankton blooms, Ecology, 91, 977–989, 2010.

Behrenfeld, M. J. and Boss, E. S.: Resurrecting the ecological underpinnings of ocean plankton blooms, Ann. Rev. Mar. Sci., 6, 167–194, 2014.

Behrenfeld, M. J., Worthington, K., Sherrell, R. M., Chavez, F. P., Strutton, P., McPhaden, M., and Shea, D. M.: Controls on tropical Pacific Ocean productivity revealed through nutrient stress diagnostics, Nature, 442, 1025–1028, 2006.

带格式的: 字体:非 斜体

带格式的: 字体:非 斜体

Biller, S. J., Berube, P. M., Lindell, D. and Chisholm, S. W.: *Prochlorococcus*: the structure and function of collective diversity, Nat. Rev. Microb., 13, 13-27, 2015.

Bonachela, J. A., Klausmeier, C. A., Edwards, K. F., Litchman, E. and Levin, S. A.: The role of phytoplankton diversity in the emergent oceanic stoichiometry, J. Plankton Res., 38, 1021–1035, 2016.

Bruggeman, J.: Succession in plankton communities: A trait-based perspective, Ph.D. thesis, 160 pp, 2009.

Buitenhuis, E., Le Quéré, C., Aumont, O., Beaugrand, G., Bunker, A., Hirst, A., Ikeda, T., O'Brien, T., Piontkovski, S. and Straile, D.: Biogeochemical fluxes through mesozooplankton, Global Biogeochem. Cycles, 20, GB2003, doi:10.1029/2005GB002511, 2006.

Buitenhuis, E. T., Rivkin, R. B., Sailley, S., and Le Quéré, C.: Biogeochemical fluxes through microzooplankton, Global Biogeochem. Cycles, 24, GB4015, doi:10.1029/2009GB003601, 2010.

Calderhead, B.: A general construction for parallelizing Metropolis− Hastings algorithms, Proc. Nat. Acad. Sci., 111, 17408–17413, 2014.

Campbell, L., Nolla, H. A. and Vaulot, D.: The importance of *Prochlorococcus* to community structure in the central North Pacific Ocean, Limnol. Oceanogr., 39, 954–961, 1994.

Cavender-Bares, K. K., Rinaldo, A. and Chisholm, S.W.: Microbial size spectra from natural and nutrient enriched ecosystems, Limnol. Oceanogr., 46, 778–789, 2001.

Cermeño, P., Marañón, E., Harbour, D. and Harris, R. P.: Invariant scaling of phytoplankton abundance and cell size in contrasting marine environments, Ecol. Let., 9, 1210–1215, 2006.

Chai, F., Dugdale, R. C., Peng, T. H., Wilkerson, F. P. and Barber, R. T.: One-dimensional ecosystem model of the equatorial Pacific upwelling system. Part I: model development and silicon and nitrogen cycle, Deep Sea Res. II, 49, 2713–2745, 2002.

Chavez, F. P., Messié, M. and Pennington, J. T.: Marine primary production in relation to climate variability and change, Ann. Rev. Mar. Sci., 3, 227–260, 2011.

Chen, B., and Laws, E. A.: Is there a difference of temperature sensitivity between marine phytoplankton and heterotrophs? Limnol. Oceanogr., 62, 806–817, doi: 10.1002/lno.10462, 2017.

带格式的: 字体:斜体

带格式的: 字体:非 斜体

带格式的: 字体:非 斜体

带格式的: 字体:非 斜体

带格式的: 字体:非 斜体

删除的内容: ,

删除的内容: .

带格式的: 字体:非 斜体

带格式的: 字体:非 斜体

带格式的: 字体:非 斜体

带格式的: 字体:非 斜体

Chen, B., and Liu, H.: Comment: Unimodal relationship between phytoplankton mass–specific growth rate and size: A reply to the comment by Sal and López-Urrutia (2011), Limnol. Oceanogr., 56, 1956–1958, 2011.

Chen, B., and Liu, H.: Relationships between phytoplankton growth and cell size in surface oceans: Interactive effects of temperature, nutrients, and grazing, Limnol. Oceanogr., 55, 965–972, 2010.

Chen, B.: Patterns of thermal limits of phytoplankton, J. Plankton Res., 37, 285–292, 2015.

Chen, B., Liu, H., Landry, M. R., Dai, M., Huang, B. and Sun, J.: Close coupling between phytoplankton growth and microzooplankton grazing in the western South China Sea, Limnol. Oceanog., 54, 1084-1097, 2009.

Chesson, P.: Mechanisms of maintenance of species diversity, Ann. Rev. Ecol. Syst., 31, 343–366, 2000.

Chisholm, S.W., Olson, R. J., Zettler, E. R., Goericke, R., Waterbury, J. B. and Welschmeyer, N.A.: A novel free-living prochlorophyte abundant in the oceanic euphotic zone, Nature, 334, 340–343, 1988.

Christian, J. R.: Biogeochemical cycling in the oligotrophic ocean: Redfield and non-Redfield models, Limnol. Oceanogr., 50, 646–657, 2005.

Clauset, A., Shalizi, C. R. and Newman, M. E.: Power-law distributions in empirical data, SIAM review, 51, 661–703, 2009.

Coutinho, R.M., Klauschies, T. and Gaedke, U.: Bimodal trait distributions with large variances question the reliability of trait-based aggregate models, Theor. Ecol., 9, 389–408, 2016.

Dowle, E. J., Morgan-Richards, M., and Trewick, S. A.: Molecular evolution and the latitudinal biodiversity gradient, Heredity, 110, 501–510, 2013.

Edwards, K.F., Klausmeier, C.A. and Litchman, E.: Evidence for a three-way trade-off between nitrogen and phosphorus competitive abilities and cell size in phytoplankton. Ecology, 92, 2085–2095, 2011.

Edwards, K. F., Thomas, M. K., Klausmeier, C. A. and Litchman, E.: Light and growth in marine phytoplankton: allometric, taxonomic, and environmental variation, Limnol. Oceanogr., 60, 540–552, 2015.

删除的内容: .

Edwards, K. F., Thomas, M. K., Klausmeier, C.A. and Litchman, E.: Allometric scaling and taxonomic variation in nutrient utilization traits and maximum growth rate of phytoplankton. Limnol. Oceanogr., 57, 554–566, 2012.

Falkowski, P.: Ocean science: the power of plankton, Nature, 483, S17–S20, 2012.

Fennel, K. and Boss, E.: Subsurface maxima of phytoplankton and chlorophyll: Steady-state solutions from a simple model. Limnol. Oceanogr., 48, 1521–1534, 2003.

Fennel, K., Wilkin, J., Levin, J., Moisan, J., O'Reilly, J. and Haidvogel, D., Nitrogen cycling in the Middle Atlantic Bight: Results from a three-dimensional model and implications for the North Atlantic nitrogen budget, Global Biogeochem. Cycles, 20, GB3007, doi:10.1029/2005GB002456, 2006.

Fernández-Castro, B., Pahlow, M., Mouriño-Carballido, B., Marañón, E. and Oschlies, A.: Optimality-based *Trichodesmium* diazotrophy in the North Atlantic subtropical gyre, J. Plankton Res., 38, 946–963, doi: 10.1093/plankt/fbw047, 2016.

Finkel, Z. V.: Light absorption and size scaling of light-limited metabolism in marine diatoms, Limnol. Oceanogr., 46, 86–94, 2001.

Finkel, Z. V.: Does phytoplankton cell size matter? The evolution of modern marine food webs (pp. 333-350). Boston, Elsevier, 2007.

Finkel, Z. V., Beardall, J., Flynn, K. J., Quigg, A., Rees, T. A. V. and Raven, J. A.: Phytoplankton in a changing world: cell size and elemental stoichiometry, J. Plankton Res., 32, 119–137, 2010.

Flynn, K. J.: Do we need complex mechanistic photoacclimation models for phytoplankton? Limnol. Oceanogr., 48, 2243–2249, 2003.

Flynn, K.J. and Raven, J.A.: What is the limit for photoautotrophic plankton growth rates? J. Plankton Res., doi:10.1093/plankt/fbw067, 2016.

Franks, P.J.: Has Sverdrup's critical depth hypothesis been tested? Mixed layers vs. turbulent layers. ICES J. Mar. Sci., 72, 1897–1907, 2015.

Follows, M. J., Dutkiewicz, S., Grant, S., and Chisholm, S. W.: Emergent biogeography of microbial communities in a model ocean. Science, 315, 1843–1846, 2007.

Follows, M. J., and Dutkiewicz, S.: Modeling diverse communities of marine microbes, Ann. Rev. Mar. Sci. 3, 427-451, 2011.

Frost, B. W.: Effects of size and concentration of food particles on the feeding behavior of the marine planktonic copepod *Calanus pacificus*. Limnol. Oceanogr., 17, 805–815, 1972.

Fujiki, T., Matsumoto, K., Mino, Y., Sasaoka, K., Wakita, M., Kawakami, H., Honda, M. C., Watanabe, S., and Saino, T.: Seasonal cycle of phytoplankton community structure and photophysiological state in the western subarctic gyre of the North Pacific. Limnol. Oceanogr., 59, 887–900, 2014.

Fujiki, T., Sasaoka, K., Matsumoto, K., Wakita, M., and Mino, Y.: Seasonal variability of phytoplankton community structure in the subtropical western North Pacific, J. Oceanogr., 72, 343–358, 2016.

Gelman, A., Carlin, J. B., Stern, H. S., and Rubin, D. B.: Bayesian data analysis (Vol. 2), Boca Raton, FL, USA, Chapman & Hall/CRC, 2014.

Geider, R. J., MacIntyre, H. L. and Kana, T. M.: Dynamic model of phytoplankton growth and acclimation: responses of the balanced growth rate and the chlorophyll a: carbon ratio to light, nutrient-limitation and temperature, Mar. Ecol. Prog. Ser., 148, 187–200, 1997.

Gin, K. Y., Chisholm, S.W. and Olson, R. J.: Seasonal and depth variation in microbial size spectra at the Bermuda Atlantic time series station, Deep Sea Res, I, 46, 1221–1245, 1999.

Gregg, W. W., Ginoux, P., Schopf, P. S. and Casey, N.W.: Phytoplankton and iron: validation of a global three-dimensional ocean biogeochemical model, Deep Sea Res. II, 50, 3143–3169, 2003.

Haario, H., Saksman, E., and Tamminen, J.: An adaptive Metropolis algorithm, Bernoulli, 7, 223–242, 2001.

Haario, H., Laine, M., Mira, A. and Saksman, E.: DRAM: efficient adaptive MCMC, Stat. Comput., 16, 339–354, 2006.

Hansen, B., Bjornsen, P. K. and Hansen, P. J.: The size ratio between planktonic predators and their prey, Limnol. Oceanogr., 39, 395-403, 1994.

Hashioka, T., Sakamoto, T.T., and Yamanaka, Y.: Potential impact of global warming on North Pacific spring blooms projected by an eddy-permitting 3-D ocean ecosystem model, Geophys. Res. Let., 36, L20604, doi:10.1029/2009GL038912, 2009.

删除的内容: .

带格式的: 字体:非 斜体

带格式的: 字体:非 斜体

带格式的: 字体:非 斜体

带格式的: 字体:非 斜体

带格式的: 字体:非 斜体

删除的内容: .

删除的内容: .

Hashioka, T., Vogt, M., Yamanaka, Y., Le Quere, C., Buitenhuis, E.T., Aita, M.N., Alvain, S., Bopp, L., Hirata, T., Lima, I.D. and Sailley, S. F.: Phytoplankton competition during the spring bloom in four plankton functional type models, Biogeosciences, 10, 6833–6850, doi: 10.5194/bg-10-6833-2013, 2013.

Honda, M. C.: Short introduction to the K2S1 project, J. Oceanogr., 72, 341–342, 2016.

Huston, M.: A general hypothesis of species diversity, Am. Nat., 113, 81–101, 1979.

Johnson, Z. I., Zinser, E. R., Coe, A., McNulty, N. P., Woodward, E. M. S., and Chisholm, S. W.: Niche partitioning among *Prochlorococcus* ecotypes along ocean-scale environmental gradients, Science 311, 1737–1740, 2006.

Khatiwala, S.: A computational framework for simulation of biogeochemical tracers in the ocean, Global Biogeochem. Cycles, 21, GB3001, doi:10.1029/2007GB002923, 2007.

Kriest, I., Sauerland, V., Khatiwala, S., Srivastav, A. and Oschlies, A.: Calibrating a global three-dimensional biogeochemical ocean model (MOPS-1.0), Geosc. Model Dev., 10, 127-154, 2017.

Kooistra, W. H., Sarno, D., Balzano, S., Gu, H., Andersen, R. A., and Zingone, A.: Global diversity and biogeography of *Skeletonema* species (Bacillariophyta), Protist, 159, 177-193, 2008.

Laine, M.: Adaptive MCMC methods with applications in environmental and geophysical models, Ph.D. thesis, 48 pp, Finnish Meteorological Institute, 2008.

Latasa, M., Landry, M. R., Louise, S. and Bidigare, R. R.: Pigment specific growth and grazing rates of phytoplankton in the central equatorial Pacific, Limnol. Oceanogr., 42, 289–298, 1997.

Large, W. G., McWilliams, J. C., and Doney, S. C., Oceanic vertical mixing: A review and a model with a nonlocal boundary layer parameterization, Rev. Geophys., 32, 363–403, 1994.

Le Quéré, C., Harrison, S. P., Prentice, I. C., Buitenhuis, E. T., Aumont, O., Bopp, L., Claustre, H., et al.: Ecosystem dynamics based on plankton functional types for global ocean biogeochemistry models, Global Change Biol., 11, 2016–2040, 2005.

Litchman, E., and Klausmeier, C.A.: Trait-based community ecology of phytoplankton, Ann. Rev. Ecol. Evol. Syst., 39, 615–639, 2008.

删除的内容: .

带格式的: 字体:非 斜体

带格式的: 字体:非 斜体

带格式的: 字体:非 斜体

删除的内容: .

删除的内容: .

Liu, H., Nolla, H. A., and Campbell, L.: *Prochlorococcus* growth rate and contribution to primary production in the equatorial and subtropical North Pacific Ocean, Aquat. Microb. Ecol., 12, 39–47, 1997.

Liu, H., Dagg, M. J., and Strom, S.: Grazing by the calanoid copepod Neocalanus cristatus on the microbial food web in the coastal Gulf of Alaska, J. Plankton Res., 27, 647–662, 2005.

Loreau, M., Naeem, S., Inchausti, P., Bengtsson, J., Grime, J. P., Hector, A., Hooper, D. U., Huston, M. A., Raffaelli, D., Schmid, B. and Tilman, D.: Biodiversity and ecosystem functioning: current knowledge and future challenges, Science, 294, 804-808, 2001.

Luo, C., Mahowald, N., Bond, T., Chuang, P. Y., Artaxo, P., Siefert, R., Chen, Y., and Schauer, J.: Combustion iron distribution and deposition, Global Biogeochem. Cycles, 22, GB1012, doi:10.1029/2007GB002964, 2008.

Maranón, E., Cermeño, P., Latasa, M., and Tadonléké, R.D.: Temperature, resources, and phytoplankton size structure in the ocean, Limnol. Oceanogr., 57, 1266–1278, 2012.

Marañón, E., Cermeño, P., López-Sandoval, D. C., Rodríguez-Ramos, T., Sobrino, C., Huete-Ortega, M., Blanco, J. M., and Rodríguez, J.: Unimodal size scaling of phytoplankton growth and the size dependence of nutrient uptake and use, Ecol. Let., 16, 371–379, 2013.

Marañón, E.: Cell size as a key determinant of phytoplankton metabolism and community structure, Ann. Rev. Mar. Sci., 7, 241–264, 2015.

Masuda, Y., Yamanaka, Y., Hirata, T. and Nakano, H.: Competition and community assemblage dynamics within a phytoplankton functional group: Simulation using an eddy-resolving model to disentangle deterministic and random effects, Ecol. Mod., 343, 1–14, 2017.

Matsumoto, K., Honda, M. C., Sasaoka, K., Wakita, M., Kawakami, H., and Watanabe, S., Seasonal variability of primary production and phytoplankton biomass in the western Pacific subarctic gyre: control by light availability within the mixed layer, J. Geophys. Res. Oceans, 119, 6523–6534, 2014.

Matsumoto, K., Abe, O., Fujiki, T., Sukigara, C. and Mino, Y., Primary productivity at the time-series stations in the northwestern Pacific Ocean: is the subtropical station unproductive? J. Oceanogr., 72, 359–371, 2016.

带格式的: 字体:非 斜体
带格式的: 字体:非 斜体
带格式的: 字体:非 斜体

带格式的: 字体:非 斜体
带格式的: 字体:非 斜体

带格式的: 字体:非 斜体
带格式的: 字体:非 斜体
带格式的: 字体:非 斜体

删除的内容: .

带格式的: 字体:非 斜体
带格式的: 字体:非 斜体
带格式的: 字体:非 斜体
带格式的: 字体:非 斜体
带格式的: 字体:非 斜体

Merico, A., Brandt, G., Smith, S. L., and Oliver, M.: Sustaining diversity in trait-based models of phytoplankton communities, Front. Ecol. Evol., 2, 59, doi: 10.3389/fevo.2014.00059, 2014.

Merico, A., Bruggeman, J., and Wirtz, K.: A trait-based approach for downscaling complexity in plankton ecosystem models, Ecol. Mod., 220, 3001–3010, 2009.

Mitzenmacher, M.: A brief history of generative models for power law and lognormal distributions, Internet Math., 1, 226–251, 2004.

Mira, A.: On Metropolis-Hastings algorithms with delayed rejection, Metron, 59, 231–241, 2001.

Moon-van der Staay, S. Y., De Wachter, R., and Vaulot, D.: Oceanic 18S rDNA sequences from picoplankton reveal unsuspected eukaryotic diversity, Nature, 409, 607–610, 2001.

Moore, L. R., Rocap, G., Chisholm, S. W.: Physiology and molecular phylogeny of coexisting *Prochlorococcus* ecotypes, Nature, 393, 464–467, 1998.

Newman, M. E. J.: Power laws, Pareto distributions and Zipf's law, Contemp. Phys., 46, 323–351, 2005.

Nickelsen, L., Keller, D. and Oschlies, A.: A dynamic marine iron cycle module coupled to the University of Victoria Earth System Model: the Kiel Marine Biogeochemical Model 2 for UVic 2.9, Geosci. Model Dev., 8, 1357–1381, doi:10.5194/gmd-8-1357-2015, 2015.

Norberg, J., Swaney, D. P., Dushoff, J., Lin, J., Casagrandi, R., and Levin, S. A.: Phenotypic diversity and ecosystem functioning in changing environments: a theoretical framework, Proc. Nat. Acad. Sci., 98, 11376–11381, 2001.

Norberg, J.: Biodiversity and ecosystem functioning: a complex adaptive systems approach, Limnol. Oceanogr., 49, 1269–1277, 2004.

Palenik, B., Ren, Q., Dupont, C. L., Myers, G. S., Heidelberg, J. F., Badger, J. H., Madupu, R., et al.: Genome sequence of *Synechococcus* CC9311: insights into adaptation to a coastal environment, Proc. Nat. Acad. Sci., 103, 13555–13559, 2006.

Poulin, F. J. and Franks, P. J.: Size-structured planktonic ecosystems: constraints, controls and assembly instructions, J. Plankton Res., 32, 1121–1130, 2010.

带格式的: 字体:非 斜体

带格式的: 字体:非 斜体

带格式的: 字体:非 斜体

带格式的: 字体:非 斜体

带格式的: 字体:非 斜体

Quintana, X. D., Brucet, S., Boix, D., López- Flores, R., Gascón, S., Badosa, A., Sala, J., Moreno-Amich, R. and Egozcue, J. J.: A nonparametric method for the measurement of size diversity with emphasis on data standardization, Limnol. Oceanogr. Methods, 6, 75–86, 2008.

Quintana, X. D., Egozcue, J. J., Martínez-Abella, O., López-Flores, R., Gascón, S., Brucet, S. and Boix, D.: Update: A non-parametric method for the measurement of size diversity, with emphasis on data standardization. The measurement of the size evenness. Limnol. Oceanogr. Methods, 14, 408–413, 2016.

Rohde, K.: Latitudinal gradients in species diversity: the search for the primary cause, Oikos, 65, 514–527, 1992.

Rosenzweig, M. L.: Species diversity in space and time, Cambridge University Press, 1995.

Sasai, Y., Yoshikawa, C., Smith, S. L., Hashioka, T., Matsumoto, K., Wakita, M., Sasaoka, K. and Honda, M. C., Coupled 1-D physical–biological model study of phytoplankton production at two contrasting time-series stations in the western North Pacific, J. Oceanogr., 72, 509–526, 2016.

Shchepetkin, A. F., and McWilliams, J. C., The regional oceanic modeling system (ROMS): a split-explicit, free-surface, topography-following-coordinate oceanic model, Ocean Mod., 9, 347–404, 2005.

Shigemitsu, M., Okunishi, T., Nishioka, J., Sumata, H., Hashioka, T., Aita, M. N., Smith, S. L., Yoshie, N., Okada, N. and Yamanaka, Y., Development of a one-dimensional ecosystem model including the iron cycle applied to the Oyashio region, western subarctic Pacific, J. Geophys. Res., 117, C06021, doi:10.1029/2011JC007689, 2012.

Smith, S. L., Vallina, S. M., and Merico, A.: Phytoplankton size-diversity mediates an emergent trade-off in ecosystem functioning for rare versus frequent disturbances. Sci. Rep., 6, 34170, doi: 10.1038/srep34170, 2016.

Sournia, A., Chrdtiennot-Dinet, M-J., Ricard, M.: Marine phytoplankton: how many species in the world ocean? J. Plankton Res. 13, 1093–1099, 1991.

Strzepek, R. F., and Harrison, P. J.: Photosynthetic architecture differs in coastal and oceanic diatoms, Nature, 431, 689–692, 2004.

带格式的: 字体:非 斜体

带格式的: 字体:非 斜体

带格式的: 字体:非 斜体

带格式的: 字体:非 斜体

带格式的: 英语(美国)

带格式的: 英语(美国)

带格式的: 英语(美国)

Terseleer, N., Bruggeman, J., Lancelot, C. and Gypens, N.: Trait-based representation of diatom functional diversity in a plankton functional type model of the eutrophied southern North Sea. Limnol. Oceanogr., 59, 1958–1972, 2014.

Thomas, M. K., Kremer, C. T., Klausmeier, C. A., and Litchman, E.: A global pattern of thermal adaptation in marine phytoplankton, Science, 338, 1085–1088, 2012.

Tilman, D.: Resource competition and community structure, Princeton university press, 1982.

Tilman, D., Isbell, F., and Cowles, J. M., Biodiversity and ecosystem functioning. Ann. Rev. Ecol. Evol. Syst., 45, 471–493, 2014.

Tilman, D., Lehman, C. L., and Thomson, K. T.: Plant diversity and ecosystem productivity: theoretical considerations. Proc. Nat. Acad. Sci., 94, 1857–1861, 1997.

Vallina, S. M., Follows, M. J., Dutkiewicz, S., Montoya, J. M., Cermeno, P. and Loreau, M.: Global relationship between phytoplankton diversity and productivity in the ocean, Nat. Commun., 5, 4299, doi: 10.1038/ncomms5299, 2014.

Villagran, A., Huerta, G., Jackson, C. S. and Sen, M. K.: Computational methods for parameter estimation in climate models, Bayesian Analysis, 3, 823-850, 2008.

Villareal, T. A.: Abundance of the giant diatom *Ethmodiscus* in the southwest Atlantic Ocean and central Pacific gyre, Diatom Res., 8, 171–177, 1993.

Villareal, T.A., Pilskaln, C., Brzezinski, M., Lipschultz, F., Dennett, M. and Gardner, G.B.: Upward transport of oceanic nitrate by migrating diatom mats, Nature, 397, 423–425, 1999.

Wakita, M., Honda, M. C., Matsumoto, K., Fujiki, T., Kawakami, H., Yasunaka, S., Sasai, Y., Sukigara, C., Uchimiya, M., Kitamura, M. and Kobari, T.: Biological organic carbon export estimated from the annual carbon budget observed in the surface waters of the western subarctic and subtropical North Pacific Ocean from 2004 to 2013, J. Oceanogr., 72, 665-685, 2016.

Ward, B.A., Friedrichs, M.A., Anderson, T.R. and Oschlies, A.: Parameter optimisation techniques and the problem of underdetermination in marine biogeochemical models, J. Mar. Sys., 81, 34-43, 2010.

Ward, B.A., Dutkiewicz, S., Jahn, O. and Follows, M.J.: A size-structured food-web model for the global ocean, Limnol. Oceanogr., 57, 1877-1891, 2012.

删除的内容: Tegen, I., and Fung, I., Contribution to the atmospheric mineral aerosol load from land surface modification, J. Geophys. Res.: Atmospheres, 100(D9), 18707-18726, 1995.

带格式的: 字体:非 斜体

带格式的: 字体:非 斜体

带格式的: 字体:非 斜体

Welschmeyer, N. A.: Fluorometric analysis of chlorophyll a in the presence of chlorophyll b and pheopigments, Limnol. Oceanogr., 39, 1985–1992, 1994.

Wirtz, K. W., and Eckhardt, B.: Effective variables in ecosystem models with an application to phytoplankton succession, Ecol. Mod., 92, 33–53, 1996.

Zhou, L., Tan, Y., Huang, L. and Li, G.: Does microzooplankton grazing contribute to the pico-phytoplankton dominance in subtropical and tropical oligotrophic waters? Acta Ecol. Sin., 35, 29–38, 2015.

带格式的: 英语(美国)

Figure captions

Fig. 1. Schematic description of the CITRATE model. Thick arrows indicate nitrogen flows and dashed lines indicate the simplified iron cycle. The inset denotes an example of phytoplankton community with a lognormal distribution for cell volume.

Fig. 2. (a) Locations of the three stations, K2, S1 and ALOHA, overlaid on annual Chl *a* climatology of the North Pacific. (b-e) Seasonal forcing of vertical eddy diffusivity (K_v), temperature, surface PAR, and atmospheric dust deposition, respectively, at station S1. The white squares are measured mixed layer depths from *in situ* temperature and salinity profiles. The thick tan line represents mixed layer depths calculated from a threshold of 10^{-4} m^2 s^{-1}. (f-i) The same as (b-e), but for station K2. (j-m) The same as (b-e), but for station ALOHA.

Fig. 3. An example of modelled patterns of total inorganic nitrogen (DIN), Chl *a* (Chl), mean size, and ln size variance for four years at stations K2 (a-d) and S1 (e-h).

Fig. 4. (a) Time evolution of log-likelihood of the MHMC chain. (b-i) Time evolution of sum of squared errors (*SSqE*) for DIN, Chl, net primary production (NPP), particulate organic nitrogen (PON), and fractions of size-fractionated Chl *a* concentrations of > 10 μm (P10), 3–10 μm (P03), 1–3 μm (P01), and <1 μm (P_1). (j-q) The same as (b-j), but for station S1.

Fig. 5. Time evolution of fitted model parameters.

Fig. 6. Model fittings to vertical profiles of (a-d) DIN, (e-h) CHL, (i-l) NPP, and (m-p) PON at four seasons at station K2. Black dots represent observational data and red thick solid lines represent the averaged seasonal values predicted by the model. Thin dashed lines represent 95% percentiles of the seasonal data.

Fig. 7. The same as Fig. 6, but for station S1.

Fig. 8. Model fittings for the percentages of the four size fractions of Chl *a* at station K2. (a-d) Percentages of > 10 μm fraction. (e-h) 3-10 μm. (i-l) 1-3 μm. (m-p) <1 μm.

Fig. 9. The same as Fig. 8, but for station S1.

删除的内容: wo

删除的内容: and

带格式的: 字体:斜体

带格式的: 上标

带格式的: 上标

带格式的: 上标

删除的内容: d

删除的内容: TIN

删除的内容: s

带格式的: 字体:斜体

删除的内容: TIN

删除的内容: TIN

Fig. 10. Modelled seasonal patterns at station K2: (a) DIN, (b) dissolved iron, (c) Chl *a*, (d) phytoplankton mean size, (e) size variance, (f) community-based specific growth rate (μ_{com}), (g) first derivative of phytoplankton growth rate against ln volume evaluated at mean size, (h) second derivative of phytoplankton growth rate evaluated at mean size, (i) Chlorophyll-to-carbon ratios, and (j) Nitrogen-to-carbon ratios.

Fig. 11. The same as Fig. 10, but for station S1.

Fig. 12. (a) Scatterplots of size variance versus phytoplankton community growth rate (μ_{com}). (b) Contributions of various factors to the dynamics of size variance in surface waters at S1. The term "Competition" equates to $v^2 \frac{d^2\mu}{dl^2}$. *MIC* and *MES* grazing equates to $-v^2 \frac{d^2 g_i}{dl^2}$. "d4$\mu$/dL4" equates to $v^2 u \frac{d^4\mu}{dl^4}$. "Trait diffusion" equates to $2u\mu$. All the derivatives are evaluated at the mean size. "Diffusion" means the contribution to the changes of size variance induced by diffusion with the underlying grid. "Net effect" means the sum of the above terms. "Net changes" mean the difference of size variance between adjacent days. (c) The same as (b), but at station K2.

Fig. 13. The same as Fig. 6, but for station ALOHA.

Fig. 14. Schematic diagrams for mixing of two phytoplankton communities with different biomass, mean size, and size variance, each following a lognormal size distribution.

删除的内容: TIN

删除的内容: phytoplankton biomass in terms of nitrogen (PHY), (e)

删除的内容: f

删除的内容: ln

删除的内容: s

删除的内容: g

带格式的: 字体:斜体, 下标

删除的内容: h

带格式的: 字体:斜体

删除的内容: size

删除的内容: i

删除的内容: trait diffusion effects

带格式的: 字体:斜体

带格式的: 字体:斜体

带格式的: 字体:斜体

带格式的: 字体:斜体

删除的内容: .

删除的内容:

删除的内容: 2

删除的内容: A s

删除的内容: the transport

删除的内容:

删除的内容: mean size of two idealized communities

删除的内容: having

删除的内容: The hypothetical biomass, log mean size, and log size variance are 1, 5, 1 for community A, and 0.2, 4, 0.8 for B, respectively.

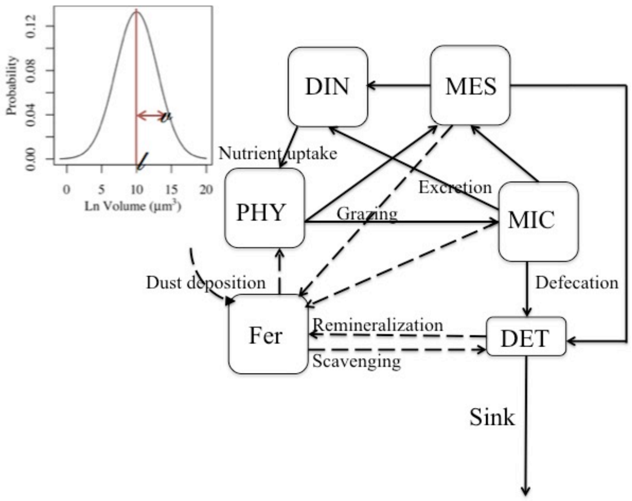

Fig. 1

带格式的: 居中

带格式表格

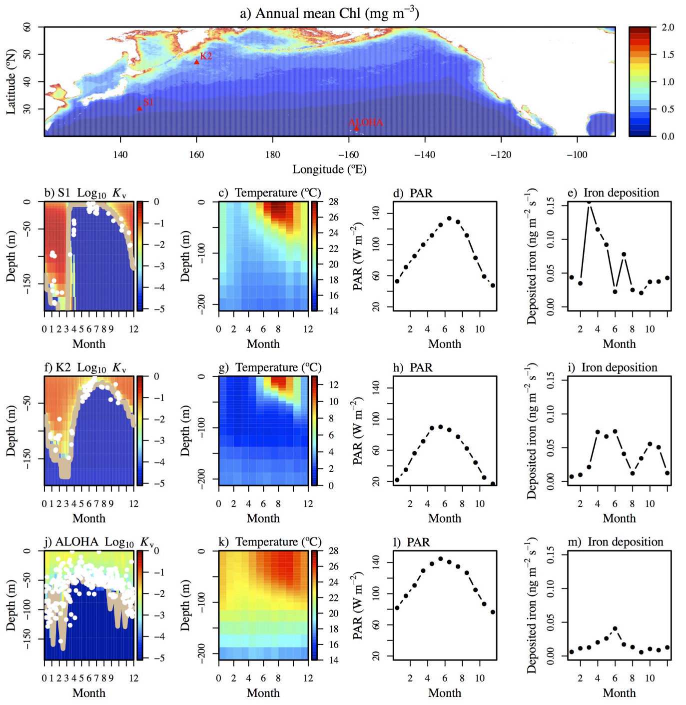
a) Annual mean Chl (mg m^{-3})
Latitude (°N)
Longitude (°E)
K2
S1
ALOHA
b) S1 Log$_{10}$ K_v
c) Temperature (°C)
d) PAR
e) Iron deposition
f) K2 Log$_{10}$ K_v
g) Temperature (°C)
h) PAR
i) Iron deposition
j) ALOHA Log$_{10}$ K_v
k) Temperature (°C)
l) PAR
m) Iron deposition
Depth (m)
PAR (W m^{-2})
Deposited iron (ng m^{-2} s^{-1})
Month

Fig. 2

删除的内容: <sp>

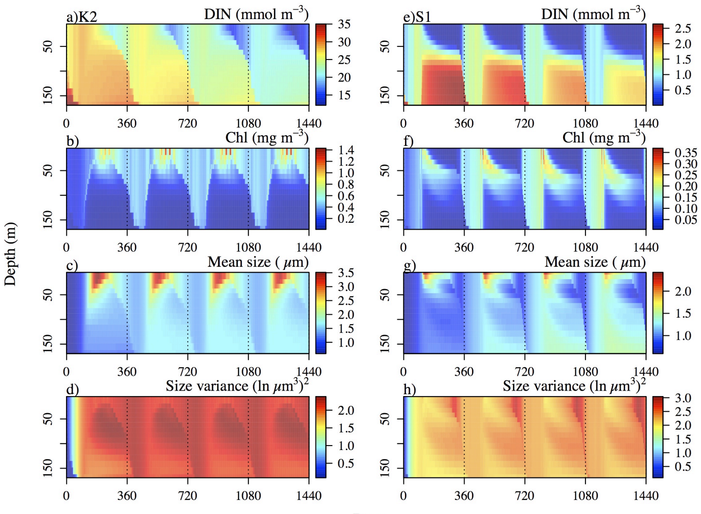

Fig. 3 An example of modelled 4 year patterns at K2 and S1

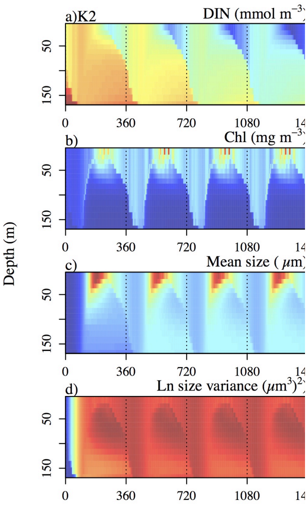

Fig. 3 An example of modelled 4 year patt

删除的内容:

删除的内容: <sp>

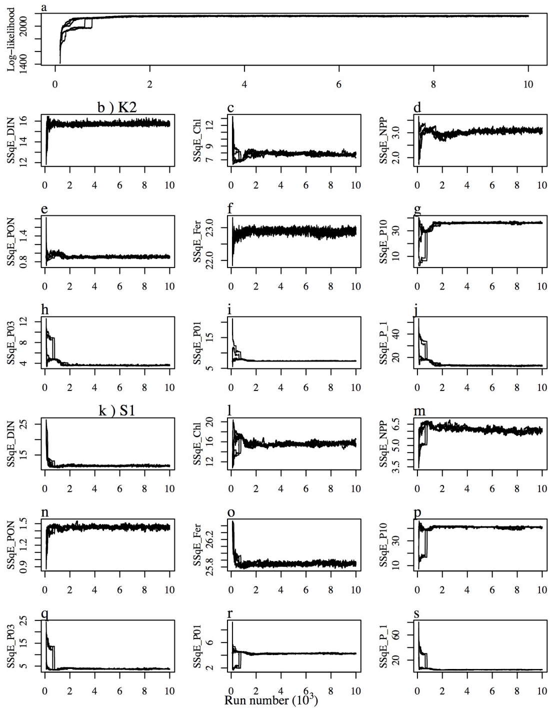
a
Log−likelihood
1400
2000
b) K2
SSqE_DIN
c
SSqE_Chl
d
SSqE_NPP
e
SSqE_PON
f
SSqE_Fer
g
SSqE_P10
h
SSqE_P03
i
SSqE_P01
j
SSqE_P_1
k) S1
SSqE_DIN
l
SSqE_Chl
m
SSqE_NPP
n
SSqE_PON
o
SSqE_Fer
p
SSqE_P10
q
SSqE_P03
r
SSqE_P01
s
SSqE_P_1
0
2
4
6
8
10
Run number (10^3)

Fig. 4

删除的内容: <sp>

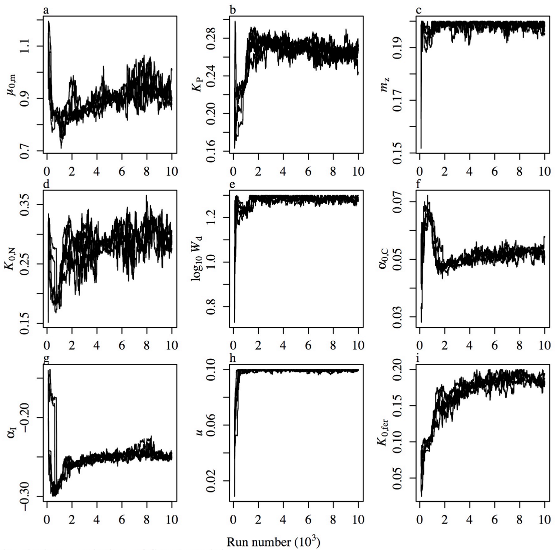

Fig. 5 Time evolution of fitted model parameters.

删除的内容: **<sp>**

删除的内容: **<sp>**

删除的内容: <sp>

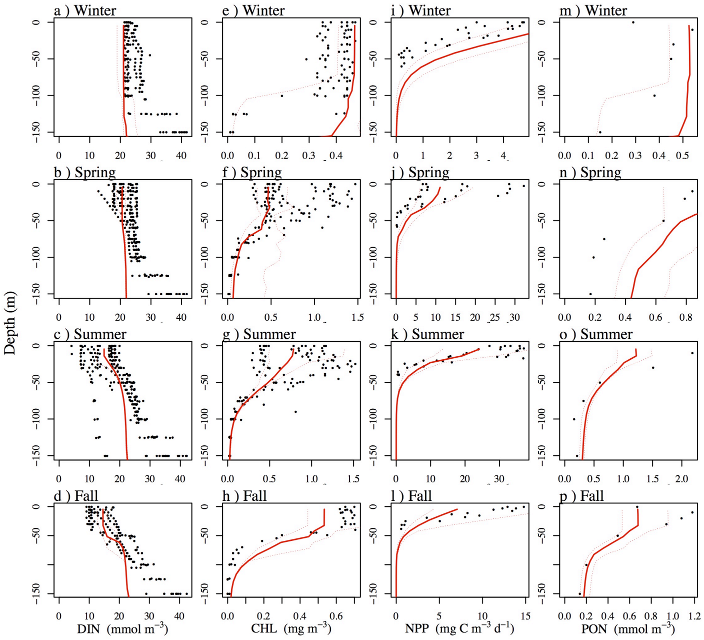

Fig. 6 . Model fittings to vertical profiles of DIN, CHL, NPP, and PON at K2

删除的内容: <sp>

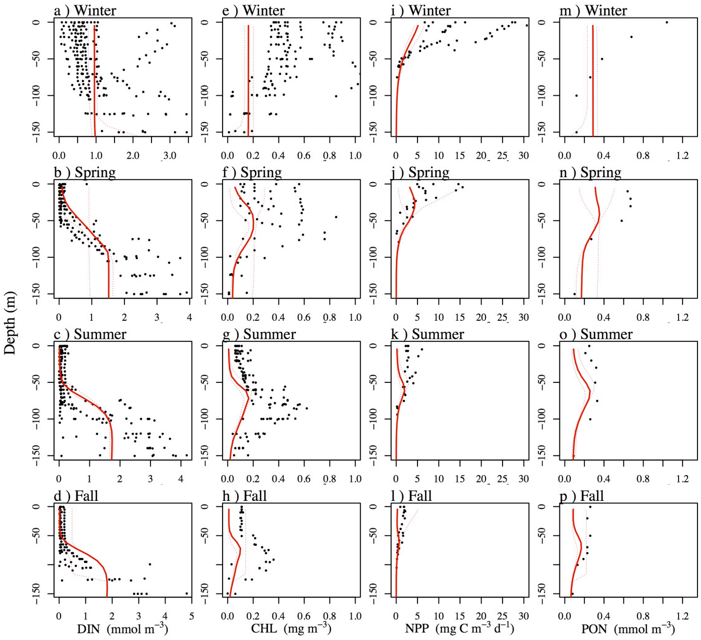

Fig. 7 . Model fittings to vertical profiles of DIN, CHL, NPP, and PON at S1

删除的内容: <sp>

删除的内容: <sp>

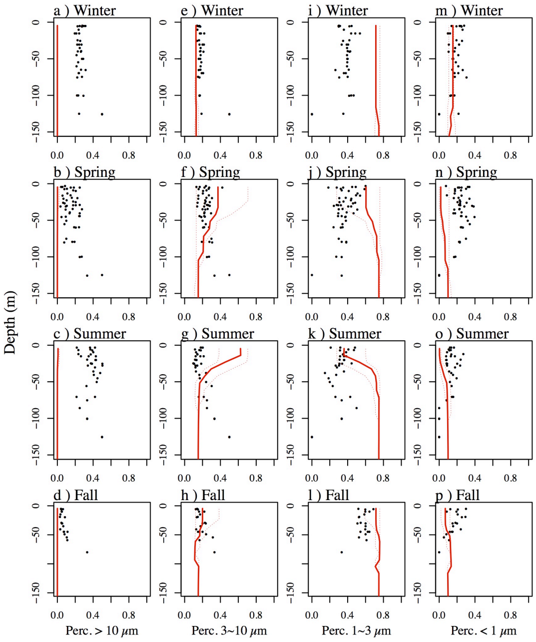

Fig. 8 . Model fittings to vertical profiles of four size fractions at K2

删除的内容: <sp>

删除的内容: <sp>

...

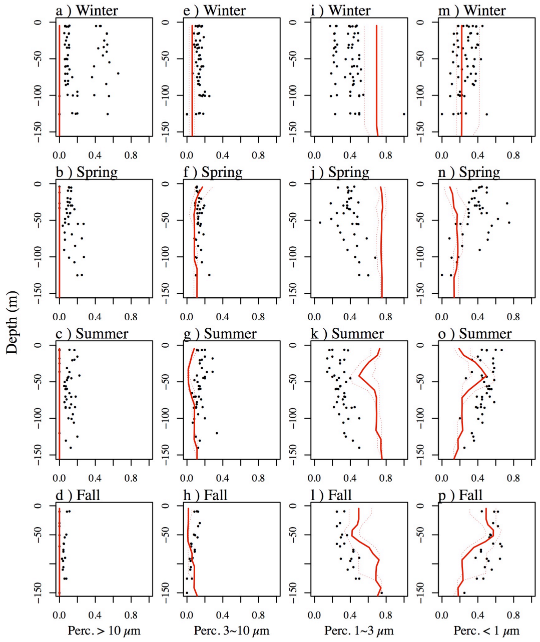

Fig. 9 . Model fittings to vertical profiles of four size fractions at S1

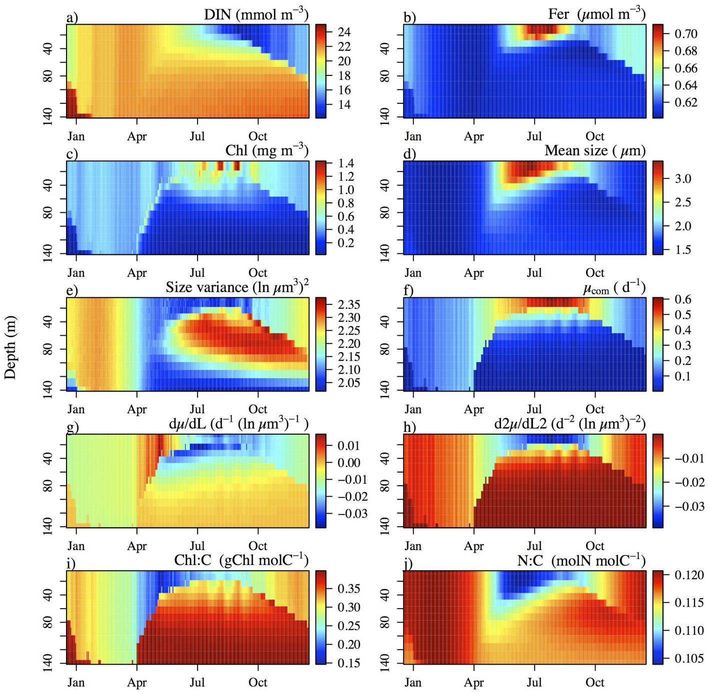

Fig. 10 . Modelled seasonal patterns at K2

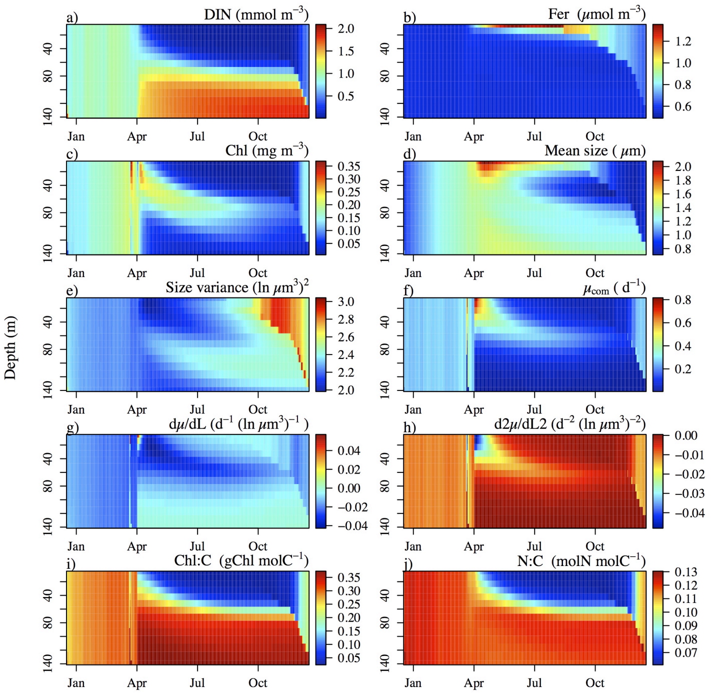

Fig. 11 . Modelled seasonal patterns at S1

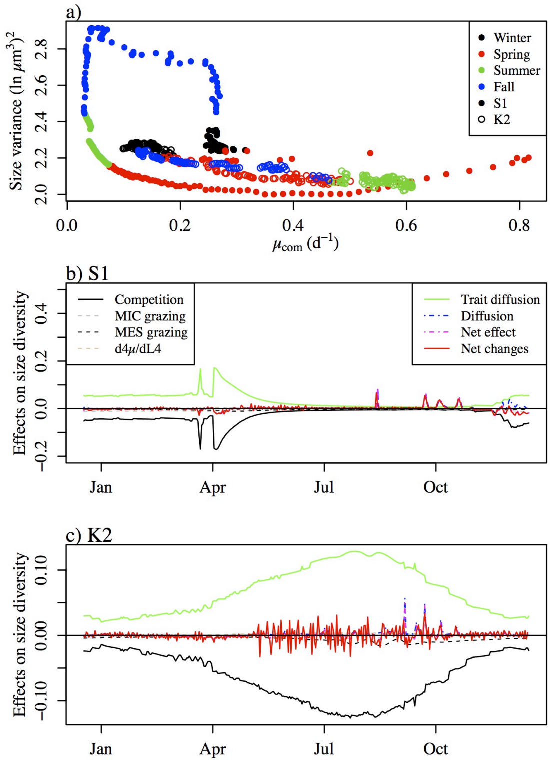

Fig. 12. (a) Scatterplots of size variance versus phytoplankton community growth rate (μ_{com}). (b) Contributions of various factors to the dynamics of size variance in surface waters at S1. The term “Competition” equates to $v^2\frac{d^2\mu}{dl^2}$. *MIC* and *MES* grazing equates to -$v^2\frac{d^2g_i}{dl^2}$. “d4μ/dL4” equates to $v^2u\frac{d^4\mu}{dl^4}$. “Trait diffusion” equates to 2$u\mu$. All the derivatives are evaluated at the mean size. “Diffusion” means the contribution to the changes of size variance induced by diffusion with the underlying grid. “Net effect” means the sum of the above terms. “Net changes” mean the difference of size variance between adjacent days. (c) The same as (b), but at station K2.

带格式的: 居中

带格式的: 行距: 单线

带格式的: 字体:10 pt

带格式的: 字体:10 pt

带格式的: 字体:10 pt

带格式的: 字体:10 pt

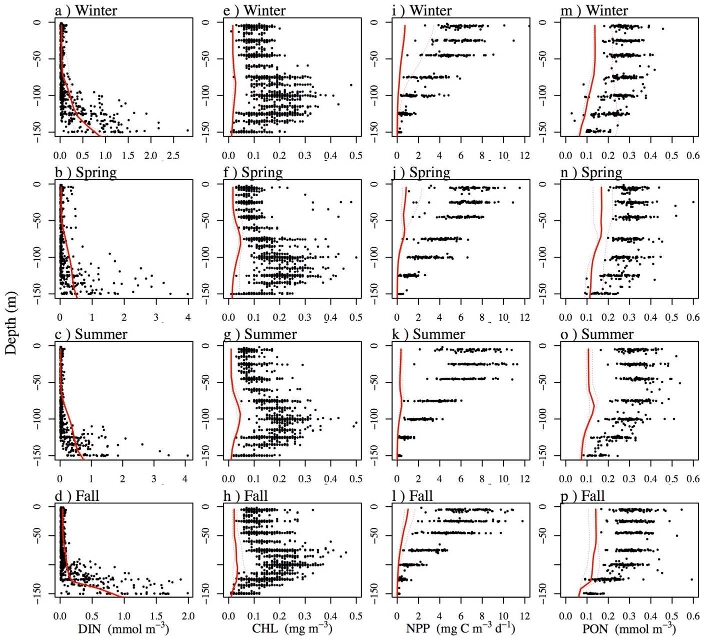

Fig. 13 . Model fittings to vertical profiles of DIN, CHL, NPP, and PON at ALOHA

带格式的: 居中

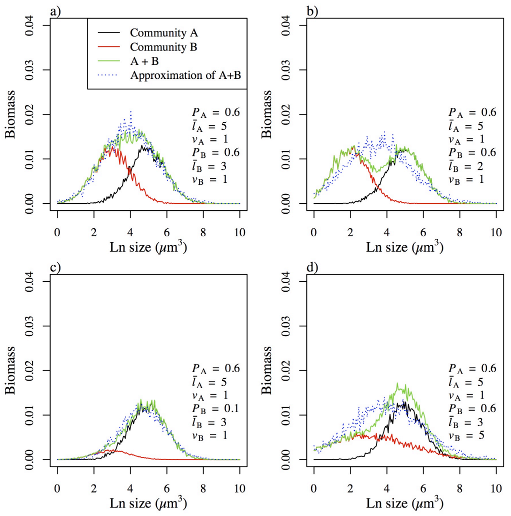

Fig. 14. Schematic diagrams for mixing of two phytoplankton communities with different biomass, mean size, and size variance, each following a lognormal size distribution

带格式的: 两端对齐, 缩进: 左: 0 cm, 悬挂缩进: 2.83 字符, 首行缩进: -2.83 字符, 行距: 1.5 倍行距

删除的内容: .

页 6: [1] 删除的内容 Bingzhang Chen 2017/11/18 AM10:56:00

overall

页 6: [1] 删除的内容 Bingzhang Chen 2017/11/18 AM10:56:00

overall

页 6: [2] 删除的内容 Bingzhang Chen 2017/11/18 AM10:57:00

the

页 6: [2] 删除的内容 Bingzhang Chen 2017/11/18 AM10:57:00

the

页 6: [2] 删除的内容 Bingzhang Chen 2017/11/18 AM10:57:00

the

页 6: [3] 删除的内容 Bingzhang Chen 2017/11/18 AM11:00:00

for modeling phytoplankton size diversity under realistic environmental conditions at the two representative stations in the North Pacific.

页 6: [3] 删除的内容 Bingzhang Chen 2017/11/18 AM11:00:00

for modeling phytoplankton size diversity under realistic environmental conditions at the two representative stations in the North Pacific.

页 6: [3] 删除的内容 **Bingzhang Chen** **2017/11/18 AM11:00:00**

for modeling phytoplankton size diversity under realistic environmental conditions at the two representative stations in the North Pacific.

页 6: [4] 带格式的 **Bingzhang Chen** **2017/9/29 AM11:11:00**

字体:倾斜

页 6: [4] 带格式的 **Bingzhang Chen** **2017/9/29 AM11:11:00**

字体:倾斜

页 6: [5] 删除的内容 **Bingzhang Chen** **2017/9/29 AM10:54:00**

and

页 6: [5] 删除的内容 **Bingzhang Chen** **2017/9/29 AM10:54:00**

and

页 6: [5] 删除的内容 **Bingzhang Chen** **2017/9/29 AM10:54:00**

and

页 6: [5] 删除的内容 **Bingzhang Chen** **2017/9/29 AM10:54:00** and

页 6: [6] 删除的内容 Bingzhang Chen 2017/9/30 PM1:12:00

General d

页 6: [6] 删除的内容 Bingzhang Chen 2017/9/30 PM1:12:00

General d

页 6: [7] 带格式的 Chen Bingzhang 2017/8/3 PM12:07:00

字体: 粗体, 斜体

页 6: [7] 带格式的 Chen Bingzhang 2017/8/3 PM12:07:00

字体: 粗体, 斜体

页 6: [7] 带格式的 Chen Bingzhang 2017/8/3 PM12:07:00

字体: 粗体, 斜体

页 6: [7] 带格式的 Chen Bingzhang 2017/8/3 PM12:07:00

字体: 粗体, 斜体

页 6: [7] 带格式的 Chen Bingzhang 2017/8/3 PM12:07:00

字体:粗体, 斜体

页 6: [7] 带格式的 **Chen Bingzhang** **2017/8/3 PM12:07:00**

字体:粗体, 斜体

页 6: [7] 带格式的 **Chen Bingzhang** **2017/8/3 PM12:07:00**

字体:粗体, 斜体

页 6: [7] 带格式的 **Chen Bingzhang** **2017/8/3 PM12:07:00**

字体:粗体, 斜体

页 10: [8] 删除的内容 **Bingzhang Chen** **2017/11/24 PM3:43:00**

The initial condition of inorganic nitrogen was set to the vertical profile of nitrate in January of the World Ocean Atlas (WOA) 2013 monthly climatology. Initial phytoplankton, zooplankton, and detritus biomass wereare all set to 0.1 μmol L^{-1} in each grid. Initial phytoplankton mean log size (

页 10: [9] 删除的内容 **Bingzhang Chen** **2017/9/30 PM1:15:00**

) and log size variance (v) wereare set to be 1. Initial dissolved iron concentration wais set to the vertical profile of iron in January from a 3D global biogeochemical model output (Aumont et al., 2003). The time step of the model wasis

30 minutes. All the fixed model parameters are shown in Table 1 and the model parameters that are optimized to match observational data are shown in Table 2. We employed a Dirichlet boundary condition at the bottom for DIN and ***fer*** with the values predefined by the WOA2013 climatology and the model output from Aumont et al. (2003), respectively. For other tracers, we assumed no diffusive flux at the bottom. Detritus wasis allowed to sink out of the system with the loss of nitrogen and iron replenished by diffusion.

页 13: [10] 删除的内容 **Bingzhang Chen** **2017/9/30 PM1:42:00**

Light levels (I_z) at depth z were calculated based on PAR_0 and Chl a concentrations following the Beer-Lambert law:

页 13: [11] 删除的内容 **Bingzhang Chen** **2017/9/30 PM1:42:00**

(12)

in which K_w and K_{chl} are the attenuation coefficients for seawater and Chl a, respectively. To realistically estimate the average light field that a phytoplankton cell should experience in a mixing water column (Franks, 2015), the ambient light level for phytoplankton within the surface mixed layer (ML) is calculated as the average light throughout the surface mixed layerML, which is defined as the deepest depth with $K_v > 10^{-3}$ m^2 s^{-1}. This calculation is based on eq. (1) in Franks (2015), which gives that the average time for a phytoplankton cell to move 100 m at the local diffusivity of 10^{-3} m^2 s^{-1} is roughly half a day. However, to compare with *in situ NPP* estimates that were calculated from incubation bottles without continuous mixing, phytoplankton μ, θ, and Q_N are recalculated from I_z based on the Beer-Lambert law (Eq. 12).

页 13: [12] 删除的内容 **Chen Bingzhang** **2017/8/3 AM11:58:00**

2.2 General description of the 1D model (nutrient, zooplankton (*Z*), detritus (*D*), iron (*fer*), and light)

The 1D model focuses on the upper 250 meters of the ocean. The vertical grid, a total of 30 layers, follows a stretched vertical coordinate with increasing resolution towards the sea surface (surface stretching parameter = 2.0), similar to that used in the Regional Ocean Modelling System (ROMS) (Shchepetkin and McWilliams, 2005). For computational efficiency, the 1D model contains only biological tracers. The physics variables are imported as external data (*see* Sect. 2.3 for details).

For simplicity, phytoplankton cells are assumed not to excrete inorganic nitrogen or to have any natural mortality to be converted into detritus. We assume a generic zooplankton compartment that feeds only on phytoplankton following a Holling Type III functional response without any size-dependent feeding preference:

页 13: [13] 删除的内容 **Chen Bingzhang** **2017/8/3 AM11:58:00**

(6)

where g_{max} is the maximal zooplankton ingestion rate, K_P is the half-saturation constant for zooplankton grazing.

The total amount of phytoplankton ingested by zooplankton is divided among three fates: zooplankton net growth, excretion into the inorganic nitrogen pool, and defecation of unassimilated food into the detritus pool (Buitenhuis et al., 2010). The mortality rate of zooplankton is set to be proportional to the squares of zooplankton biomass. The dynamics of zooplankton follow:

页 13: [14] 删除的内容	Chen Bingzhang	2017/8/3 AM11:58:00

(7a)

where E_z is the activation energy for heterotrophic processes. NGE is the net growth efficiency of zooplankton. m_z is the zooplankton mortality coefficient. z is water depth (m).

Detritus is converted to inorganic nitrogen at a rate (R_{dn}, d^{-1}) that has the same temperature sensitivity with zooplankton grazing. Detritus is also assumed to have a constant sinking rate (W_d).

页 13: [15] 删除的内容	Chen Bingzhang	2017/8/3 AM11:58:00

(7b)

The dynamics of inorganic nutrients follow:

页 13: [16] 删除的内容 Chen Bingzhang 2017/8/3 AM11:58:00

(7c)

The dynamics of dissolved iron largely follow Aumont et al. (2003), Nikelsen et al. (2015), and the PlankTOM10 model (Buitenhuis et al., 2010):

页 13: [17] 删除的内容 Chen Bingzhang 2017/8/3 AM11:58:00

(7d)

To translate between nitrogen and iron in particles, a constant fer:N ratio (R_{fer_N}) of 0.0265 is assumed. Monthly atmospheric dust deposition data are extracted from Tegen and Fung (1995). Following the PlankTOM10 model, iron scavenging rate (fer_{scav}) is composed of both background scavenging rate (k_{scm}) and particle absorption rate (k_{sc}):

页 13: [18] 删除的内容 Chen Bingzhang 2017/8/3 AM11:58:00

(8a)

where k_{eq} is the equilibrium constant between free iron and ligands and organic complexes:

页 13: [19] 删除的内容 Chen Bingzhang 2017/8/3 AM11:58:00

(8b)

Note that T is in absolute temperature. l_{fe} is the total iron ligand concentration that is assumed constant (0.6 nM).

Light levels (I_z) at depth z were calculated based on PAR_0 and Chl a concentrations following the Beer-Lambert law:

页 13: [20] 删除的内容 **Chen Bingzhang** **2017/8/3 AM11:58:00**

(9)

in which K_w and K_{chl} are the attenuation coefficients for seawater and Chl a, respectively. To realistically estimate the average light field that a phytoplankton cell should experience in a mixing water column (Franks, 2015), the ambient light level for phytoplankton within the surface mixed layer (ML) is calculated as the average light throughout the surface ML, which is defined as the deepest depth with $K_v > 10^{-3}$ m^2 s^{-1}. This calculation is based on eq. (1) in Franks (2015), which gives that the average time for a phytoplankton cell to move 100 m at the local diffusivity of 10^{-3} m^2 s^{-1} is roughly half a day. However, to compare with *in situ NPP* estimates that were calculated from incubation bottles without continuous mixing, phytoplankton μ, θ, and Q_N are recalculated from I_z based on the Beer-Lambert law.

The initial condition of inorganic nitrogen is set to the vertical profile of nitrate in January of the World Ocean Atlas (WOA) 2013 monthly climatology. Initial phytoplankton, zooplankton, and detritus biomass are all set to 0.1 μmol L^{-1} in each grid. Initial phytoplankton mean log size (

页 13: [21] 删除的内容 **Chen Bingzhang** **2017/8/3 AM11:58:00**

) and log size variance (v) are set to be 1. Initial dissolved iron concentration is set to the vertical profile of iron in January from a 3D global biogeochemical model output (Aumont et al., 2003). The time step of the model is 10 minutes. All the fixed model parameters are shown in Table 1 and the model parameters that are optimized to match observational data are shown in Table 2.

The adaptive component uses information from previous model runs to approximate the distribution of parameter values as a multivariate Gaussian, which it periodically updates as more simulations are conducted. Based on this, the algorithm alters the magnitude and direction of proposed 'jumps' in parameter space (i.e., the proposal covariance matrix (P_{cvm})) in order to more efficiently explore the parameter space. Specifically, the P_{cvm} is tuned based on the covariance matrix (C_{vm}) of the already accepted parameter sets after a fixed number of iterations following Gelman et al. (2014) (i.e. $P_{cvm} = C_{vm} \bullet 2.4^2/d$, where d is the dimension of the target parameter vector).

With the delayed rejection MCMC, when a newly proposed set of parameters is rejected, P_{cvm} is temporarily downscaled (to 1% of the original P_{cvm} in our case) and a second set of parameters is proposed based on the rejected parameters and the downscaled P_{cvm}. DRAM has the advantage of speeding up the mixing properties of MHMC and has been shown to better explore the parameter space than some other algorithms such as the families of Simulated Annealing possibly due to the use of two-stage proposal covariance matrices (Villagran et al., 2008). Compared with the widely used ensemble Kalman filter, DRAM is perhaps more suitable for the nonlinear ecosystems (Annan and Hargreaves, 2007).

页 22: [23] 删除的内容	Chen Bingzhang	2017/9/14 PM5:06:00

The vertical and seasonal patterns of Chl *a* concentrations, including the deep chlorophyll maximum at the subtropical station S1, could also be well reproduced at both stations. The patterns of NPP at station K2 were also well reproduced. One noticeable problem at station S1 is that the surface peak of NPP during summer and fall could not be well reproduced, probably due to the lack of N_2 fixation in the model that is expected to enhance NPP within the surface mixed layer. The model fits of PON were less satisfying at station K2, probably due to the use of a single parameter for the sinking velocity of detritus at both stations.

页 23: [24] 删除的内容	Chen Bingzhang	2017/9/22 PM3:47:00

Light also played a role in affecting size dynamics. At station S1, even though phytoplankton mean size also increased during winter, it increased most dramatically in early spring when light level increased and there were still nutrients left from winter mixing (Fig. 11e,h).

页 25: [25] 删除的内容	Chen Bingzhang	2017/8/8 AM11:21:00

positively correlated to μ, indicating that higher growth rates induced greater resource competition. This agrees well with the “dynamic equilibrium theory” proposed by Huston (1979).

The patterns of trait diffusion, calculated as the sum of all components containing u in the right side of Eq. (1c) to sustain diversity, mirrored those of growth rates. From late fall to early spring, because the values of

页 26: [26] 删除的内容 S. Lan Smith 2017/10/22 PM11:04:00

We believe that t

页 26: [26] 删除的内容 S. Lan Smith 2017/10/22 PM11:04:00

We believe that t

页 26: [27] 删除的内容 Chen Bingzhang 2017/9/26 PM4:48:00

overweighs other technical advantages such a

页 26: [27] 删除的内容 Chen Bingzhang 2017/9/26 PM4:48:00

overweighs other technical advantages such a

页 26: [28] 删除的内容 S. Lan Smith 2017/10/22 PM11:04:00

can

页 26: [28] 删除的内容 S. Lan Smith 2017/10/22 PM11:04:00

can

页 26: [28] 删除的内容 S. Lan Smith 2017/10/22 PM11:04:00

can

页 26: [29] 删除的内容 Chen Bingzhang 2017/9/26 PM4:51:00

equations themselves (Eq. 1) have already provided the genuine insights for

页 26: [29] 删除的内容 Chen Bingzhang 2017/9/26 PM4:51:00

equations themselves (Eq. 1) have already provided the genuine insights for

页 26: [30] 删除的内容 S. Lan Smith 2017/10/22 PM11:06:00

for

页 26: [30] 删除的内容 S. Lan Smith 2017/10/22 PM11:06:00

for

页 26: [30] 删除的内容 S. Lan Smith 2017/10/22 PM11:06:00

for

页 26: [31] 删除的内容 S. Lan Smith 2017/10/22 PM11:06:00

at mean size

页 26: [31] 删除的内容　S. Lan Smith　2017/10/22 PM11:06:00

at mean size

页 26: [31] 删除的内容　S. Lan Smith　2017/10/22 PM11:06:00

at mean size

页 26: [31] 删除的内容　S. Lan Smith　2017/10/22 PM11:06:00

at mean size

页 26: [32] 带格式的　Chen Bingzhang　2017/8/7 AM11:11:00

字体斜体

页 26: [32] 带格式的　Chen Bingzhang　2017/8/7 AM11:11:00

字体斜体

页 26: [33] 删除的内容　Bingzhang Chen　2017/10/18 AM11:45:00

since

页 26: [33] 删除的内容　Bingzhang Chen　2017/10/18 AM11:45:00

since

页 26: [34] 删除的内容　S. Lan Smith　2017/11/27 PM2:10:00

Thus, we propose that

页 26: [34] 删除的内容 S. Lan Smith 2017/11/27 PM2:10:00

Thus, we propose that

页 26: [34] 删除的内容 S. Lan Smith 2017/11/27 PM2:10:00

Thus, we propose that

页 26: [34] 删除的内容 S. Lan Smith 2017/11/27 PM2:10:00

Thus, we propose that

页 26: [34] 删除的内容 S. Lan Smith 2017/11/27 PM2:10:00

Thus, we propose that

页 26: [34] 删除的内容 S. Lan Smith 2017/11/27 PM2:10:00

Thus, we propose that

页 26: [34] 删除的内容 S. Lan Smith 2017/11/27 PM2:10:00

Thus, we propose that

页 26: [35] 删除的内容 S. Lan Smith 2017/10/22 PM11:12:00

a

页 26: [35] 删除的内容 S. Lan Smith 2017/10/22 PM11:12:00

a

页 26: [35] 删除的内容 **S. Lan Smith** **2017/10/22 PM11:12:00**

a

页 26: [35] 删除的内容 **S. Lan Smith** **2017/10/22 PM11:12:00**

a

页 26: [36] 删除的内容 **Bingzhang Chen** **2017/11/25 PM1:02:00**

‘adaptive dynamics’, it is easier to ability to easily quantify competition intensity (and other ecological quantities), which makes

页 26: [36] 删除的内容 **Bingzhang Chen** **2017/11/25 PM1:02:00**

‘adaptive dynamics’, it is easier to ability to easily quantify competition intensity (and other ecological quantities), which makes

页 26: [37] 删除的内容 **S. Lan Smith** **2017/10/22 PM11:15:00**

positively

页 26: [37] 删除的内容 **S. Lan Smith** **2017/10/22 PM11:15:00**

positively

页 26: [37] 删除的内容 **S. Lan Smith** **2017/10/22 PM11:15:00** positively

页 26: [38] 删除的内容 S. Lan Smith 2017/10/22 PM11:16:00

the

页 26: [38] 删除的内容 S. Lan Smith 2017/10/22 PM11:16:00

the

页 26: [39] 删除的内容 Bingzhang Chen 2017/11/25 PM1:08:00

This is because when environmental conditions favour highfast growth rates, it takes less time for the dominant species to predominate, thusand reducing diversitydiversity decreases. The positive correlation between the absolute value of

页 26: [39] 删除的内容 Bingzhang Chen 2017/11/25 PM1:08:00

This is because when environmental conditions favour highfast growth rates, it takes less time for the dominant species to predominate, thusand reducing diversitydiversity decreases. The positive correlation between the absolute value of

页 26: [40] 删除的内容 S. Lan Smith 2017/10/22 PM11:20:00

also gives

页 26: [40] 删除的内容 S. Lan Smith 2017/10/22 PM11:20:00

also gives

页 **26: [40]** 删除的内容 **S. Lan Smith** **2017/10/22 PM11:20:00**

also gives

页 **26: [40]** 删除的内容 **S. Lan Smith** **2017/10/22 PM11:20:00**

also gives

页 **26: [40]** 删除的内容 **S. Lan Smith** **2017/10/22 PM11:20:00**

also gives

页 **26: [40]** 删除的内容 **S. Lan Smith** **2017/10/22 PM11:20:00**

also gives

页 **27: [41]** 带格式的 **Chen Bingzhang** **2017/9/26 PM4:58:00**

字体:斜体

页 **27: [41]** 带格式的 **Chen Bingzhang** **2017/9/26 PM4:58:00**

字体:斜体

页 **27: [42]** 删除的内容 **S. Lan Smith** **2017/10/22 PM11:24:00**

also

页 **27: [42]** 删除的内容 **S. Lan Smith** **2017/10/22 PM11:24:00**

also

页 27: [42] 删除的内容 **S. Lan Smith** **2017/10/22 PM11:24:00**

also

页 27: [42] 删除的内容 **S. Lan Smith** **2017/10/22 PM11:24:00**

also

页 27: [42] 删除的内容 **S. Lan Smith** **2017/10/22 PM11:24:00**

also

页 27: [42] 删除的内容 **S. Lan Smith** **2017/10/22 PM11:24:00**

also

页 27: [43] 删除的内容 **Chen Bingzhang** **2017/9/27 PM10:57:00**

evolutionary theory

页 27: [43] 删除的内容 **Chen Bingzhang** **2017/9/27 PM10:57:00**

evolutionary theory

页 27: [44] 删除的内容 **S. Lan Smith** **2017/11/27 PM2:17:00**

and

页 27: [44] 删除的内容 S. Lan Smith 2017/11/27 PM2:17:00

and

页 27: [44] 删除的内容 S. Lan Smith 2017/11/27 PM2:17:00

and

页 27: [44] 删除的内容 S. Lan Smith 2017/11/27 PM2:17:00

and

页 27: [44] 删除的内容 S. Lan Smith 2017/11/27 PM2:17:00

and

页 27: [44] 删除的内容 S. Lan Smith 2017/11/27 PM2:17:00

and

页 27: [45] 删除的内容 S. Lan Smith 2017/11/27 PM2:19:00

a population with the

页 27: [45] 删除的内容 S. Lan Smith 2017/11/27 PM2:19:00

a population with the

页 27: [45] 删除的内容 S. Lan Smith 2017/11/27 PM2:19:00

a population with the

页 27: [45] 删除的内容　　S. Lan Smith　　2017/11/27 PM2:19:00

a population with the

页 27: [45] 删除的内容　　S. Lan Smith　　2017/11/27 PM2:19:00

a population with the

页 27: [45] 删除的内容　　S. Lan Smith　　2017/11/27 PM2:19:00

a population with the

页 27: [45] 删除的内容　　S. Lan Smith　　2017/11/27 PM2:19:00

a population with the

页 27: [46] 带格式的　　Bingzhang Chen　　2017/9/28 PM3:26:00

字体斜体

页 27: [46] 带格式的　　Bingzhang Chen　　2017/9/28 PM3:26:00

字体斜体

页 27: [46] 带格式的　　Bingzhang Chen　　2017/9/28 PM3:26:00

字体斜体

页 27: [46] 带格式的　　Bingzhang Chen　　2017/9/28 PM3:26:00

字体:斜体

页 27: [46] 带格式的 **Bingzhang Chen** **2017/9/28 PM3:26:00**

字体:斜体

页 27: [46] 带格式的 **Bingzhang Chen** **2017/9/28 PM3:26:00**

字体:斜体

页 27: [46] 带格式的 **Bingzhang Chen** **2017/9/28 PM3:26:00**

字体:斜体

页 27: [46] 带格式的 **Bingzhang Chen** **2017/9/28 PM3:26:00**

字体:斜体

页 27: [46] 带格式的 **Bingzhang Chen** **2017/9/28 PM3:26:00**

字体:斜体

页 27: [46] 带格式的 **Bingzhang Chen** **2017/9/28 PM3:26:00**

字体:斜体

页 27: [46] 带格式的 **Bingzhang Chen** **2017/9/28 PM3:26:00**

字体:斜体

页 27: [46] 带格式的 **Bingzhang Chen** **2017/9/28 PM3:26:00**

字体斜体

页 27: [46] 带格式的 **Bingzhang Chen** **2017/9/28 PM3:26:00**

字体斜体

页 27: [46] 带格式的 **Bingzhang Chen** **2017/9/28 PM3:26:00**

字体斜体

页 27: [46] 带格式的 **Bingzhang Chen** **2017/9/28 PM3:26:00**

字体斜体

页 27: [46] 带格式的 **Bingzhang Chen** **2017/9/28 PM3:26:00**

字体斜体

页 29: [47] 删除的内容 **Chen Bingzhang** **2017/8/29 PM5:01:00**

Compared to previous continuous trait-based models (Terseleer et al., 2014; Acevedo-Trejos et al., 2015, 2016), **CITRATE** 1.0

页 29: [47] 删除的内容 **Chen Bingzhang** **2017/8/29 PM5:01:00**

Compared to previous continuous trait-based models (Terseleer et al., 2014; Acevedo-Trejos et al., 2015, 2016), **CITRATE** 1.0

页 29: [47] 删除的内容 Chen Bingzhang 2017/8/29 PM5:01:00

Compared to previous continuous trait-based models (Terseleer et al., 2014; Acevedo-Trejos et al., 2015, 2016), **CITRATE** 1.0

页 29: [48] 删除的内容 S. Lan Smith 2017/10/22 PM11:35:00

the

页 29: [48] 删除的内容 S. Lan Smith 2017/10/22 PM11:35:00

the

页 29: [48] 删除的内容 S. Lan Smith 2017/10/22 PM11:35:00

the

页 29: [48] 删除的内容 S. Lan Smith 2017/10/22 PM11:35:00

the

页 29: [49] 删除的内容 S. Lan Smith 2017/11/27 AM11:28:00

of

页 29: [49] 删除的内容 S. Lan Smith 2017/11/27 AM11:28:00

of

页 29: [49] 删除的内容 S. Lan Smith 2017/11/27 AM11:28:00

of

页 29: [49] 删除的内容 S. Lan Smith 2017/11/27 AM11:28:00

of

页 29: [49] 删除的内容 S. Lan Smith 2017/11/27 AM11:28:00

of

页 29: [49] 删除的内容 S. Lan Smith 2017/11/27 AM11:28:00

of

页 29: [50] 删除的内容 S. Lan Smith 2017/10/22 PM11:37:00

the growth superiority of

页 29: [50] 删除的内容 S. Lan Smith 2017/10/22 PM11:37:00

the growth superiority of

页 29: [51] 删除的内容 Bingzhang Chen 2017/9/28 PM5:07:00

oligotrophic

页 29: [51] 删除的内容 Bingzhang Chen 2017/9/28 PM5:07:00

oligotrophic

页 29: [52] 删除的内容 S. Lan Smith 2017/10/22 PM11:38:00

.

页 29: [52] 删除的内容 S. Lan Smith 2017/10/22 PM11:38:00

.

页 29: [52] 删除的内容 S. Lan Smith 2017/10/22 PM11:38:00

.

页 29: [53] 删除的内容 S. Lan Smith 2017/10/22 PM11:40:00

opposite

页 29: [53] 删除的内容 S. Lan Smith 2017/10/22 PM11:40:00

opposite

页 29: [53] 删除的内容 S. Lan Smith 2017/10/22 PM11:40:00

opposite

页 29: [53] 删除的内容 S. Lan Smith 2017/10/22 PM11:40:00

opposite

页 29: [54] 删除的内容 S. Lan Smith 2017/10/22 PM11:40:00

also

页 29: [54] 删除的内容 S. Lan Smith 2017/10/22 PM11:40:00

also

页 29: [54] 删除的内容 S. Lan Smith 2017/10/22 PM11:40:00

also

页 29: [54] 删除的内容 S. Lan Smith 2017/10/22 PM11:40:00

also

页 29: [54] 删除的内容 S. Lan Smith 2017/10/22 PM11:40:00

also

页 29: [54] 删除的内容 S. Lan Smith 2017/10/22 PM11:40:00

also

页 29: [54] 删除的内容 S. Lan Smith 2017/10/22 PM11:40:00

also

页 29: [54] 删除的内容 S. Lan Smith 2017/10/22 PM11:40:00

also

页 29: [54] 删除的内容 S. Lan Smith 2017/10/22 PM11:40:00

also

页 29: [54] 删除的内容 S. Lan Smith 2017/10/22 PM11:40:00

also

页 29: [54] 删除的内容 S. Lan Smith 2017/10/22 PM11:40:00

also

页 29: [54] 删除的内容 S. Lan Smith 2017/10/22 PM11:40:00

also

页 29: [54] 删除的内容 S. Lan Smith 2017/10/22 PM11:40:00

also

页 29: [54] 删除的内容 S. Lan Smith 2017/10/22 PM11:40:00

also

页 29: [54] 删除的内容 S. Lan Smith 2017/10/22 PM11:40:00

also

页 29: [54] 删除的内容 S. Lan Smith 2017/10/22 PM11:40:00

also

页 29: [55] 删除的内容 **S. Lan Smith** **2017/11/27 AM11:31:00**

,

页 29: [55] 删除的内容 **S. Lan Smith** **2017/11/27 AM11:31:00**

,

页 29: [55] 删除的内容 **S. Lan Smith** **2017/11/27 AM11:31:00**

,

页 29: [55] 删除的内容 **S. Lan Smith** **2017/11/27 AM11:31:00**

,

页 29: [55] 删除的内容 **S. Lan Smith** **2017/11/27 AM11:31:00**

,

页 29: [55] 删除的内容 **S. Lan Smith** **2017/11/27 AM11:31:00**

,

页 29: [55] 删除的内容 **S. Lan Smith** **2017/11/27 AM11:31:00**

,

页 29: [55] 删除的内容 **S. Lan Smith** **2017/11/27 AM11:31:00**

,

页 29: [56] 删除的内容 S. Lan Smith 2017/10/22 PM11:44:00

addition

页 29: [56] 删除的内容 S. Lan Smith 2017/10/22 PM11:44:00

addition

页 29: [56] 删除的内容 S. Lan Smith 2017/10/22 PM11:44:00

addition

页 29: [56] 删除的内容 S. Lan Smith 2017/10/22 PM11:44:00

addition

页 30: [57] 删除的内容 S. Lan Smith 2017/11/27 AM11:36:00

. And also b

页 30: [57] 删除的内容 S. Lan Smith 2017/11/27 AM11:36:00

. And also b

页 30: [57] 删除的内容 S. Lan Smith 2017/11/27 AM11:36:00

. And also b

页 30: [57] 删除的内容 S. Lan Smith 2017/11/27 AM11:36:00

. And also b

页 30: [57] 删除的内容 S. Lan Smith 2017/11/27 AM11:36:00

. And also b

页 30: [58] 删除的内容 S. Lan Smith 2017/11/27 AM11:41:00

lognormal is not the only

页 30: [58] 删除的内容 S. Lan Smith 2017/11/27 AM11:41:00

lognormal is not the only

页 30: [59] 删除的内容 Bingzhang Chen 2017/11/24 PM1:44:00

I

页 30: [59] 删除的内容 Bingzhang Chen 2017/11/24 PM1:44:00

I

页 30: [60] 带格式的 Bingzhang Chen 2017/11/24 AM11:13:00

字体斜体

页 30: [60] 带格式的 Bingzhang Chen 2017/11/24 AM11:13:00

字体斜体

页 30: [60] 带格式的 Bingzhang Chen 2017/11/24 AM11:13:00

字体:斜体

页 30: [60] 带格式的 Bingzhang Chen 2017/11/24 AM11:13:00

字体:斜体

页 30: [60] 带格式的 Bingzhang Chen 2017/11/24 AM11:13:00

字体:斜体

页 30: [61] 删除的内容 Bingzhang Chen 2017/11/24 PM1:44:00

usually

页 30: [61] 删除的内容 Bingzhang Chen 2017/11/24 PM1:44:00

usually

页 30: [62] 带格式的 Bingzhang Chen 2017/11/24 AM11:22:00

字体:斜体

页 30: [62] 带格式的 Bingzhang Chen 2017/11/24 AM11:22:00

字体:斜体

页 30: [63] 带格式的 Bingzhang Chen 2017/11/24 AM11:13:00

字体:斜体

页 30: [63] 带格式的 Bingzhang Chen 2017/11/24 AM11:13:00

字体:斜体

页 30: [64] 删除的内容 S. Lan Smith 2017/11/27 AM11:42:00

with

页 30: [64] 删除的内容 S. Lan Smith 2017/11/27 AM11:42:00

with

页 30: [64] 删除的内容 S. Lan Smith 2017/11/27 AM11:42:00

with

页 30: [64] 删除的内容 S. Lan Smith 2017/11/27 AM11:42:00

with

页 30: [65] 删除的内容 S. Lan Smith 2017/11/27 AM11:43:00

the common unit of

页 30: [65] 删除的内容 S. Lan Smith 2017/11/27 AM11:43:00

the common unit of

页 30: [66] 带格式的 Bingzhang Chen 2017/11/24 AM11:20:00

右对齐, 缩进: 首行缩进: 2.36 字符, 允许文字在单词中间换行

页 30: [67] 删除的内容	S. Lan Smith	2017/11/27 PM2:23:00

While

页 30: [67] 删除的内容	S. Lan Smith	2017/11/27 PM2:23:00

While

页 30: [67] 删除的内容	S. Lan Smith	2017/11/27 PM2:23:00

While

页 30: [67] 删除的内容	S. Lan Smith	2017/11/27 PM2:23:00

While

页 30: [67] 删除的内容	S. Lan Smith	2017/11/27 PM2:23:00

While

页 30: [67] 删除的内容	S. Lan Smith	2017/11/27 PM2:23:00

While

页 30: [68] 删除的内容	Bingzhang Chen	2017/11/24 AM11:26:00

The slope of log abundance versus log size (e.g. cell volume)

页 30: [69] 删除的内容 S. Lan Smith 2017/11/27 PM2:25:00

with the consequence tha

页 30: [69] 删除的内容 S. Lan Smith 2017/11/27 PM2:25:00

with the consequence tha

页 30: [70] 带格式的 Bingzhang Chen 2017/11/24 PM1:41:00

右对齐, 缩进: 首行缩进: 1.18 字符, 允许文字在单词中间换行

页 30: [71] 删除的内容 Bingzhang Chen 2017/11/27 PM3:12:00

$$B(V)= N□0□\ V□\alpha+1□\ e□\text{-}\gamma V□B(V)= N□0□\ V□\alpha+1□\ e□\text{-}\lambda V□$$

页 30: [72] 批注 S. Lan Smith 2017/11/27 AM11:49:00

Is this term simply added to the eq. above? If so, I’d suggest writing out the full equation.

页 30: [73] 带格式的 Bingzhang Chen 2017/11/24 PM12:07:00

字体: 斜体

页 30: [73] 带格式的 Bingzhang Chen 2017/11/24 PM12:07:00

字体: 斜体

页 30: [74] 删除的内容 S. Lan Smith 2017/11/27 PM2:27:00

In the literature, there have been lots of debates on whether

页 31: [75] 删除的内容 **S. Lan Smith** **2017/11/27 AM11:51:00**

might

页 31: [75] 删除的内容 **S. Lan Smith** **2017/11/27 AM11:51:00**

might

页 31: [75] 删除的内容 **S. Lan Smith** **2017/11/27 AM11:51:00**

might

页 31: [75] 删除的内容 **S. Lan Smith** **2017/11/27 AM11:51:00**

might

页 31: [75] 删除的内容 **S. Lan Smith** **2017/11/27 AM11:51:00**

might

页 31: [76] 删除的内容 **Bingzhang Chen** **2017/11/24 PM2:35:00**

unicellular

页 31: [76] 删除的内容 **Bingzhang Chen** **2017/11/24 PM2:35:00**

unicellular

页 31: [76] 删除的内容 **Bingzhang Chen** **2017/11/24 PM2:35:00**

unicellular

页 31: [76] 删除的内容	Bingzhang Chen	2017/11/24 PM2:35:00

unicellular

页 31: [77] 删除的内容	Bingzhang Chen	2017/11/24 AM11:59:00

However, aside from fact that the power-law distribution is unrealistic in predicting phytoplankton biomass at the size limits (there must be upper and lower limits of size at which phytoplankton biomass becomes close to zero, which cannot be predicted bywhich the power-law cannot reproduce), the power-law distribution is much more inconvenient in terms of for mathematical manipulations (e.g. calculating mean and variance) thancompared to the normal distribution. TheA lognormal distribution is usually appropriatea much better alternative for phytoplankton size in terms of mathematic properties (e.g., zero probability of negative size) and can be fit well to empirical data (Finkel, 2007Quintana et al., 2008). Therefore, it is not surprising that the lognormal distribution has been widely used in continuous size models; (Terseleer et al., 2014; Acevedo-Trejos et al., 2015, 2016; Smith et al., 2016). However, this does not guarantee that a fixed type of probability distribution can hold for all situations (Coutinho et al., 2016). In oligotrophic waters where picophytoplankton, particularly the unicellular cyanobacteria *Prochlorococcus* and *Synechococcus*, dominate (Campbell et al., 1994; Liu et al., 1997), the distribution of phytoplankton log size is more likely right skewed. In other words, abundances of large species are higher than expected from a pure lognormal distribution, which is consistent with the observation that some large diatoms, with significant contributions to new production, can be found in the oligotrophic gyres (Villareal et al., 1999). This is probably one of the major reason that our model tends to underestimate the fraction of > 10 μm size.

页 31: [78] 删除的内容	S. Lan Smith	2017/10/22 PM11:48:00

ces

页 31: [78] 删除的内容	S. Lan Smith	2017/10/22 PM11:48:00

ces

页 31: [78] 删除的内容	S. Lan Smith	2017/10/22 PM11:48:00

ces

页 31: [78] 删除的内容	S. Lan Smith	2017/10/22 PM11:48:00

ces

页 31: [78] 删除的内容	S. Lan Smith	2017/10/22 PM11:48:00

ces

页 31: [78] 删除的内容	S. Lan Smith	2017/10/22 PM11:48:00

ces

页 31: [78] 删除的内容 **S. Lan Smith** **2017/10/22 PM11:48:00**

ces

页 31: [78] 删除的内容 **S. Lan Smith** **2017/10/22 PM11:48:00**

ces

页 31: [79] 删除的内容 **S. Lan Smith** **2017/11/27 PM2:29:00**

The immediate summation of

页 31: [79] 删除的内容 **S. Lan Smith** **2017/11/27 PM2:29:00**

The immediate summation of

页 31: [79] 删除的内容 **S. Lan Smith** **2017/11/27 PM2:29:00**

The immediate summation of

页 31: [79] 删除的内容 **S. Lan Smith** **2017/11/27 PM2:29:00**

The immediate summation of

页 31: [79] 删除的内容 **S. Lan Smith** **2017/11/27 PM2:29:00**

The immediate summation of

页 31: [79] 删除的内容 **S. Lan Smith** **2017/11/27 PM2:29:00**

The immediate summation of

页 31: [79] 删除的内容	S. Lan Smith	2017/11/27 PM2:29:00

The immediate summation of

页 31: [80] 删除的内容	S. Lan Smith	2017/11/27 PM2:29:00

usually

页 31: [80] 删除的内容	S. Lan Smith	2017/11/27 PM2:29:00

usually

页 31: [80] 删除的内容	S. Lan Smith	2017/11/27 PM2:29:00

usually

页 31: [81] 删除的内容	Bingzhang Chen	2017/9/28 PM5:30:00

2

页 31: [81] 删除的内容	Bingzhang Chen	2017/9/28 PM5:30:00

2

页 31: [81] 删除的内容	Bingzhang Chen	2017/9/28 PM5:30:00

2

页 31: [81] 删除的内容　Bingzhang Chen　2017/9/28 PM5:30:00

2

页 31: [82] 删除的内容　S. Lan Smith　2017/11/27 AM11:55:00

al

页 31: [82] 删除的内容　S. Lan Smith　2017/11/27 AM11:55:00

al

页 31: [83] 带格式的　Bingzhang Chen　2017/9/28 PM10:31:00

字体:非粗体, 斜体

页 31: [83] 带格式的　Bingzhang Chen　2017/9/28 PM10:31:00

字体:非粗体, 斜体

页 31: [83] 带格式的　Bingzhang Chen　2017/9/28 PM10:31:00

字体:非粗体, 斜体

页 31: [84] 删除的内容　S. Lan Smith　2017/10/22 PM11:51:00

From t

页 31: [84] 删除的内容　S. Lan Smith　2017/10/22 PM11:51:00

From t

页 31: [84] 删除的内容 S. Lan Smith 2017/10/22 PM11:51:00

From t

页 31: [84] 删除的内容 S. Lan Smith 2017/10/22 PM11:51:00

From t

页 31: [84] 删除的内容 S. Lan Smith 2017/10/22 PM11:51:00

From t

页 32: [85] 删除的内容 Bingzhang Chen 2017/9/28 PM5:35:00

) should be similar due to strong mixing, the approximation is not a big concern. The problem mainly lies at the bottom of the mixed layer where there is a sharp gradient of phytoplankton properties particularly biomass (Fig. 12c). We can roughly estimate that, based on the eddy diffusivity (~2 x 10^5 m^2 s^{-1}), grid distance (20 m), and the phytoplankton biomass differences (0.2 μmol N L^{-1}), the transported phytoplankton biomass from the upper grid (higher $\boldsymbol{P}$) to the lower grid (lower $\boldsymbol{P}$) at one time step (0.5 min) is roughly 0.0002 μmol N L^{-1}, 1% of the $\boldsymbol{P}$ in the lower grid. Therefore, oOur tentative conclusion is that

页 32: [86] 删除的内容 Chen Bingzhang 2017/8/8 AM10:58:00

and may potentially be a concern only under the presence of large gradients of phytoplankton biomass or trait moments

页 34: [87] 删除的内容	S. Lan Smith	2017/10/23 AM12:00:00

Future

➢

页 35: [88] 删除的内容	Chen Bingzhang	2017/9/20 PM3:19:00

The code for **CITRATE** 1.0 is written in Fortran90 with the Intel Fortran compiler used. The running environment is Linux or Unix. The user is supposed to be familiar with the Fortran language.

For each station, four different physical forcing data including vertical profiles of eddy diffusive coefficients and temperatures, surface PAR and atmospheric dust deposition. We already provided the relevant data for stations S1 and K2. The temporal resolution is one day for the vertical eddy diffusivity and one month for three other types of data.

After downloading the folder *FlexEFT1D*, go to the directory *FlexEFT1D/DRAM_0.9/NPZDcont/BOTH* and type *vi run*. The user can change the value of *Test* inside the bash script *run*. The *Test* value being 0 means a fast run, usually for a formal model run for a large number of iterations. The *Test* value being 1 means running a model for debugging, which is much slower than the fast run. The user can also modify the compiler flags depending on the purpose in the script. Having chosen the right compiler option, type *./run*, the model will compile and an executable file (NPZDCONT) will be generated.

The next step is to type *vi Model.nml*, the file containing two namelists. The namelist *&Model* contains the options for station names, the type of ecological model, the type of nutrient uptake function (1 only for **CITRATE**), and the type for grazing function (four different grazing functions including the three Holling type functions and the Ivlev function). The station name determines the right physics files to be read and the filenames for model output. For now we only allow three possible stations: S1, K2, and HOT. Other station names will generate an error. If the user wants to add more station names, the subroutine *Setup_OBSdata* within *MOD_1D.f90* is the place to be modified. A number of ecological models besides CITRATE have been developed. It is beyond the scope of the present study to describe all of them in detail. Just note that the model lists are in the fortran file bio_MOD.f90 and some other details are in choose_model.f90 and MOD_1D.f90.

The namelist *&MCMCrun* contains the options for defining the total length of the MCMC chain which is at least 2, the number of the ensemble runs, the number of days for each model run, whether the model should start from previous runs (*Readfile* = 1) or start a new run (*Readfile* = 0), and the number of runs in the historical files (*enssig* and *enspar*).

After defining all the model settings, type "./NPZDCONT" and then the model will run and some outputs will be shown on the screen. Type "./NPZDCONT > out" to make the model outputs stored in the "out" file.

For each model run, the model saves the current parameters into the "enspar" file and the current values of σ and SSqE into the 'enssig' file. In this way, even if the model crashes, the user can pick up the current parameter position and updated parameter covariance matrix. The model also generates the files of best parameters, best σ and SSqE files, best model output files that correspond to observational data, and model output files at daily resolution at each grid after an ensemble run.

页 36: [89] 删除的内容 **Bingzhang Chen** **2017/9/29 AM11:58:00**

页 37: [90] 删除的内容 **Chen Bingzhang** **2017/9/13 PM2:40:00**

K_p	Grazing half-saturation constant of zooplankton	0.5^e	μM N

页 38: [91] 删除的内容 **Chen Bingzhang** **2017/9/14 PM4:46:00**

“burn-in” period

页 38: [91] 删除的内容 **Chen Bingzhang** **2017/9/14 PM4:46:00**

“burn-in” period

页 38: [91] 删除的内容 **Chen Bingzhang** **2017/9/14 PM4:46:00**

“burn-in” period

页 38: [91] 删除的内容 **Chen Bingzhang** **2017/9/14 PM4:46:00**

“burn-in” period

页 38: [91] 删除的内容 **Chen Bingzhang** **2017/9/14 PM4:46:00**

“burn-in” period

页 38: [92] 删除的内容 **Chen Bingzhang** **2017/9/13 PM3:14:00**

1

页 38: [92] 删除的内容 **Chen Bingzhang** **2017/9/13 PM3:14:00**

1

页 38: [92] 删除的内容 **Chen Bingzhang** **2017/9/13 PM3:14:00**

1

页 38: [93] 删除的内容 **Chen Bingzhang** **2017/9/13 PM3:17:00**

3.3

页 38: [93] 删除的内容 **Chen Bingzhang** **2017/9/13 PM3:17:00**

3.3

页 38: [94] 删除的内容	Chen Bingzhang	2017/9/13 PM2:36:00

Q_{0N}	Phytoplankton minimal N:C ratio	0.076[a] (0.05, 0.13)	0.093 (0.0007)	mol: mol
g_{max}	Maximal zooplankton grazing rate at 15 ºC	1 (0.5, 2)	0.90 (0.024)	d^{-1}

页 38: [95] 删除的内容	Chen Bingzhang	2017/9/13 PM3:20:00

094

页 38: [95] 删除的内容	Chen Bingzhang	2017/9/13 PM3:20:00

094

页 38: [96] 删除的内容	Chen Bingzhang	2017/9/13 PM3:20:00

19

页 38: [96] 删除的内容	Chen Bingzhang	2017/9/13 PM3:20:00

19

页 38: [97] 删除的内容	Chen Bingzhang	2017/9/13 PM3:39:00

0.08

页 **38: [97]** 删除的内容 **Chen Bingzhang** **2017/9/13 PM3:39:00**

0.08

页 **38: [98]** 删除的内容 **Chen Bingzhang** **2017/9/13 PM3:20:00**

0.097

页 **38: [98]** 删除的内容 **Chen Bingzhang** **2017/9/13 PM3:20:00**

0.097

页 **38: [99]** 删除的内容 **Chen Bingzhang** **2017/9/13 PM3:26:00**

5

页 **38: [99]** 删除的内容 **Chen Bingzhang** **2017/9/13 PM3:26:00**

5

页 **38: [99]** 删除的内容 **Chen Bingzhang** **2017/9/13 PM3:26:00**

5

页 38: [100] 删除的内容 **Chen Bingzhang** **2017/9/13 PM3:22:00**

0.89

页 38: [100] 删除的内容 **Chen Bingzhang** **2017/9/13 PM3:22:00**

0.89

页 38: [101] 删除的内容 **Chen Bingzhang** **2017/9/13 PM2:36:00**

α_K	Size scaling exponent for K_N	0.27^c (0.1, 0.3)	0.24 (0.001)	dimensio

页 38: [102] 删除的内容 **Chen Bingzhang** **2017/9/13 PM3:36:00**

d

页 38: [102] 删除的内容 **Chen Bingzhang** **2017/9/13 PM3:36:00**

d

页 38: [103] 删除的内容 **Chen Bingzhang** **2017/9/14 PM2:56:00**

1.34

页 38: [103] 删除的内容 **Chen Bingzhang** **2017/9/14 PM2:56:00**

1.34

页 38: [104] 删除的内容 Chen Bingzhang 2017/9/13 PM2:36:00

α_{μ}	First-order size scaling component for μ_{m}	0.25^{e} (0.1, 0.4)	0.27 (0.005)	dimensio
β_{μ}	Second-order size scaling component for μ_{m}	-0.025^{e} (–0.05, 0)	–0.013 (0.0002)	dimensio

页 38: [105] 删除的内容 Chen Bingzhang 2017/9/13 PM3:36:00

f

页 38: [105] 删除的内容 Chen Bingzhang 2017/9/13 PM3:36:00

f

页 38: [106] 删除的内容 Chen Bingzhang 2017/9/22 AM11:42:00

058

页 38: [106] 删除的内容 Chen Bingzhang 2017/9/22 AM11:42:00

058

页 38: [106] 删除的内容 Chen Bingzhang 2017/9/22 AM11:42:00

058

页 38: [107] 删除的内容	**Chen Bingzhang**	**2017/9/13 PM2:36:00**

α_{fer}	Size scaling exponent for $K_{0,fer}$	0.27^{c} (0.1, 0.3)	0.30 (0.001)	dimensio

页 38: [108] 删除的内容	**Chen Bingzhang**	**2017/9/13 PM3:36:00**

g

页 38: [108] 删除的内容	**Chen Bingzhang**	**2017/9/13 PM3:36:00**

g

页 38: [108] 删除的内容	**Chen Bingzhang**	**2017/9/13 PM3:36:00**

g

页 38: [109] 删除的内容	**Chen Bingzhang**	**2017/9/13 PM3:25:00**

092

页 38: [109] 删除的内容	**Chen Bingzhang**	**2017/9/13 PM3:25:00**

092

页 38: [109] 删除的内容	**Chen Bingzhang**	**2017/9/13 PM3:25:00**

092

页 **38: [110]** 删除的内容 **Chen Bingzhang** **2017/8/7 PM2:58:00**

dustso	Dust iron solubility	0.02[h] (0.01, 0.05)	0.022 (0.0007)	dimensio

页 **38: [111]** 删除的内容 **Chen Bingzhang** **2017/9/13 PM3:34:00**

Marañón et al., (2013); [b]

页 **38: [111]** 删除的内容 **Chen Bingzhang** **2017/9/13 PM3:34:00**

Marañón et al., (2013); [b]

页 **38: [111]** 删除的内容 **Chen Bingzhang** **2017/9/13 PM3:34:00**

Marañón et al., (2013); [b]

页 **38: [111]** 删除的内容 **Chen Bingzhang** **2017/9/13 PM3:34:00**

Marañón et al., (2013); [b]

页 **38: [111]** 删除的内容 **Chen Bingzhang** **2017/9/13 PM3:34:00**

Marañón et al., (2013); [b]

页 38: [111] 删除的内容 Chen Bingzhang 2017/9/13 PM3:34:00

Marañón et al., (2013); [b]

页 38: [111] 删除的内容 Chen Bingzhang 2017/9/13 PM3:34:00

Marañón et al., (2013); [b]

页 55: [112] 删除的内容 Bingzhang Chen 2017/9/28 PM11:32:00

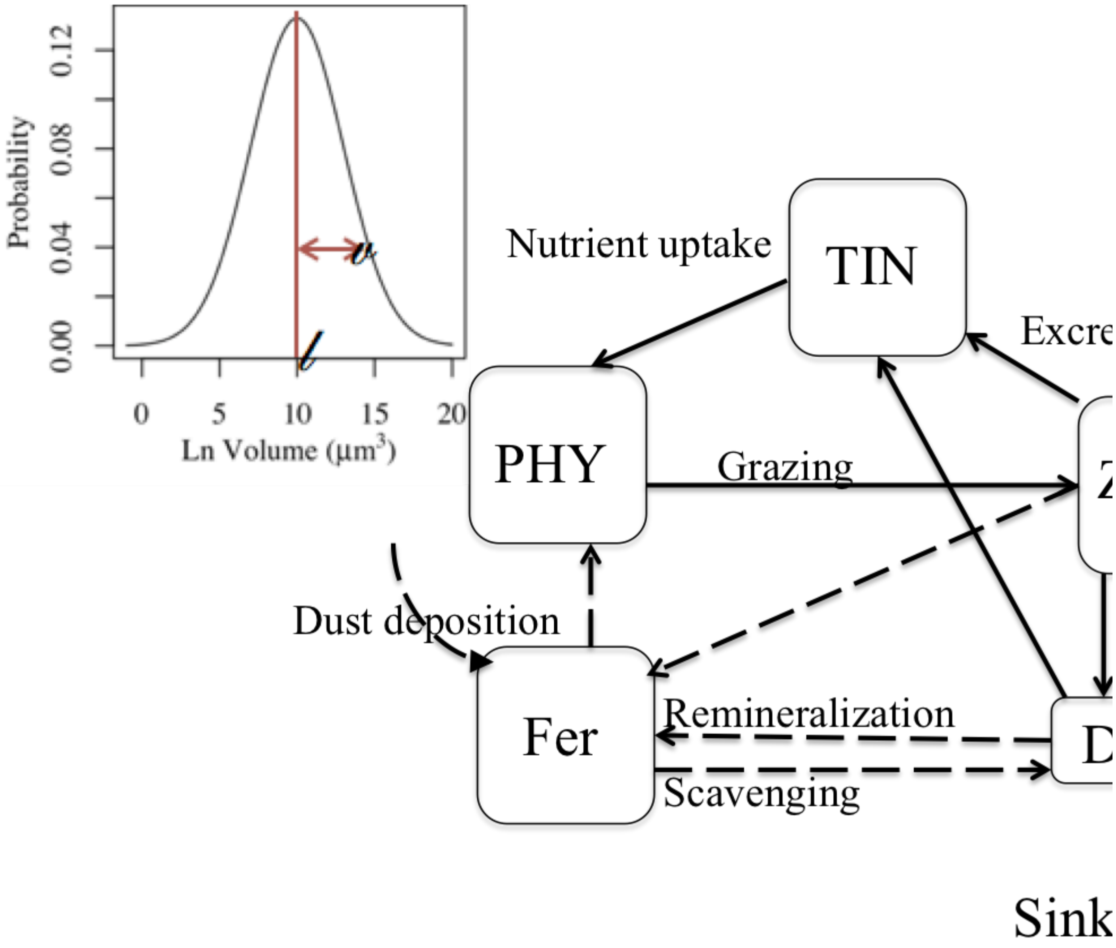

页 59: [113] 删除的内容 Bingzhang Chen 2017/9/29 PM2:50:00

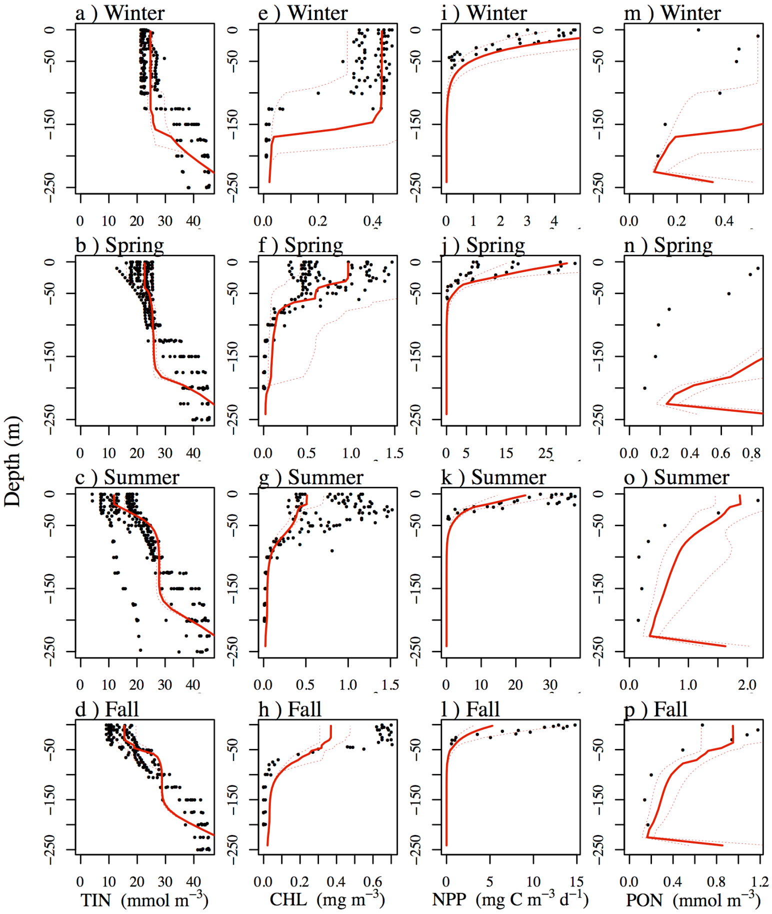

Fig. 6 . Model fittings to vertical profiles of TIN, CHL, NPP, and PON at K2

页 60: [114] 删除的内容 **Bingzhang Chen** **2017/9/29 PM2:50:00**

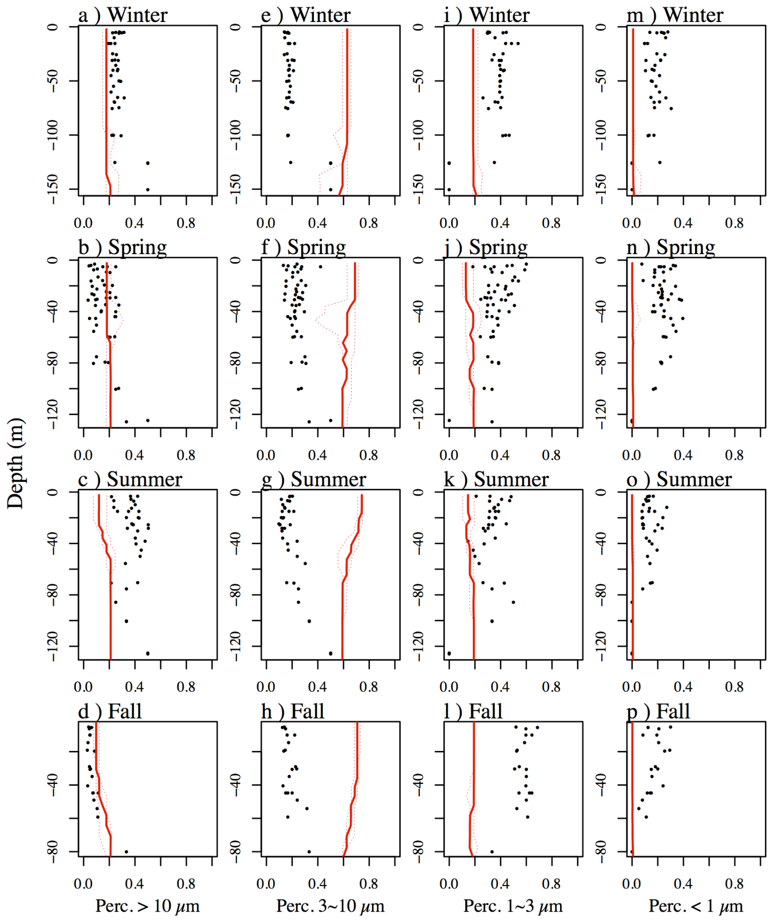

Fig. 8 . Model fittings to vertical profiles of four size fractions at K2

页 61: [115] 删除的内容 **Bingzhang Chen** **2017/9/29 PM2:50:00**

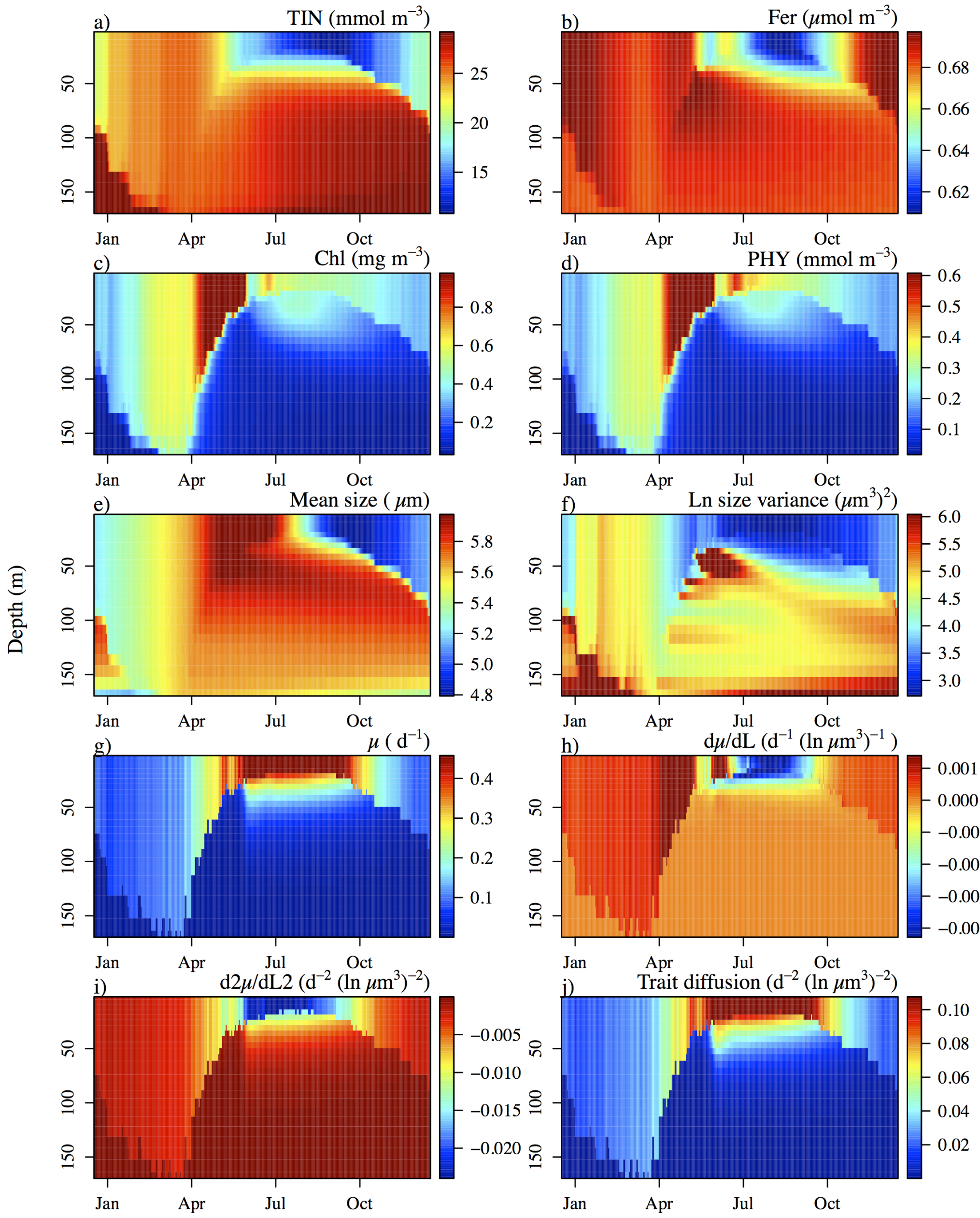

Fig. 10 . Modelled seasonal patterns at K2

页 62: [116] 删除的内容 **Bingzhang Chen** **2017/9/29 PM2:51:00**

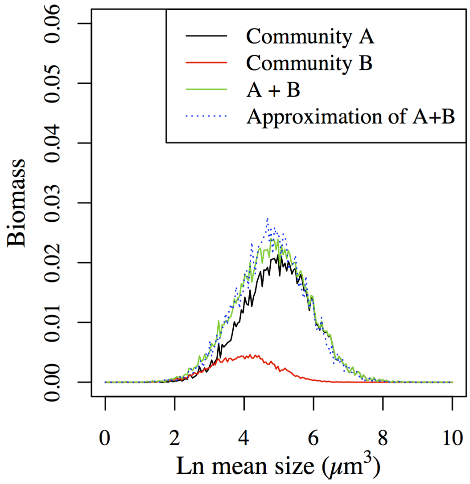
Community A
Community B
A + B
Approximation of A+B
Biomass
0.00
0.01
0.02
0.03
0.04
0.05
0.06
0
2
4
6
8
10
Ln mean size (μm^3)

Fig. 12